This page intentionally left blank

© Copyright by Farid Ahmed 2013
All Rights Reserved

ENVIRONMENTAL APPLICATIONS AND IMPLICATIONS OF CARBON-BASED NANOMATERIALS

A Dissertation
Presented To
the Faculty of the Department of Civil and Environmental Engineering
University of Houston

In Partial Fulfillment
of the Requirements for the Degree
Doctor of Philosophy
in Environmental Engineering

by
Farid Ahmed
August, 2013

ENVIRONMENTAL APPLICATIONS AND IMPLICATIONS

OF

CARBON-BASED NANOMATERIALS

Farid Ahmed

Approved:

Chair of the Committee
Debora F. Rodrigues, Assistant Professor,
Civil and Environmental Engineering

Committee Members:

Hanadi Rifai, Professor,
Civil and Environmental Engineering

William G. Rixey, Associate Professor,
Civil and Environmental Engineering

Megan Robertson, Assistant Professor,
Chemical and Biomolecular Engineering

Xin Wei, Associate Professor,
Department of Chemistry,
Texas Southern University

Suresh K. Khator, Associate Dean,
Cullen College of Engineering

Hanadi Rifai, Director,
Environmental Engineering
Graduate Program

Acknowledgements

It is my pleasure to acknowledge the help and support I have received from my colleagues, UH faculty members, friends and family members during the course of my doctoral study. I would like to thank all of you for positively contributing towards my research and personal life. I just want to mention that all your kind words and deeds will be a source of inspiration for the rest of my life.

First of all, I would like to acknowledge the contribution of my advisor, Professor Debora F. Rodrigues, for selecting me as her first doctoral student. I believe without her constructive guidance and constant inspiration, it would be impossible to come this far. The two most important lessons I learned from her are systematic approach to solve a challenge and effective time management. The research methods and strategies, I learned from her, will help me to develop my career in the coming years. I would also like to extend my acknowledgements to all the Environmental faculty for enriching my knowledge in Environmental Engineering and beyond. I would like to thank Professor Debora F. Rodrigues again for helping to enrich my knowledge in advanced biomolecular techniques, which I was not familiarized with at all before joining this program. Dr. Bill Rixey deserves special thanks for efficiently teaching two mass transfer related courses in Environmental systems and often sharing ideas and suggestions regarding my research. Many thanks go to Dr. Hanadi Rifai, for providing instructions and guidance since my first day in the Environmental Engineering program. I truly admire her wisdom and extending her help whenever needed. I would also like to thank Professor Rigoberto Advincula (Case School of Engineering, Case Western Reserve University) for providing

collaborative research opportunities. It was a great experience to learn about various aspects of polymer nanocomposite synthesis and characterization while working with his group.

I was particularly lucky to work within a group of very helpful and vibrant young researchers. I am very thankful to Dr. Catherine M. Santos for sharing her research expertise with me and extending help whenever needed. I would also like to thank Isis Mejias, Tugba Onal, Sean Smith, Ruji P. Medina, Hang Nguyen and Yvonne Musico for their continuous support and help. Also, I extend my thanks to the authority of Sims South Bayou Treatment Plant for providing the wastewater sample used in my studies.

I specially acknowledge the financial support from the National Science Foundation Career Award (NSF Award #104093), the University of Houston New Faculty Research Program (proposal # 102556) and the Provost Fellowship Award for supporting my doctoral research.

My wife, Ruksana Rahman, deserves great acknowledgement for being a constant source of love and joy in my life. Her help and encouragements kept me going through many stressful times. I am also very much thankful to my brother, Forhad Ahmed and sister, Mahbuba Akther, for their unconditional love and affection throughout my life. Lastly, I am in debt to my parents for everything in my life. Special thanks to them for showing me how to live an honest and happy life.

ENVIRONMENTAL APPLICATIONS AND IMPLICATIONS
OF
CARBON-BASED NANOMATERIALS

An Abstract
Presented To
the Faculty of the Department of Civil and Environmental Engineering
University of Houston

In Partial Fulfillment
of the Requirements for the Degree
Doctor of Philosophy
in Environmental Engineering

by
Farid Ahmed
August, 2013

Abstract

In recent years, carbon-based nanomaterials have advanced significantly in terms of synthesis and chemical modifications for diverse applications in nanotechnology. Among the carbon-based nanomaterials, single-walled carbon nanotubes (SWNT) and graphene oxides (GO) have been attracting researchers' interest due to their unique electronic and physicochemical properties. On the other hand, studies focusing on the understanding of their toxicological properties and potential antimicrobial applications are still in their infancy. The major barriers for such applications are their poor dispersion in most mediums, high cost and high cytotoxicity towards mammalian cells.

In this study, we overcome these limitations by incorporating only 3% (weight %) of these nanomaterials into aromatic polymer matrices of poly-vinyl carbazole (PVK) to improve their dispersion and antibacterial effects. The higher antimicrobial effects of PVK-SWNT and PVK-GO nanocomposites were attributed to a better contact of the nanomaterial with the bacterial cells by enhanced dispersion of the nanomaterial in the polymer matrix. The antimicrobial property of theses nanocomposites was observed on free swimming cells and on biofilms in solutions and coated surfaces, respectively. Cytotoxic effects of PVK-SWNT nanocomposite to mammalian cells was also found to be minimal due to low amount of the nanomaterial (only 3%) in the nanocomposite, which is promising in terms of applications where humans can be exposed to these nanomaterials, such as biomedical devices and water treatment systems. Furthermore, nanomaterials, such as SWNT and GO, were also demonstrated to be effective in removing biofouling agents, like protein, from aqueous solutions. GO exhibited the

highest protein sorption capacity (~500 mg protein/g nanomaterial). The adsorption phenomena were found to be dependent on the surface charge of the nanomaterial and solution chemistry. Besides investigating the potential applications for these nanomaterials, their fate and impact in the environment were investigated. Acute exposure of GO to wastewater microbial communities involved in the carbon, nitrogen and phosphorous biogeochemical cycles was investigated. A dose dependent inhibitory effect of GO was observed on the wastewater microbial metabolic activity. Furthermore, GO was found to adversely affect the bioremoval of carbon, nitrogen and phosphorus in the wastewater treatment process at concentrations as low as 10 mg/L.

Table of Contents

List of Figures

List of Tables

Chapter 1 Research Hypothesis and Literature Review

1.1 Research Hypothesis

There has been significant development in synthesis and applications of different types of nanomaterials with the advancement of nanotechnology. One of the most promising class of nanomaterials is the carbon-based nanomaterials, which possess unique properties compared to their bulk counterparts; therefore, they have various potential applications [1]. All carbon-based nanomaterials are essentially derived from graphene, which is a single layer of carbon atoms arranged in a 2-dimensional honey-comb lattice [1].

In recent years, broad groups of graphene-based nanomaterials have been synthesized, either by different physical orientation (like carbon nanotubes) or surface functionalization (graphene oxide) or both. Among all the carbon-based nanomaterials, we evaluated in this study mainly graphene oxide (GO) and single-walled carbon nanotubes (SWNT) for their significant antimicrobial and adsorption properties. Up to date, several studies demonstrated inhibitory effects of carbon-based nanomaterials on pure bacterial cultures [2-5]. The two main common mechanisms of toxicity were hypothesized to be cell membrane damage via direct physical contact with the nanomaterials, and oxidative stress via production of reactive oxygen species (ROS). In general ROS are oxygen containing chemical species (O_2^-, OH^- and H_2O_2) with reactive chemical properties, which can interact with cell membrane and cell organelles [6]. Although these nanomaterials possess significant toxic effects towards various microorganisms, the investigation of their applications as antimicrobial agents is very limited. The major challenges for the wide application of these nanomaterials are that

some of these nanomaterials present high mammalian cell cytotoxicity, high cost, and lack of dispersion in most polar solvents (especially for SWNT). However, cytotoxic properties can significantly be reduced by incorporating the carbon-based nanomaterials into biocompatible polymers. The polyethylene glycol (PEG) and other polymers mixed with SWNT and GO were reported to be able to penetrate mammalian cells without damaging the plasma membrane, and their accumulation did not show significant toxic effect on the cell cycle [7-9]. Therefore, it was hypothesized that successful dispersion of GO and SWNT in a biocompatible polymer may be a promising way to reduce mammalian cytotoxicity and at the same time produce an antimicrobial material.

Although numerous studies have demonstrated antimicrobial properties of carbon-based nanomaterials on pure bacterial cultures, their effects on diverse groups of environmental microorganisms are mostly unknown. Because of the possibility of wide applications and the likelihood of large-scale production, it is highly likely that carbon-based nanomaterials will find their way into the environment and, as a consequence, may impact it negatively. In both natural and engineered (wastewater treatment plants) aquatic systems, diverse microbial communities carry out degradation of organic matter, remediation of toxic or carcinogenic compounds and removal of excess nutrient (nitrogen and phosphorus) by biogeochemical cycles, to reduce the pollution of receiving waters . Considering the toxic effects on pure culture, it can be hypothesized that carbonaceous nanomaterials may also affect microbial communities in natural and engineered aquatic systems. In a recent study, it was found that single walled carbon nanotubes (SWNT) can differentially impact microbial communities in activated sludge processes and adversely affect treatment efficiency [10]. Hence, it is necessary to extend

the antimicrobial study from pure culture microorganisms to diverse microbial communities found in natural aquatic systems and wastewater treatment plants. The understanding of environmental toxicity of nanomaterials is essential to help designing better and safer nanomaterial-based products and to determine safe ways to dispose them in the environment.

In my research work, both implications and applications of carbon-based nanomaterials were investigated. More precisely, I investigated single-walled carbon nanotubes (SWNT) and Graphene Oxide (GO) and their polymer (poly-N-vinyl carbazole, PVK) based nanocomposites in terms of toxicity, cytotoxicity and possible applications. The main goals of this research study were: (a) Investigation of the toxicity mechanisms of nanomaterials and nanocomposites on pure bacterial culture; (b) Application of nanomaterials and nanocomposites for biomedical and water treatment applications. (c) Investigation of the effects of nanomaterials on microbial communities involved in the biogeochemical cycles of wastewater treatment.

The main hypotheses behind my study are:

Hypothesis 1

Nanocomposites, with small load of carbon-based nanomaterials in a biocompatible aromatic polymer matrix, will improve dispersion of SWNT and GO, reduce cytotoxic effects, but still maintain the antimicrobial properties.

Hypothesis 2

Carbon-based nanomaterials and nanocomposites deposited on surfaces maintain identical antimicrobial properties as their counterparts dispersed in solutions.

Hypothesis 3

Unregulated environmental disposal of antimicrobial SWNT and GO can pose a threat to the biological functions of different microbial communities found in wastewater treatment.

This dissertation is divided in literature review of carbon-based nanomaterials (Chapter 1); synthesis and characterization of SWNT and GO nanocomposites, as well as their antimicrobial applications in suspension and on coated surfaces (Chapter 2 and 3). In Chapter 4 and 5, their anti-microbial and anti-fouling characteristics are applied for the development of anti-microbial coated membranes filters and as adsorbent for the removal of biofouling agents, such as proteins, respectively. Lastly, in Chapter 6, the effects of GO on biogeochemical cycles in wastewater treatment plant is presented.

1.2. Carbon-Based Nanomaterials

Nanomaterials are defined as particles ranging from 1 to 100 nm. Their unique thermal, mechanical, electrical and biological properties are currently applied across physics, chemistry and biological fields [1]. Carbon-based nanomaterials are of carbon origin and share the same bonding configurations as macroscopic carbon structures, but their properties and morphology are dominated by the stability of select resonance structures rather than the bulk averages of their crystalline forms. The physicochemical configurations and properties are strongly related to carbon's structural conformations and thus hybridization state [11]. Depending on the bonding relationships with neighboring atoms, the carbon atoms can hybridize into different configurations and form various carbon-based nanomaterials with different structures [1, 11]. The most studied carbon-based nanomaterials are single-walled carbon nanotube (SWNT), fullerene, graphene (G), graphene oxide (GO), and nanodiamonds (Figure 1). In this chapter, we will concentrate our discussions mostly on SWNT, G and GO.

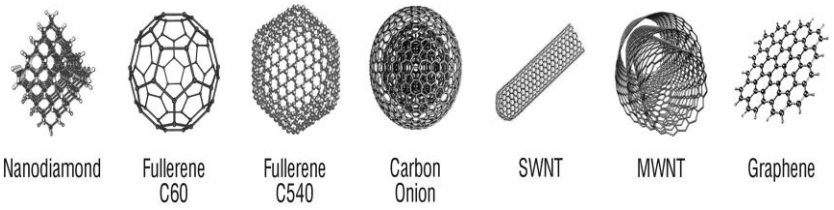

Figure 1.1. Examples of carbon-based nanomaterials.

1.3. Synthesis of SWNT, G and GO

There are several methods for synthesizing different carbon-based nanomaterials. Here we will discuss some methods for synthesizing SWNT, G and GO.

The basic small scale methods for synthesizing SWNT are arc discharge and laser ablation, which utilizes carbon rod and graphite rod, respectively, as a source of carbon. In the arc discharge method, direct current vaporizes the surface of one carbon rod and forms SWNT deposits on another carbon rod. In the laser ablation method, a pulsed laser is used to vaporize graphite inside a reactor and the vapor is cooled to form SWNT [12]. Both of these methods produce limited quantities of SWNT with high quality. For large scale production, Chemical Vapor Deposition (CVD) is the most widely used method for both SWNT and G. In this method, either Co or Ni is usually used as the substrate. These substrates are heated at 700-1000°C and hydrocarbon gas is injected as the source of carbon for the synthesis of these nanomaterials. In this method physical properties, like the thickness and number of layers, can be controlled by the concentration of the hydrocarbon gas and the reaction conditions. This method can produce large quantities of nanomaterials but with metal and catalyst impurities [11, 12].

A common method for synthesis of G is through mechanical or chemical exfoliation. In mechanical exfoliation, a graphite sheet is broken down to 5 μm thick sheets with plasma. The sheets are then stuck on a photoresist and peeled off layer by layer with scotch tape. The thin layer left on the photoresist usually is a single or a few layers of graphene. The process produces very low yields of graphene sheets. On the other hand, chemical exfoliation involves reaction with solvents like N-methyl-

pyrrolidone or surfactants like sodium dodecylbenzene sulfonate and sodium cholate. Usually G solutions in these solvents or surfactant tend to be quite stable as the surfactant coats G sheets, which make the sheets repeal each other to allow them to be well dispersed. Further purification can be achieved with density gradient ultracentrifugation (DGU). The disadvantages of this process are the high costs and high boiling points of the solvents [1].

In recent years, modified Hummers method has become the most common synthesis method for production of GO and G. Generally graphite flakes are highly oxidized with concentrated sulfuric acid or potassium permanganate to form graphite oxide. Graphite oxide is highly oxygenated with OH^- and $COOH^-$ groups which make it hydrophilic. In water, graphite oxide readily exfoliates and yields a stable suspension of single layered GO. Graphene oxide can be further reduced with agents like Hydrazine or sodium borohydrate to produce graphene [1].

1.4. Characterization Techniques

Optical imaging is the most common used method for characterization of nanomaterials. Optical imaging techniques include atomic force microscopy (AFM), scanning electron microscopy (SEM), and transmission electron microscopy (TEM). Most often, two or more methods are applied simultaneously for complete visual imaging and physical evaluation of thickness and size of the nanomaterial. Usually, AFM provides a topographical contrast image of the nanomaterial and determines the thickness of the nanosheets, such as G. SEM and TEM are obtained by passing an electron beam through the ultrathin nanomaterials to produce an image with atomic scale resolution [1, 11].

Raman spectroscopy, on the other hand, is used frequently to identify any specific carbon-based nanomaterials in terms of its characteristic spectra [13]. Every band in the raman spectrum corresponds to a specific vibrational frequency of a specific bond in the molecule. The vibrational frequency depends on the orientation of the band and the weight of the atoms in that bond [1, 14]. Raman spectroscopy is often used to determine the defects and alignment of carbon-based nanomaterials like carbon nanotubes. Another method to investigate the quality of the nanomaterial and the presence of impurities from byproducts or catalyst are the thermo gravimetric analysis (TGA). In the TGA, materials undergo a gradual increase in temperature and the variation of mass is determined as a function of temperature. The important parameters in a TGA curve are the oxidation temperature and residual mass. TGA is often used to determine the purity and thermal stability of synthesized carbon-based nanomaterials [15].

In some applications, carbon-based nanomaterials can be modified with functional groups or blended/modified with polymers to enhance or modify the original properties of the nanomaterial and/or the polymer. The presence and intensity of such functional groups and characteristic bonds of polymers are usually examined by Fourier transformed infrared spectroscopy (FTIR), UV-vis absorption measurements (UV-vis) and X-ray photoelectron spectroscopy (XPS) [1, 14, 16]. FTIR is used to qualitatively determine the functional groups and also the chemical structure of functionalized nanomaterials. UV-vis is used to quantitatively determine highly conjugated compounds like graphene, graphite, electroactive polymers or conjugated polymer networks [17]. XPS is a surface chemical analysis technique to determine quantitatively elements present on a surface, as well as their chemical and electronic states. For carbon-based nanomaterials, it is often

used to quantitatively determine the concentration of carbon and oxygen groups after functionalization [18].

1.5. Brief Descriptions of the Carbon-Based Nanomaterials Presented in This Work

1.5.1. Graphene (G)

Graphene, the building block of graphite, is a one-atom-thick planar sheet of sp^2-bonded carbon atoms densely packed in a honeycomb crystal lattice. Graphene possesses excellent electrical conductivity, mechanical flexibility, optical transparency, thermal conductivity, and low coefficient of thermal expansion. However in most applications, achieving single layer graphene can be challenging due to agglomeration or re-stacking as graphite by pi-pi stacking or van der Waals forces. This problem can be tackled with surface functionalization, which converts hydrophobic surfaces to hydrophilic. The presence of these groups prevents the aggregation by polar-polar interactions or by their bulky size. The thickness of the graphene layer has been reported to be between 0.35 nm and 1.0 nm [1].

1.5.2. Graphene Oxides (GO)

Pristine graphene is not suitable for many applications; therefore surface modifications are necessary, which can be attained by functionalization of graphene sheets. Proper functionalization generally prevents agglomeration of graphene sheets in aqueous systems and at the same time can retain some of graphene's inherent properties. Usually functionalized graphene with hydroxyl, epoxide, diol, ketone, and carboxyl functional groups, are called GO. The presence of these groups significantly alters the

Van der Waals force and dispersion of this material in water and various organic solvents. Among many chemical synthesis processes of GO from natural graphite, the modified Hummers method is the most widely used [1, 19].

1.5.3. Single-Walled Carbon Nanotube (SWNT)

Carbon nanotube can be described as the cylindrical form of a graphene sheet. The diameter usually is nanoscale while the length is microscale. SWNT is one of the most investigated carbon-based nanomaterials, hence their synthesis techniques and properties are well-established. SWNT can have a metallic, semi-metallic and semi-conducting behavior. SWNT particles are highly hydrophobic and tend to agglomerate. However it is possible to achieve good dispersion of SWNTs in aquatic media by surface modification and debundling via sonication. SWNT are considered to be one of the most utilized carbon-based nanomaterials with applications in bioengineering, electronics, and packaging industries [11].

1.5.4. Carbon-Based Nanocomposites

Due to potential of various applications, in recent years, many researchers have successfully synthesized carbon-based nanocomposites. In most cases, nanocomposites are mixtures of small loads of carbon-based nanomaterials in a bulk volume of polymeric materials [1]. Essentially in all nanocomposites, nanomaterials or their derivatives are used as filler material [1, 20]. Due to the progress in manufacturing of nanomaterials in bulk volumes, there has been growing interest in synthesizing nanocomposites for specialized industrial applications. However major challenges still remain in terms of homogenous dispersion of nanomaterials, effective mixing of nanomaterials with the

polymer and ensuring the physical integrity of the nanomaterials inside the polymeric matrix. To achieve better dispersion of the carbon-based nanomaterials within the polymeric matrix, various surface functionalization methods have been adopted. Often, appropriate functional groups are selected to maximize the interfacial interaction between the polymeric matrix and the nanomaterial [21, 22].

The most common nanocomposite synthesis techniques include solution blending, melt mixing, and *in situ* polymerization [1, 20]. In the solution blending method, the polymer is dissolved in a suitable solvent which is later blended with a well dispersed nanomaterial, e.g. graphene, graphene oxide or SWNT, and subsequently the solvent is removed from the suspension. During the blending process, the polymer wraps the nanoparticles and interconnects the nanoparticles inside the matrix [1, 23-25]. The disadvantage of this process is mainly the use of toxic solvents. In the melt mixing process, the polymer is liquefied at high temperatures and then mixed to the nanoparticles. This procedure allows the dispersion of the nanoparticles in the nanocomposite. However, the high temperature used in this process can reduce the functional groups on the nanomaterial surface, hence potentially reducing the interfacial bonding with the polymer. In the case of the *in situ* polymerization process, nanoparticles are mixed with the monomers and the resultant mixture is subsequently polymerized to produce the nanocomposite. Presence of functional groups increases the initial dispersion of nanoparticles and hence their homogeneous distribution in the final nanocomposite. In nanocomposites, the interaction between the polymer and the carbon-based nanomaterial can be either non-covalent or covalent [20, 26]. The non-covalent interaction involves physical adsorption and/or wrapping of the polymer to the surface of the nanotubes. In

the case of carbon-based nanomaterials, such as the nanotubes or graphene sheets, some polymers, specially aromatics, will form pi-pi stacking with the polymer, other can have Van der Walls or electrostatic interactions [20]. In the covalent bonding, a strong chemical bonding occurs between polymers and the functional groups present on the surface of the nanomaterial.

The incorporation of nanomaterials into a polymer matrix can bring new properties to the nanocomposites. In the case of carbon-based nanomaterials, their unique stiffness and conductivity can significantly enhance the mechanical strength and electrical conductivity of the polymer when incorporated in it. For example, incorporation of only 0.7 wt% of GO sheets into polyvinyl alcohol (PVA) has shown to improve its mechanical strength by ~70% [23]. Some of the most common polymers used in nanocomposite synthesis include polyacrylic acid (PAA), polyethylene glycol (PEG), polyethylene terephthalate (PET), polypropylene (PP), polyvinyl alcohol (PVA) and poly vinylidene fluoride (PVDF) [20]. Overall, the incorporation of small loads of nanoparticles inside the polymer matrix generates nanocomposites with exceptional electrical and thermal conductivity, mechanical strength and stability. These light weight and high strength materials have found applications in automotive, aerospace, electronics, packaging and biomedical industries [1, 20].

1.6. Important Physicochemical, Toxic and Cytotoxic Properties

1.6.1. Physicochemical Properties

Diameter, length, shape, and material purity of the nanomaterials are important factors to attain different properties in the nanomaterials [27]. The very narrow diameter/thickness and long tube/sheets that many nanomaterials possess, like SWNT or G, leads to high aspect ratio. Hence, nanomaterials have very high surface area to volume ratio, which makes them significantly more advantageous for many applications than their macro or micro-scale counterparts [28]. For instance, this property is essential for applications as sorbent or scaffolding material [28, 29]. The application as a sorbent, however, is affected by the nanomaterial aggregation state, which is highly dependent on solution chemistry [30, 31]. The aggregation behavior is related to hydrophobicity, electrostatic and Van der Waals interactions among nanomaterials and/or between nanomaterials and other compounds in solution. In terms of solution chemistry, pH and ionic strength are the two most important parameters. The stability of the nanomaterial in aqueous suspension is strongly dependent on the pH. Change of pH from acidic to basic was found to dissociate the functional groups on the nanomaterial surface; and hence reducing the attachment efficiency. On the other hand, increase in ionic strength (Na^{+}, Ca^{2+}) was found to reduce the electrostatic repulsions between the nanomaterials and therefore increasing the attachment efficiency [31].

1.6.2. Anti-microbial Properties of Carbon-Based Nanomaterials

The physicochemical properties of the nanomaterials have also been demonstrated to enhance or reduce their anti-microbial properties. The most common parameter for the

nanomaterial toxicity to microbes has been reported to be their nanoscale size [2]. In addition, their shape, specific surface area, chemical composition and surface structure have also been demonstrated to play an important role in toxicity [32, 33]. Although available surface area is a function of particle dispersion or agglomeration in the medium and the dispersion is dependent on the solution chemistry where the nanomaterial is found. It has been established that the larger the surface area of an individual nanomaterial the higher will be the contact area with the microbial cells [2, 30, 34].

For instance, dispersed nanotubes were reported to have significantly more toxic effects to cells than the aggregates [35, 36]. Carbon-based nanomaterials are synthesized in different shapes, i.e., tubes, sheets, spheres, and this shape factor can affect their deposition and their interaction with microorganisms [33, 37]. In the case of rod shaped nanomaterials, like SWNT, it was found that the diameter of the nanotubes is a key factor for its antibacterial properties. It was demonstrated that in the presence of small diameter nanotubes, bacteria produces more stress related gene products than in the presence of larger diameter nanotubes [2]. Similarly, sharp edges of graphene or graphene oxide sheets were described to physically damage and inactivate bacterial cells [38].

In addition of the size of the nanomaterial, the cell contact time with the nanomaterial has also been demonstrated to increase their antimicrobial effects [39-41]. Several studies have demonstrated time dependency antimicrobial effects of nanomaterials on both pure culture and environmental bacteria. Antimicrobial studies with SWNT, GO and their polymeric nanocomposites demonstrated significant increase in toxicity toward both Gram-positive and Gram-negative bacteria with increase of incubation period from 1 h to 3 h [5, 40]. It was also observed that for Gram-positive

bacteria longer exposure was needed to cause significant antimicrobial effects [40]. Similarly, a study investigating the impact of functionalized SWNT on soil microbial community showed major impacts to the microbial community functionality after 3 d exposure to SWNT. The longer the incubation period the worse was the impact to the soil community and the biogeochemical cycle of nutrients in the soil [42].

Antimicrobial effects of carbon-based nanomaterials were not only found to be dependent on the physicochemical properties of the nanomaterials and the exposure time, but also dependent on the bacterial cell wall characteristics. Several studies have shown Gram-positive bacteria, which possess thicker peptidoglycan, is more resistant to the anti-microbial properties of nanomaterials than Gram-negative bacteria [36, 40]. Besides the bacterial cell wall structure, other bacterial properties, such as ability to form spores and unique cell injury repair mechanisms of some bacteria were hypothesized to explain the different tolerances of bacteria to nanomaterials [4, 43, 44].

Most of the investigations so far have been against diverse groups of planktonic microorganisms including bacteria (both Gram-positive and Gram-negative), protozoa, and viruses [45-50]. Few studies have shown that SWNT and GO-coated surfaces significantly inhibit bacterial biofilm formation, such as *E. coli* and *B. subtilis* [5, 40, 41] [41]. On the other hand, toxicity studies of graphene and graphene oxide is still very limited when compared to carbon nanotubes. Recently, few studies have shown that like carbon nanotube, graphene also possess antibacterial properties, but the toxicity mechanisms might be different [5, 38, 51, 52]. The two most common hypothesized mechanisms for SWNTs are physical damage of cell membranes and production of

harmful reactive oxygen species [2, 4, 40, 53-55]. In the case of the nanotubes, the cell membrane damage was derived by direct cell contact with the nanomaterials. In this mechanism, SWNT was found to have direct physical interaction with cellular materials and cause cell injury and death [33, 56]. Similarly, sharp edges of G and GO were reported to cause damage to bacterial cell membrane and induce cell death [38, 57]. Additionally, unlike carbon nanotubes, GO sheets were described to wrap around the bacterial cells and isolate them from their environment, preventing them to grow [5, 38]. In general, the main mechanisms behind toxicity of all the carbon-based nanomaterials have been described to be physical membrane damage and oxidative stress t [38, 53, 57, 58]. In the presence of carbon-based nanomaterials, production of reactive oxygen species (ROS), like O_2^- and H_2O_2, was demonstrated and reported to cause toxicity toward bacterial cells [53, 57]. Excessive ROS can oxidize the fatty acids in the cell membrane and damage the cell permeability, which will affect essential cell functions [37, 58].

Overall, from the antimicrobial studies it is evident that carbon-based nanomaterials can induce toxicity to both Gram-positive and Gram-negative bacteria in pure culture and in environmental conditions. The antimicrobial effects were attributed to the physicochemical characteristics of the nanomaterial as well as the experimental conditions like contact time and solution chemistry. The principal antimicrobial mechanism was reported to be cell membrane damage via physical contact with the nanomaterials and oxidative stress.

1.6.3. Cytotoxic Properties

Besides the antimicrobial properties of nanomaterials, the cytotoxic effects of carbon-based nanomaterials on different types of mammalian cells have been extensively investigated. As observed in antimicrobial studies, size and shape of nanomaterials also found to play an important role in their cytotoxic properties. A comprehensive study investigating the correlation of GO size with its cytotoxicity showed that smaller nanosheets were capable of causing much higher cytotoxicity than larger sheets [59]. *In vivo* toxicological studies of GO using mice shows its accumulation in kidney and lung tissues and only 0.4 mg was found to be of lethal dose.

Several studies demonstrated the effects of dose and contact time on cytotoxic effects of nanomaterials. The first published cytotoxicty study was done on human epidermal keratinocytes cells exposed to SWNT concentrations between 0.06-0.24 mg/ml for 18 h. Significant loss of cell viability and morphological changes were described to be caused by oxidative stress [54]. Similarly, cytotoxicity effects of multi-walled carbon nanotube (MWNT) were also confirmed with human epidermal keratinocyte cells. Dose and time dependent cytotoxic effects were observed and accumulation of MWNTs inside the cells were demonstrated [60]. This study further demonstrated that purified MWNT still presented cytotoxicity, which suggested that the presence of metal catalysts were not responsible for the cytotoxicity of the nanomaterial. Other studies also investigated the cytotoxic effects of the aggregation state of the nanotubes. In one study, MWNT were homogenized by a grinding process to make the tubes more available to the macrophage cells as compared to unground aggregated nanotubes. This higher nanotube dispersion

increased the cytotoxicity and cell inflammation [61]. A comparative study with macrophages showed that the cytotoxic properties of SWNT are more pronounced than MWNT. However both SWNT and MWNT were found to cause significant loss in cell viability [62].

Similar to nanotubes, cytotoxic effects of GO was also found to be dose and time dependent. GO nanosheets were demonstrated to exhibit cytotoxicity to human fibroblast cells at concentrations as low as 20 μg/ml. In the presence of GO, cells were morphologically deformed and significant cell death occurred [9]. More detailed toxicological studies with GO demonstrated presence of GO not only in the cytoplasm, but also in lysosomes, mitochondria and even in the nucleus.

Overall, all the cytotoxicity studies showed adverse effects of SWNT, MWNT and GO on mammalian cells at various extent. However comparative toxicological studies showed, that in general, SWNTs are the most toxic nanomaterial when compared to GO [63].

1.7. Applications of Nanomaterials as Coatings and for Water Treatment

1.7.1. Antimicrobial Coatings

Biomedical surfaces often need to possess antimicrobial properties to prevent colonization and growth of pathogenic microorganisms. Conventional antimicrobial surfaces contain antibiotics and metal ions (silver) that resist bacterial colonization for short periods of time. In these antimicrobial surfaces, active anti-bacterial agents are loaded in the coating polymer matrix and are released to the surface via diffusion [64, 65]. The diffused antibacterial agents (for example, Ag^{+}) may interact with the bacterial

cell wall and adversely affect its functionality [65]. However due to continuous diffusion, the loading of antibacterial agents get exhausted and the surface loses its effectiveness over time [66, 67]. Recently, coatings with permanently attached antimicrobial agents have gained more attractiveness since these coatings will ensure long term effectiveness against microorganisms. Carbon-based nanomaterials, like SWNT and GO, have become potential candidates as antimicrobial agents for surface modifications, due to their antimicrobial properties. However, pristine SWNT, G and GO are not suitable for such applications since they cannot easily coat surfaces, and also as pure materials, they have cytotoxic effects to humans. These challenges prevent their use for biomedical and other applications related to human exposure.

As a solution, recent studies have investigated the production of biocompatible nanocomposites, which combine carbon-based nanomaterials with biocompatible polymers. For instance, GO nanocomposites with polyethylene glycol (PEG) was found to have impressive solubility and stability in aqueous solvents, and not shown any cytotoxic effect to human cells. Therefore this new nanocomposite presents various potential biomedical applications [68]. Another study with this nanocomposite investigated the biodistribution and bioaccumulation of PEG-GO. This study demonstrated that PEG-GO does not accumulate inside the mammalian organs and therefore does not pose any long term toxicity issues [69]. Several other studies also successfully synthesized benign GO nanocomposites with biocompatible polymers like chitosan, perylene tetracarboxylic acid (PTCA) and polyelthylenimine (PEI) [68, 70-72]. These nanocomposites have been successfully used in various biomedical applications, i.e., sensor, drug carrier, without causing any cytotoxicity.

Similarly, previous studies with other mammalian cells, such as the human umbilical vein endothelial cells, demonstrated that a SWNT mixture with the phosphorycholine polymer exhibited a cytotoxicity of only ~8-10%, while SWNT/MWNT suspended with polyethylene glycol (PEG) showed no considerable toxicity to mammalian cells [7]. SWNT in a block polymer Poly(styrene-isobutylene-styrene) nanocomposite film was shown to not cause growth inhibition of mouse fibroblast cells [73]. The PEG and other polymers mixed with SWNT/MWNT were reported to be able to penetrate mammalian cells without damaging the plasma membrane, and their accumulation did not show significant toxic effect on the cell cycles [74].

Although there have been successes in terms of reducing cytotoxicity of carbon-based nanomaterials by incorporating them into biocompatible polymers, their use for the preparation of antimicrobial coatings is still very limited. A recent study showed that nanocomposites of reduced GO with polyoxyethylene sorbitan laurate can be synthesized as a paper like structure, which possess antimicrobial activity toward Gram-positive bacteria. In addition, this nanocomposite was found to exhibit negligible cytotoxicity to several types of mammalian cells [75]. In another study, nanocomposite films of SWNT (2 wt %) in poly(lactic-co-glycolic acid) and poly(L-lysine) polymers were demonstrated to inactivate bacteria (~90 %) [36, 76]. Most of these findings were done in short-time studies and in very controlled environments. Therefore the effectiveness of these nanocomposites after long-time exposures to bacteria needs to be investigated at various environmental conditions.

1.7.2. Traditional Water Treatment Technology: Target Contaminants and Limitations

Water treatment processes aim to remove both biological and chemical contaminants from water sources. Biological contaminants include different groups of pathogenic microorganism (bacteria, virus and protozoa) [30, 77, 78]. On the other hand, heavy metals and natural organic matter (NOM) are important components of the chemical contaminants present in various natural water sources [79, 80].

Microbial disinfection is a major step in conventional water treatment systems. The most common forms of disinfection techniques include chlorination, ultra-violet (UV) disinfection and ozone treatment. Filtration devices, such as granular activated carbon (GAC) and sand filters do not disinfect water but physically remove them from the influent. Whenever available, the combination of these treatment techniques is very successful in preventing outbreaks. However, not all countries have access to them, therefore outbreaks around the world still occur at high rates [81]. Furthermore, all these techniques have limitations. The limitations of current disinfection methods are two-fold: firstly, certain pathogens can form cysts or spores that protect them against certain types of disinfection methods, and secondly, some disinfection methods also produce carcinogenic disinfection byproducts (DBPs) [78, 81]. DBPs are undesired products formed by reactions between various constituents of natural organic matters (NOM) and disinfection agents like chlorine and ozone [82-84]. NOM is a complex mixture of humic substances and acts as carbon source for bacteria [30, 78]. Dissolved NOMs increase the bacterial regrowth and biofilm formation in the water distribution systems [85].

Traditional activated carbon filters are widely used for NOM removal by adsorption process [86]. However the adsorption process is limited by the molecular size of the adsorbate components and porosity of the adsorbent [30]. In addition, chemical compounds, such as pharmaceuticals and pesticides, have been quantified at alarming concentrations in natural and engineered aquatic systems [87, 88]. Many of them are termed as emerging contaminants since their health consequences and removal processes still need to be investigated [89-91]. Heavy metals are also one of the major contaminants to be removed during water treatment. Due to their acute and chronic toxicity effects, regulatory limits have been set for concentrations in drinking water [92]. In conventional treatment plants, GAC filters are used to remove heavy metals by adsorption. However, poor removal efficiency at low concentrations of heavy metals and slow adsorption rate often fails to meet regulatory requirements [93-95].

1.7.3. Application of Nanomaterials and Nanocomposites for Water Treatment

1.7.3.1. Removal of Biological Contaminants

The anti-microbial properties and high adsorption capacity of carbon-based materials led to several investigations on their potential applications for the removal of bacteria and viruses from contaminated water sources. Studies of bacterial adsorption to carbon-based nanomaterials demonstrated that carbon-based nanomaterials, like SWNT, possess large surface area, and therefore, superior adsorption capacity than traditional adsorbents [78, 96]. It was calculated that, 0.1 g of SWNT has a surface area of approximately 250 m^2/g. Furthermore, a surface availability of 10% SWNT, can remove 3.18 $x10^{12}$ CFU/mL (Colony forming units/mL). Some nanomaterials, such as SWNT,

were also reported to present affinity to certain bacteria. This adsorption preference is important, since it can potentially selectively remove pathogens from non-pathogenic microorganisms. For example, an adsorption study with mixed bacterial cultures of *Staphylococcus aureus* (*S. aureus*) and *E. coli* demonstrated that *S. aureus* was adsorbed 100 times more than *E. coli* [97]. Additionally, microbial adsorption rate on nanomaterial surfaces tend to be rapid, which is a desirable characteristic for adsorbents, point of use (POU) water treatment devices, and for the development of sensors [78, 97]. For instance, SWNT was found to remove 95% of *E. coli* and *S. aureus* within 5-30 minutes of contact. In traditional drinking water treatment, removal of bacterial spores is very difficult by chemical disinfection or activated carbon adsorption . It was reported that in aqueous solution, SWNT particles can absorb almost 27-37 times more *B. subtilis* spores than powdered activated carbon [98]. This high adsorption capacity was due to the high aspect ratio and the fibrous structure of SWNTs, which increased significantly the surface availability for the attachment of spores [78].

In addition to bacterial removal, viruses also have been successfully removed by carbon-based nanomaterials through adsorption. Several studies demonstrated that commercial membrane filters coated with carbon nanotubes can completely remove all viruses from an influent containing 10^7-10^8 plaque forming units (PFU)/ml [96, 99]. Removal of virus in traditional drinking water treatment systems bring challenges as nanometer sized virus can easily escape regular filtration membranes and activated carbon-based filtration systems. A linear relationship was established between the thickness of the nanotube layer and removal of viral particles [96, 100]. The important parameters governing efficiency of virus removal was reported to be ionic strength, pH

and NOMs [100]. Addition of Ca^{2+} ions improved virus removal via surface complexation with the virus. Higher attachment of virus with SWNT was observed at pH values lower than the virus isoelectric point (3.9). Presence of NOM deteriorated filter effectiveness by adsorbing to both SWNT and virus and hence bring repulsive forces between them [100].

1.7.3.2. Removal of Organic Contaminants

Among the organic contaminants, natural organic matters (NOM) are the most widely found in water sources and are composed of a heterogenous mixture of humic substances, proteins, lipids and carbohydrates [32, 78, 101-103]. NOMs are traditionally removed by adsorption with granular activated carbon and powdered activated carbon. The NOM adsorption efficiency depends on the surface properties of the adsorbent and the chemical characteristics of the NOM along with the water solution chemistry, *e.g.* pH, salinity [30, 86, 103, 104]. The main physical properties of adsorbents are pore size (micro and meso) and presence of net positive surface charges. As activated carbon is a highly porous structure, size exclusion plays an important role in adsorption. NOMs with higher molecular weights will generally adsorb on the outer surface, while lower molecular fractions will adsorb inside the micropores [86].In the case of carbon-based nanomaterial, like SWNT and graphene, their large surface area plays an important role on the adsorption of different NOM fractions. For instance, it was reported that for both higher and lower molecular weight fractions of NOMs, SWNT exhibits much higher removal capacity than activated carbon [85]. Although, SWNT and graphene aggregates in aqueous medium, their large mesopores in aggregates and less negatively charged

surfaces compared to activated carbon enhances their adsorption capacity for NOMs [30, 85]. The abundance of micropores in activated carbon also bring difficulties in terms of desorption of adsorbed contaminants inside the pores for regeneration of the material. In the case of nanomaterials, NOMs are adsorbed on the outer surface, which facilitates their regeneration [85, 86]. Additionally, the presence of aromatic rings in both humic acids and carbon-based nanomaterials allows them to have pi-pi interactions, which facilitate removal of NOM from aqueous environments [105]. More importantly, the much larger surface area of nanomaterials than activated carbon allows NOMs and competitive adsorbates, such as trichloroethane and synthetic organic compounds, to be removed more efficiently by nanomaterials [86, 106, 107].

1.7.3.3. Removal of Heavy Metals

Heavy metals are one of the inorganic pollutants of most concern in drinking water and wastewater treatments. The majority of the heavy metal contaminations of water sources come from industries like metal plating, paints and textile dying industries. Heavy metals are one of the most aggressive environmental pollutants since it cannot be easily removed by conventional biological water treatment processes. In traditional water treatments, heavy metals are mostly removed by coagulation, flocculation, and activated carbon filtration processes. More recently, studies have shown that carbon nanotubes and graphene oxide can remove heavy metals from aqueous solutions. In most of these studies, SWNTs were able to successfully remove Pb^{2+}, Zn^{2+}, Cd^{2+}, Cu^{2+} from aqueous solutions [108-110]. The results from the studies investigating the affinity order of the heavy metal ions toward carbon nanotube are often contradictory [92, 111]. Furthermore,

these studies demonstrated that the adsorption capacity of carbon nanotubes are highly dependent on the pH of the solution, however presents significantly higher adsorption capacity compared to other adsorbents in similar experimental conditions [112]. The mechanisms of heavy metal removal by carbon nanotubes were demonstrated to be physical adsorption, electrostatic attraction and precipitation.

Functionalized carbon nanotubes have also been reported to adsorb heavy metals [108, 110]. A comprehensive study investigating the mechanisms of Pb^{2+} adsorption on acid treated multi-walled nanotubes demonstrated that Pb^{2+} interacts with oxygen carrying functional groups on the carbon nanotube surfaces. Other adsorption mechanism identified were physical adsorption of Pb^{2+} on non-functionalized areas on the surfaces, defect sites on the walls of the nanotubes and open ends of the tubes [113]. Similarly to functionalized nanotubes, graphene oxide studies also have showed promising results. Since most of the heavy metals are present as cations (*e.g.*, Cu^{2+}, Pb^{2+}, Cd^{2+}), the negatively charged functional groups present on the GO surface make them excellent adsorbents for heavy metals. On the other hand, non-functionalized graphene has been shown to serve as an adsorbent of both cationic and anionic heavy metal ions to some extent [114]. All studies so far have demonstrated that GO can adsorb significantly more heavy metals (Cu^{2+}, Cd^{2+}, Co^{2+}) from aqueous solutions than unmodified carbon nanotubes and activated carbon [114, 115]. Electrostatic attractions between positively charged metal ions and negatively charged functional groups on GO surfaces were reported to be the main adsorption mechanism. Additionally, small amounts of GO incorporated into chitosan or gelatin was found to significantly enhance their metal adsorption capacities [116, 117]. From all investigations with functionalized

nanomaterials, it was evident that carbon nanotubes and graphenes will have an enhanced heavy metal adsorption capacity by increasing the negative functional groups on their surfaces. This change on their surface chemistries can be achieved by activation mechanisms using oxidizing agents like $KMnO_4$, H_2O_2, HNO_3 and H_2SO_4 [1, 118, 119]. The changes on surface charges of these nanomaterials were determined by zeta potential measurements after activation. For instance, nanotubes became more negatively charged in solution due to the presence of –COOH and –OH functional groups [112].

Besides the functional groups, other reports observed that experimental conditions and solution chemistries play an important role on the nanomaterial adsorption of heavy metals. Experimental conditions like contact time, initial metal concentration and mass of carbon-based nanomaterials play an important role on the amount of heavy metal adsorbed. The pH and ionic concentrations have been reported as significant parameters for successful adsorption. If the pH solution is higher than the net zero surface charge of the carbon-based nanomaterial, then the negative surface charge facilitates adsorption of cationic heavy metal ions via electrostatic attraction [112]. On the other hand, lowering the pH will decrease the adsorption of cationic heavy metals. The pH also highly affects the speciation of heavy metals and introduces competing reactions among ionic species in the solution, which can affect the adsorption process [120, 121]. The presence of competing ions in a solution has been shown to reduce the adsorption capacity of the nanomaterial for certain metal ions. For instance, increasing ionic strengths can reduce the removal efficiency of different metal ions since they compete for the limited adsorption sites on the nanomaterial surface [122].

1.7.3.4. Applications of Nanomaterials and Nanocomposites on Membranes for Water Treatment

The anti-microbial properties and high chemical adsorption capacity of carbon-based nanomaterials make them very attractive for water treatment applications as chemical sorbents and disinfectant agents. The major challenges for their wide application in water treatment processes are their high cost of production; cytotoxicity and lack of dispersion in polar solvents. One way to overcome these issues are their combination with other polymers to form nanocomposites, since polymers can be less costly than nanomaterials [123].

In general, during the synthesis of nanocomposites very small loads of nanomaterial are efficiently dispersed into the polymeric matrix, which reduces the cost of the nanocomposite and reduces the cytotoxicity problems [124]. This new approach of incorporating nanomaterials into polymers has recently led to the development of membranes for water treatment applications [32, 123, 125]. For instance, carbon nanotubes-based nanocomposites have been successfully incorporated into membranes to improve the membrane permeability [32]. These membranes can be broadly divided into two categories: 1) carbon nanotubes are aligned onto a nonporous polymeric support where nanotubes act as pore to pass water through; 2) carbon nanomaterials are blended with the membrane polymer to alter the physicochemical properties of the membrane [32]. The tubular shape of nanotubes allows the water to pass through the inner tubes while the outer surface of the nanotubes removes contaminants via adsorption [96, 126]. The nanotubes can be functionalized or modified depending on the contaminants

intended to be removed. In theses membranes, the pore structures are highly aligned, hence eliminate any concentration polarization due to asymmetry observed in traditional membranes [32, 127]. Most importantly the permeability of this type of membrane is 4-5 times higher than predicted values, which was attributed to the nanoscale channels, hydrophobicity and minimal friction due to the smooth inner channels of the nanotubes [32]. However, despite these attractive features, such membranes are hard to synthesize, so the majority of studies are exploring the possibility of incorporating nanomaterials into the membrane matrix.

Incorporation of the nanomaterials inside the polymer matrix improves mechanical properties and also the hydrophilic and or hydrophobic nature of the membrane [48, 128, 129]. The added advantages for nanomaterial incorporation in the membranes are the increase in mechanical strength and increasing porosity inside the membrane. The embedded nanomaterials are tightly packed inside the polymer matrix and hence have lower risk of detachment. The incorporation of multi-walled nanotubes in polyvinyl alcohol (PVA) was reported to increase the stiffness and permeability of the membrane [130]. Increasing loads of carbon nanotubes (1-4% of functionalized nanotubes) was found to improve the water permeability and rejection of solute [131]. Interfacial polymerization with polyamide and nanotubes was done to effectively produce solvent resistant nanofiltration membranes. In these composites, highly porous structure was reported to enhance the solvent flux by one order of magnitude [132]. Often functionalized nanotubes are used to increase hydrophilic properties of the membrane. The most common functional groups include –COOH, -OH and $–NH_2$. Due to the functionalization of the carbon nanotubes, membrane becomes hydrophilic, rejects more

hydrophobic pollutants and significantly increases permeability flux [133]. Hydrogen bonding between functional groups and water was hypothesized to contribute to the higher hydrophilicity of the functionalized nanotube containing membranes [129]. In another study, nanocomposite membrane was formed by adding amine functionalized multi-walled nanotubes with aqueous solution of 1,3-phenylendiamine.The characterization results suggest that incorporation of NH_2-nanotube created nano-channels on the surface, in addition, -NH2 increased hydrophilicty of the membrane. These improved properties contributed 160% increase in water flux across the membrane [134].

Chapter 2 Synthesis and Characterization of the Impacts of SWNT and the PVK–SWNT Nanocomposite on Pure Bacterial Cultures

"Adapted with permission from (Ahmed, F.; Santos, C. M.; Vergara, R. A. M. V.; Tria, M. C. R.; Advincula, R.; Rodrigues, D. F., Antimicrobial Applications of Electroactive PVK-SWNT Nanocomposites. *Environmental Science & Technology* 2012, 46, (3), 1804-1810). Copyright (2012) American Chemical Society."

2.1. Rationale and Objectives

Materials used in aquatic environments and medical devices have high potential for biofilm formation [135]. Biofilms are complex aggregations of microorganisms surrounded by an extracellular matrix and have been reported to grow on conducting and exposed surfaces of biomedical devices, marine and industrial instruments, and pipes. Biofilm growth has led to several health and economic problems. The problems include antibiotic-resistant infections, increased energy consumption, excessive operational expenditures, and accelerated corrosion problems [136]. To solve these problems, different types of coatings, that can protect the surface from biofilm formation, have been developed, such as polyamide, polypropylene with silver, antibiotics, metal ions, etc [66, 67]. However the syntheses of biofilm resistant surfaces tend to be complex and expensive, and often the surfaces loose effectiveness due to leaching or depletion of the antimicrobial agents [36, 41, 137].

Recently, several studies have shown that single-walled-carbon nanotubes (SWNTs) have antimicrobial properties against diverse groups of microorganisms like bacteria (both Gram-positive and Gram-negative), protozoa, and viruses [45-49]. SWNT-coated surfaces have also been shown to significantly inhibit *E. coli* biofilm formation [41]. However, the use of SWNT as antimicrobial agent is still limited by its poor

dispersibility in most solvents as well as its high cost [29, 36, 138]. Alternatively, SWNT combined (as a filler component) with polymers provide better dispersion and can potentially increase or maintain the same antimicrobial properties of SWNT materials, while providing a broad range of structural, mechanical, and degradation properties [36, 125, 135]. Unfortunately, there have only been a handful of studies about antibacterial effects of polymer-SWNT nanocomposites. None of them have explored the possibility of using these composites as robust coating materials to resist biofilm formation. Electroactive polymers are an excellent choice for such nanocomposites, because of their anti-corrosion properties and facile surface application (via electrodeposition) [139, 140]. Among the available electroactive polymers, polyvinyl-*N*-carbazole (PVK) is an excellent candidate due to its good thermal and mechanical properties, and its ability to form robust thin films (i.e. conducting polymer network (CPN)) on any conducting surface [141, 142]. Furthermore, PVK contains the aromatic N-carbazole group that facilitate π-π stacking as well as donor-acceptor interactions making it a more compatible polymer for carbon-based nanomaterials like SWNT [143, 144].

In this study, we investigated the PVK-SWNT nanocomposite antibacterial properties to planktonic cells (i.e. cells in suspension prior to biofilm formation) and biofilms. The bacterial toxicity of different concentrations of PVK-SWNT dispersed in water were investigated against Gram-positive (*B. subtilis*) and Gram-negative (*E. coli*) bacteria, as well as the potetial inhibition properties of biofilm formation on coated surfaces with the PVK-SWNT nanocomposite.

2.2. Materials and Methods

2.2.1. Single-walled Carbon Nanotubes (SWNT) Preparation

Single-walled carbon nanotubes (SWNTs) were purchased from Cheap Tubes Inc. (Vermont, US). The characterization of these nanomaterials is presented in Table 2.1 and Figure 2.1. The SWNTs were further purified by heating at 200 ^{0}C for 6 hours prior to use.

Table 2.1. SWNT properties supplied by the manufacturer (Cheap Tubes, VT)

Outside Diameter (OD)	1-2 nm
Length	5-30 μm
Purity	>90wt%
Ash	<1.5wt%

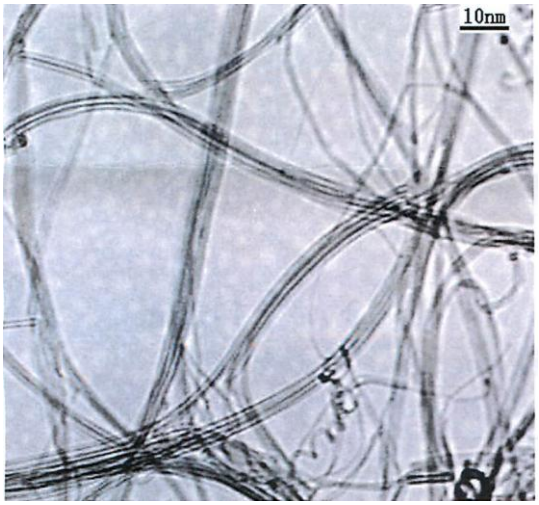

Figure 2.1. Transmission Electron Microscopy (TEM) image of SWNT supplied by the manufacturer (Cheap Tubes, VT).

2.2.2. Preparation of PVK-SWNT Nanocomposite Solutions

The poly (N-vinyl carbazole) (PVK) was purchased from Sigma-Aldrich Chemicals (USA) (ca MW= 25,000-50,000 g/mol). All solvents used for the PVK-SWNT preparation were purchased from Sigma Aldrich (USA) and were of analytical grade. The PVK-SWNT (97:3 wt% ratio PVK: SWNT) was prepared according to previously reported procedure [139]. The PVK:SWNT ratio of 97:3 (wt%) was selected based on the high dispersibility and stability of SWNT for long periods of time (several months) as described elsewhere [139].

Briefly, a 97:3 wt/vol % ratio of PVK:SWNT was prepared in *N*-cyclohexyl-2-pyrrolidone (CHP). The purified SWNT was first dissolved in CHP and sonicated for 4 h. Then, in a separate vial, the PVK was dissolved in CHP and sonicated for 30 min. The PVK solution was then slowly mixed to the SWNT solution and followed by sonication for 1 h. After which, the PVK-SWNT dispersion was centrifuged (4400 rpm, 1 h) and the black precipitate was removed. The remaining solution of PVK-SWNT dispersion was then treated with methanol (5 mL) and again centrifuged (4400 rpm) for 30 min. The black precipitate was collected and redispersed in water followed by 20 minutes of ultrasonication. This procedure furnished a stable and well dispersed PVK-SWNTs solution. For the bacterial measurements, different PVK-SWNT concentrations (1.0 mg/ml, 0.5 mg/ml, 0.05 mg/ml, and 0.01 mg/ml) dispersions in water were used. The SWNT suspension (1 mg/ml) was prepared according to method described elsewhere [145]. Briefly, SWNT was dispersed in DI water and the suspension was bath sonicated for 1 hr immediately before using for the antimicrobial tests.

2.2.3. Preparation of PVK-SWNT Nanocomposite Conducting Polymer Network (CPN) Films

Indium tin oxide (ITO)-coated glass slides (Alfa Aeser, USA) were used as substrates for the PVK-SWNT, PVK, SWNT film fabrication. The ITO-coated glass slides were cleaned by sequentially sonicating the slides in deionized (dI) water, isopropanol, hexane and toluene, each for 15 minutes and the substrates were dried under a stream of N_2. Prior to film deposition, the ITO surfaces were plasma cleaned for 3 min. The electropolymerization solution was prepared by mixing 0.1 M tetrabutylammonium hydroxide (TBAH) (2 mL) in acetonitrile with PVK (50 μL) or PVK-SWNT suspension (50 μL) at 97:3 (wt %) ratio as described above. The PVK-SWNT and PVK films were deposited onto bare ITO surfaces by repeatedly scanning the potential between 0 and 1500 mV at a scan rate of 10 mV/s for 50 cycles. Ag and Pt wires were used as reference and counter electrode, respectively, for the electrodeposition of PVK-SWNT. The deposited film was rinsed three times with acetonitrile to remove any unbound material from the surface.

2.2.4. Characterization of PVK-SWNT Nanocomposite

The PVK-SWNT dispersions were characterized by Fourier transformed infrared spectroscopy (FTIR) and UV-vis absorption measurements. FTIR images were obtained using -FTS 7000 Digilab Spectrometer in the range of 700-3500 cm^{-1}. UV-vis spectra of the PVK-SWNT dispersion and electrodeposited film were recorded using an Agilent 8453 spectrometer.

The electrodeposition of PVK-SWNT conducting polymer network (CPN) films onto ITO were monitored by acquiring the cyclic voltammogram plots (Princeton Applied Research Parsat 2263) at each cycle. The nanocomposite (PVK-SWNT) crosslinked films were characterized using X-ray photoelectron spectroscopy (XPS) and UV-vis measurements. XPS measurements of the samples were performed using a PHI 5700 X-ray photoelectron spectrometer (XPS), which was equipped with a monochromatic Al Kα X-ray source (hν = 1486.7 eV) incident at 90° relative to the axis of a hemispherical energy analyzer. The spectrometer was operated both at high and low resolutions with pass energies of 23.5 and 187.85 eV, respectively, a photoelectron take off angle of 45° from the surface, and an analyzer spot diameter of 1.1 mm. High-resolution spectra were obtained for photoelectrons emitted from C 1s and N 1s. All spectra were collected at room temperature with a base pressure of 1×10^{-8} torr. Electron binding energies were calibrated with respect to the C1s line at 284.8 eV. PHI Multipak software (ver 5.0A) was used for all data processing. The high-resolution data was first analyzed by background subtraction using the Shirley routine and a subsequent nonlinear fitting to mixed Gaussian-Lorentzian functions. Atomic compositions were derived from the high-resolution scans. Peak areas were obtained after subtraction of the integrated baseline and corrected for sensitivity factors.

2.2.5. Bacterial Culture and Antimicrobial Activity determined by Optical Density (OD) Measurements

Single isolated colonies of *E. coli* MG 1655 and *B. subtilis* 102 were inoculated and incubated in 5 ml of Tryptic Soya Broth (TSB) (Oxoid, England) overnight at 35 ^{0}C

and 200 rpm. The bacterial culture was centrifuged at 3000 rpm for 10 minutes. The cells were washed and re-suspended in phosphate buffer solution (PBS, 0.01M, pH=7.4) (Fisher Scientific, USA). The bacterial suspension was adjusted to give an optical density (OD) of 0.5 at 600 nm, which corresponds to a concentration of 10^7 colony forming units (CFU)/ml. For the antimicrobial activity assay, bacterial cultures were exposed for 3 hr to the different nanomaterials.

Briefly, aliquots of 180 µl of bacterial suspensions (10^7 CFU/ml) in PBS and non-inoculated PBS buffer with bacteria (used as blanks) were pipetted in a 96-well flat bottom plate (Costar 3370, Corning, NY) containing triplicates of 20 µl of the following samples suspended in DI water: (1) SWNT at concentration of 1.0 mg/ml; (2) PVK-SWNT nanocomposite at concentrations of 1.0 mg/ml, 0.5 mg/ml, 0.05 mg/ml, and 0.01 mg/ml; and (3) 1 mg/ml of PVK. The control samples contained 20 µl of DI water only with 180µl of bacterial suspensions. To account for the absorbance of SWNT and PVK-SWNT nanomaterials suspended in the bacterial samples, 20 µl of each concentration of SWNT and PVK-SWNT were added to 180 µl of PBS only and later used as blanks to subtract from the original samples. The plates were then incubated at 37°C at 50 rpm for 3 hr. After 3 hr, 20 µl of the bacteria exposed to the different materials, the negative controls, and the blank samples were transferred into 96 well-plates containing 200 µl TSB. The samples were then incubated at 37 °C at 50 rpm and the bacterial growth was monitored using Synergy MX Microtiter plate reader (BioTek, VT) by measuring the OD_{600} every hour until the bacteria reached stationary phase. The results for *E. coli* and *B. subtilis* growth after exposure to the nanomaterials were reported at their mid-log phases, i.e. after 3 h and 5 h, respectively. Final OD values for each bacterial solution

exposed to the different nanomaterial samples were determined by subtracting the OD values acquired from their respective blanks. The results are reported as average OD values with standard deviations of the triplicate samples from all three performed experiments. Statistical analyses (Two-sided t-Test, 95% confidence interval) were performed to determine whether the OD values of the samples with SWNT or PVK-SWNT were significantly different from the control. Same statistical analysis was also performed between OD values from SWNT and PVK-SWNT samples.

2.2.6. Bacterial Viability Assay

Live/Dead assay was performed using the LIVE/DEAD Baclight kit (Invitrogen, USA) to quantify the number of live and dead cells after interaction of the bacterial cells with the most toxic concentrations of nanomaterial samples. The assay consisted of mixing 20 µl of the most toxic concentrations of nanomaterials for each bacteria with 180 µl of bacterial suspensions at 0.5 OD and incubated for one hour at 35 ^{0}C. After 1 hr incubation, 10 µl of the suspension was stained with the LIVE/DEAD BacLight Bacterial Viability kit and observed under Fluorescence Microscope (OLYMPUS, Japan). SYTO 9 dye was used to stain live cells and propidium iodide (PI) was used to stain cells with compromised membranes [146]. Three representative images at 40x were taken for each sample and all samples were tested in duplicate. Total cells and dead cells were counted with Image-Pro Plus software (MediaCybernetics, USA). The percent of inactivated cells was determined from the ratio of the number of cells stained with PI divided by the number of cells stained with SYTO-9. The results were averaged out and the standard deviations were calculated.

2.2.7. Bacterial Re-growth Potential Test (Plate Agar Test)

The plate agar test was performed to determine the re-growth potential of bacteria in contact with nonmaterial samples. The unmodified ITO, electrodeposited PVK-SWNT (97:3 wt %), electrodeposited PVK, and spin coated SWNT-modified films on ITO were individually placed in a 12 well-plate (Falcon, USA). To each well was added 1.0 ml of bacterial culture, which was incubated at 37 °C (without shaking) for 2 h. As a control for potential contamination during manipulation of the ITO substrates, unmodified surfaces incubated in PBS were also used. The film samples were removed and gently rinsed with PBS to wash any unattached bacteria to the surface. The surfaces were then placed onto a Tryptic Soy Agar (TSA) plate with the coated side facing down onto the agar surface and incubated overnight at 35 ^{o}C. The bacterial growth around each plate was measured using a caliper micrometer Mitutoyo 500-196-20 Digital Caliper (MSI Viking Gage, USA). Averages and standard deviations were calculated from 3 replicates.

2.2.8. Inhibition of Biofilm Growth

Inhibitions of biofilm growth were determined on nanocomposite coated ITO surfaces. Unmodified ITO, electrodeposited PVK-SWNT (97:3 wt % PVK: SWNT), electrodeposited PVK, and spin coated SWNT-modified films on ITO were individually placed in a 12-well plate (FalconBD, USA). Each well of the 12-well plate, containing TSB, were inoculated with 300 µl of bacterial cells at OD of 0.5 and incubated at 37 °C for 48 hr. After incubation, the ITO surfaces were taken out and gently rinsed with sterile DI water. Biofilm fixation was done according to cell fixation method previously described.[147] Briefly, the ITO surfaces were incubated with 2% glutaraldehyde and

subsequently dehydrated with increasing concentrations of ethanol (25%, 50%, 75%, 95% and 100%). The surfaces were vacuum dried overnight prior to AFM measurements. AFM topography measurements were done on the ITO substrates under ambient conditions with a PicoSPM II (PicoPlus, Molecular Imaging-Agilent Technologies) in the intermittent contact mode. Images obtained were processed using Gwyddion software (2.13).

2.3. Results and Discussion

2.3.1. PVK-SWNT Characterization

The dispersion of PVK-SWNT (97-3 wt %) nanocomposites were characterized using FT-IR and UV-vis. FT-IR measurements confirmed the functional groups present on the nanocomposite (Figure 2.2, a). As controls, IR measurements of PVK and SWNT were also acquired. As expected, no distinctive IR peaks were observed for the pure SWNT. However, the PVK-SWNT nanocomposite showed similar peaks to pure PVK. In particular, the peak at 1255 cm^{-1}, due to the C-N stretching of vinyl carbazole, was observed in both PVK and PVK-SWNT nanocomposite. UV-vis spectra of the PVK-SWNT dispersion were acquired to measure interfacial interaction of SWNT and PVK. Results are shown in Figure 2.2 (b). Based on the results, no absorption peaks at the visible region were observed for pure SWNT. The pure PVK however showed two distinct peaks at 330 and 343 nm, which can be attributed to the transitions of the pendant carbazole moieties of PVK [17]. Similar absorption peaks were observed for the PVK-SWNT nanocomposite with a slight decrease in intensity and red-shifted by ~10 nm due to the incorporation of SWNT.

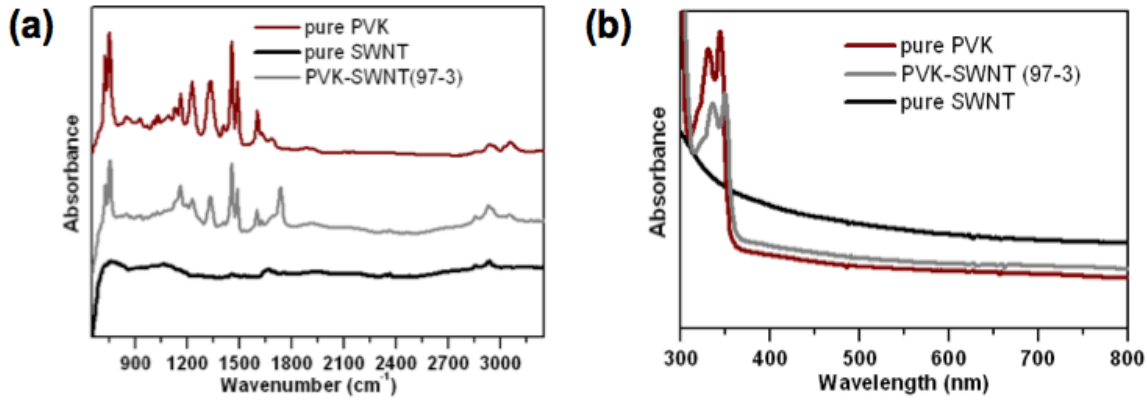

Figure 2.2. Spectroscopic characterization of the PVK-SWNT (97-3 wt %) dispersion. (a) IR and (b) UV-Vis spectra of the pure PVK, pure SWNT, and PVK-SWNT (97-3 wt %) nanocomposite.

Electrodeposited PVK-SWNT coated surfaces were characterized using XPS to determine elemental composition on the surface. Figure 2.3 (a and b) shows the narrow scans in the N1s and C1s of the electrodeposited PVK-SWNT and PVK surfaces. To estimate the amount of SWNT after electrocrosslinking, N/C ratios of PVK-SWNT and PVK were acquired. For PVK-SWNT, a calculated N/C ratio value of 9.4 was obtained while for PVK, the N/C ratio was calculated as 9.7. Using the obtained N/C ratios, the amount of PVK and SWNT on the film was 97 % and 3 %, respectively.

UV-Vis spectra after electrodeposition of the PVK-SWNT, Figure 2.3 (c), showed the disappearance of the well-defined peaks at 342 nm and 352 nm that were initially found for the PVK-SWNT dispersion (Figure 2.2. b). A new broad band centered at 450 nm was depicted after the electrodeposition process, attributed to the electrochemical crosslinking of the carbazole pendants in PVK [148, 149]. These results correlates well

with our previous studies on electropolymerized PVK and carbazole-containing precursors [17, 149].

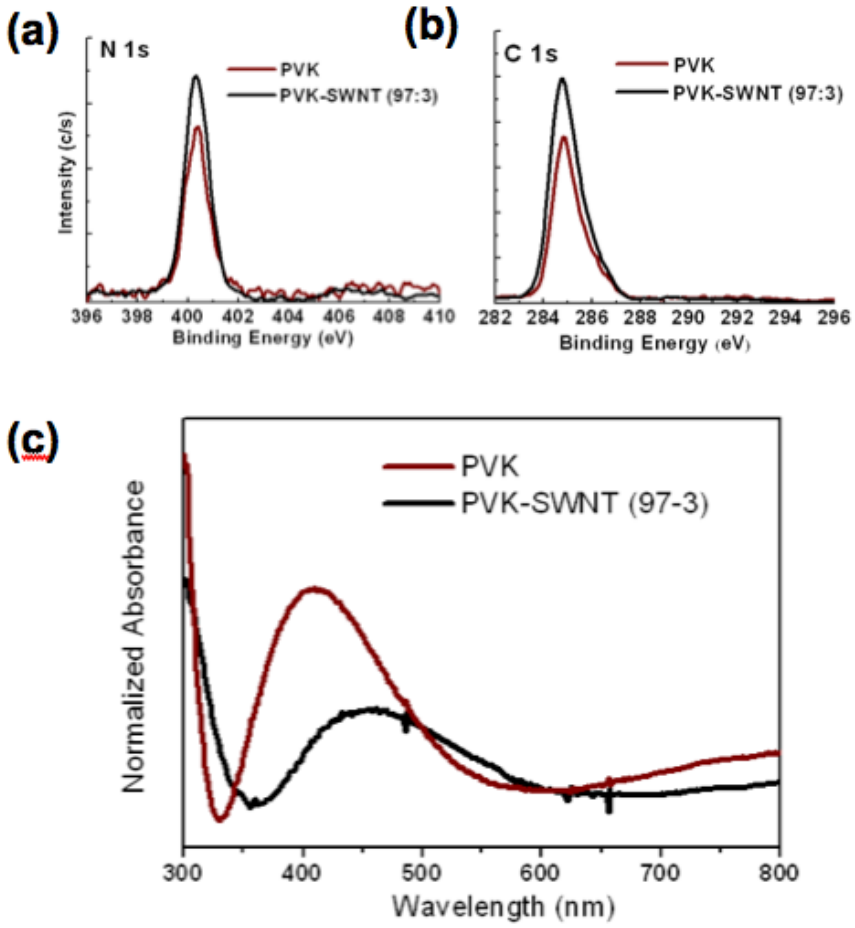

Figure 2.3. Spectroscopic characterization of the electrodeposited PVK-SWNT (97-3 wt %) film. XPS spectra on the (a) N 1s (b) C 1s regions of the electrodeposited PVK and PVK-SWNT on ITO. (c) UV-Vis spectra of the electrodeposited PVK and PVK-SWNT on ITO.

2.3.2. Antibacterial Effects of Nanocomposites on Planktonic Cells

The toxic effects of PVK-SWNT, PVK, and SWNT solutions to *E. coli* and *B. subtilis* were evaluated by OD_{600} measurements of the total bacterial growth. From Figure 2.4, it is observed that for both *E. coli* and *B. subtilis* most growth inhibition happened at SWNT (1 mg/ml) and PVK-SWNT (1 mg/ml) concentrations. For *E. coli*, growth inhibition was ~60% and ~64% for SWNT (1mg/ml) and PVK-SWNT (1 mg/ml), respectively. Similarly for *B. subtilis*, growth inhibition was ~57% and ~63% for SWNT (1 mg/ml) and PVK-SWNT (1 mg/ml), respectively. Figure 2.4 also demonstrated that the effects of SWNT and PVK-SWNT to *E. coli* and *B. subtilis* were not the same; however these findings were similar to other studies [4, 36, 44]. The different levels of tolerance of different microorganims to carbon-based nanomaterials are still a matter of continuing research. Several hypotheses for the different toxicity levels consider differences in cell wall structure, the protective effect of the outer membrane surface properties, ability to form spores and/or unique repair mechanisms of different microorganisms [43]. It is noticeable that PVK itself did not exhibit any antibacterial effects on either *E. coli* or *B. subtilis* (Figure 2.4). Furthermore, the results show that after 3 hr of exposure to SWNT and PVK-SWNT nanocomposite fewer bacteria were viable. This was demonstrated by the much longer time for the remaining microbial population to reach mid-log phase than the control samples [3, 150].

These comparable toxicity of PVK-SWNT nanocomposites with low SWNT content than pure 100% SWNT (1 mg/ml) can be explained by a better dispersion of the SWNTs in aqueous solution in the presence of PVK as previously demonstrated [151].

This better dispersion of the SWNTs particles in aqueous media is because of the effective pi-pi stacking and donor-acceptor interactions between the carbazole group and the SWNT. In the case of SWNT toxicity towards bacteria, dispersion is an important parameter and highly dispersed SWNT causes greater cell contact and can potentially increase cell damage [46, 138].

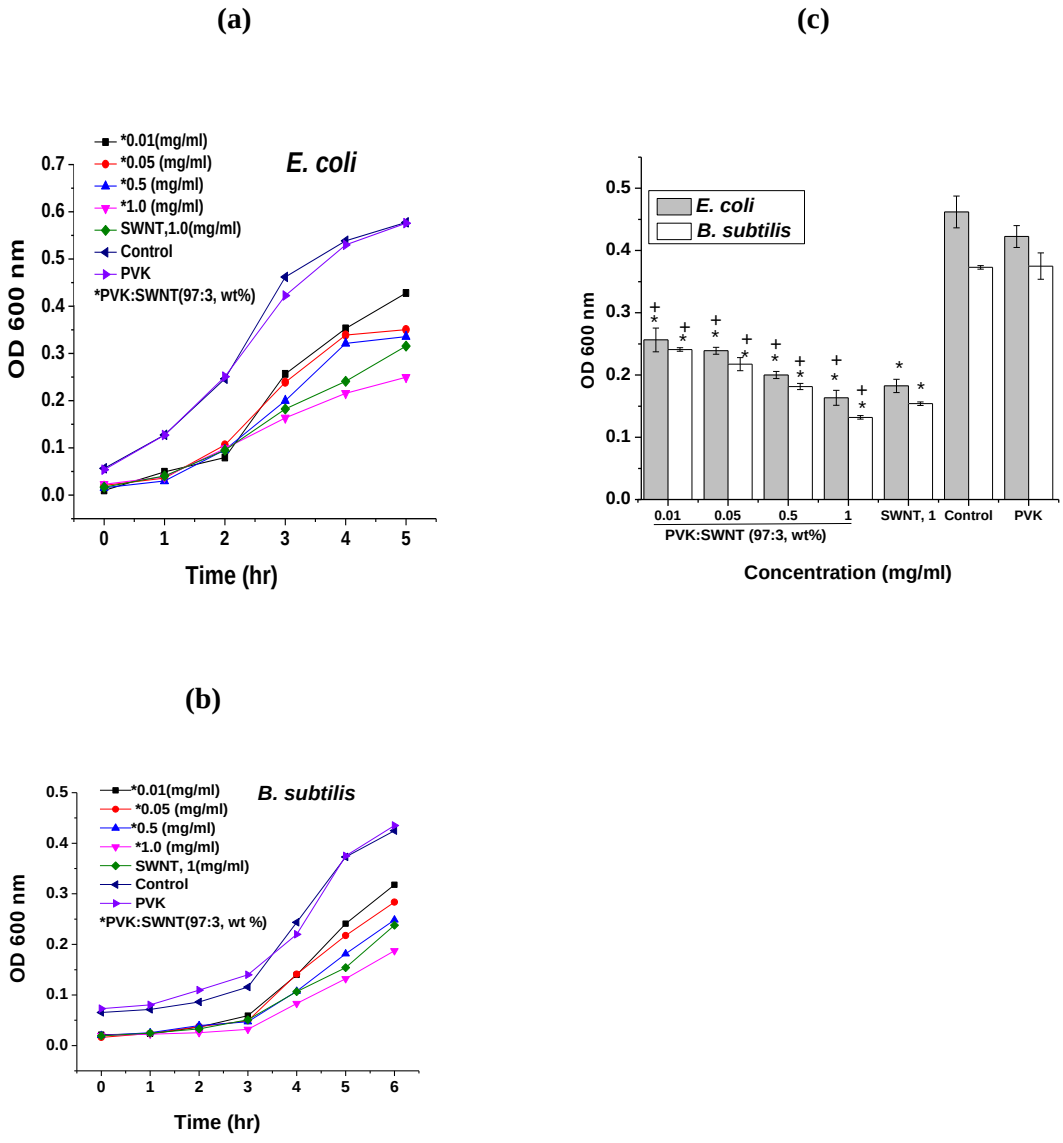

Figure 2.4. Growth curves of (a) *E. coli* and (b) *B. subtilis.* (c) OD measurements of the bacterial growth at mid-log phase. The symbols * + correspond to statistically different results between the control and the different SWNT samples, respectively.

2.3.3. Viability Assay

The Live/Dead assay was performed to determine the viability of the bacterial after interaction with nanomaterials (Figure 2.5). Fluorescence microscopy was used to assess the loss of bacterial viability after incubation. Figure 2.5 shows representative fluorescence images for the bacterial solutions incubated with the nanocomposite PVK-SWNT and the control. Results show that in the absence of the nanomaterials, all cells were alive (Figure 2.5.a). While, cellular damage was observed in ~94 % and ~98 % of the *E. coli* cells exposed to PVK-SWNT and SWNT, respectively. For *B. subtilis*, ~90 % and ~87 % of the cells were damaged after exposure to PVK-SWNT and SWNT, respectively. The two most hypothesized mechanism of SWNT toxicity to bacteria are physical disruption of bacterial membrane and oxidative stress [2, 36, 41, 152, 153]. From this study, we can say that the addition of PVK did not prevent one of these two mechanisms to happen since most of the cells exposed of PVK-SWNT were red–stained cells, which indicated that the PI dye could penetrate inside the damaged cells.

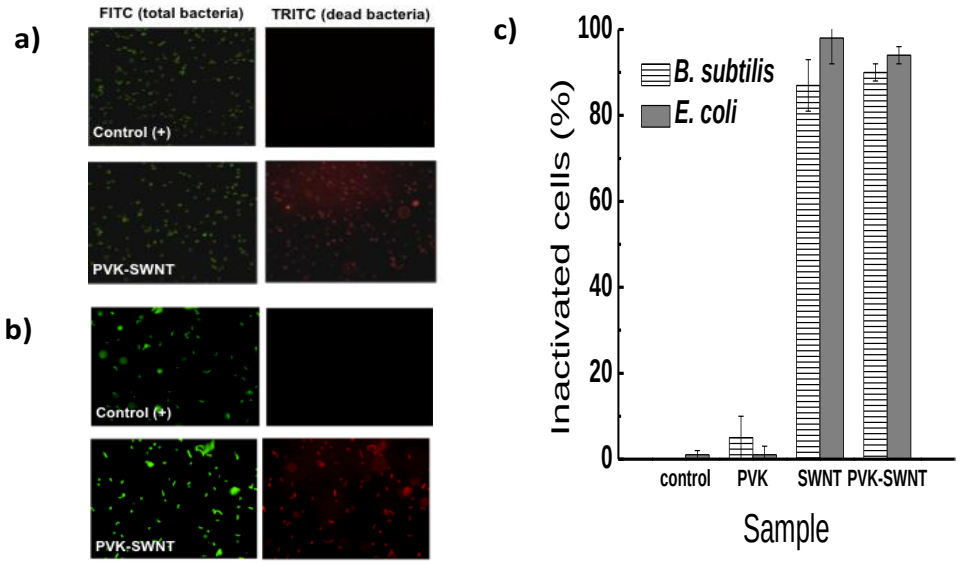

Figure 2.5. Viability assay for the bacteria exposed to nanocomposite: (a) *E. coli* (b) *B. subtilis.* (c) Correlation of the % of non-viable *E. coli* and *B. subtilis* (inactivated cells %) after exposure to PVK-SWNT, SWNT (1 mg/ml), and PVK.

2.3.4. Bacterial Re-growth Potential Test

To demonstrate the efficiency of PVK-SWNT and SWNT as potential coating materials to prevent bacterial deposition and biofilm formation, the agar printing assay was performed with *E. coli* and *B. subtilis*. For this measurement, electrodeposited PVK-SWNT and spin-coated SWNT onto ITO surfaces were used. The nanocomposite-modified film contained 3 % SWNT and 97 % PVK. The results of PVK-SWNT were compared against electro-crosslinked PVK, spin-coated SWNT on ITO surfaces, and unmodified ITO surfaces as a control. The results showed that the percent bacterial inactivation on the coated PVK-SWNT surfaces compared to the unmodified ITO

surfaces were 67% and 80 % for *B. subtilis* and *E. coli*, respectively (Figure 2.6). The PVK-coated surfaces did not show any antimicrobial property for neither *E. coli* nor *B. subtilis*, which suggests that the toxicity observed with the PVK-SWNT nanocomposite was due to the presence of SWNT only. Furthermore, these results show that antimicrobial activity for PVK-SWNT nanocomposite solutions were maintained even after electrodeposition.

Even though antibacterial properties of SWNT-coated surfaces were described in other studies, these studies used either pure SWNT or other nanocomposite materials than PVK for short incubation time [2, 41, 153]. However, this study is the first one to demonstrate that very low concentrations of SWNTs can be embedded in nanocomposites without losing its antimicrobial properties after prolonged exposure to bacteria (i. e. 48 h). In this study we embedded only 3% of SWNT in PVK-SWNT, which achieved almost similar inhibitory effects as 100 % SWNT (Figure 2.6). Furthermore, this study shows that the use of PVK improves dispersibility of SWNT in aqueous solution, achieving a more homogenous deposition of SWNTs onto surfaces [139] and at the same time maintaining the antimicrobial property of SWNT.

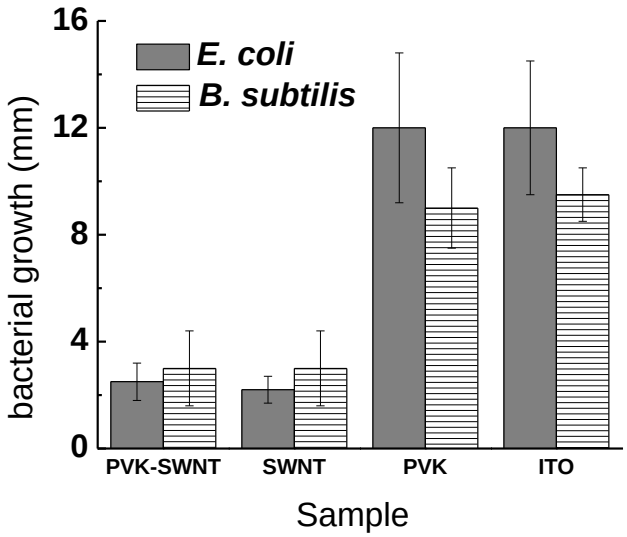

Figure 2.6. Agar printing assay to determine the survival of bacteria deposited onto ITO surfaces containing electrodeposited PVK-SWNT (97:3 wt% PVK:SWNT), spin coated SWNT (1 mg/ml), and electrodeposited PVK. Bare ITO surfaces were used as control.

To investigate the long-term bacterial toxicity of the electropolymerized PVK-SWNT films, biofilms were allowed to grow for 48 h on modified ITO surfaces. The biofilm growth and area covered by microbial growth on the surface were determined by AFM. As control, AFM images of the electropolymerized PVK, spin-coated SWNT, and the unmodified ITO substrate were also taken. The results show that biofilms were able to grow on unmodified ITO and PVK films after prolonged exposure to *E. coli* and *B. subtilis* (Figure 2.7) However, on electrodeposited PVK-SWNT and SWNT films, just a few cells, but not a biofilm, were observed on the surface after 48 h exposure. These observations demonstrate that the nanocomposite-modified surface can effectively prevent biofilm growth the same way as pure SWNT films [41]. These results are in agreement with previous studies where small amounts of incorporated SWNT into polylactic-co-glycolic acid (PLGA) or polysulfonate (PSF) exhibited almost equivalent

toxicity of 100 wt% SWNT coated surfaces [41, 153]. The mechanism of SWNT nanocomposites on bacterial colonization inhibition have been suggested as the direct contact of bacteria with SWNT ends and bundles that extend from the nanocomposite [153]. It is possible that our system (PVK-SWNT films) follows similar toxicity mechanism. It is worth mentioning that the PVK-SWNT nanocomposite can be electrodeposited onto any conducting surface, which in terms of cost and ease of application is significantly better than 100% SWNT coatings.

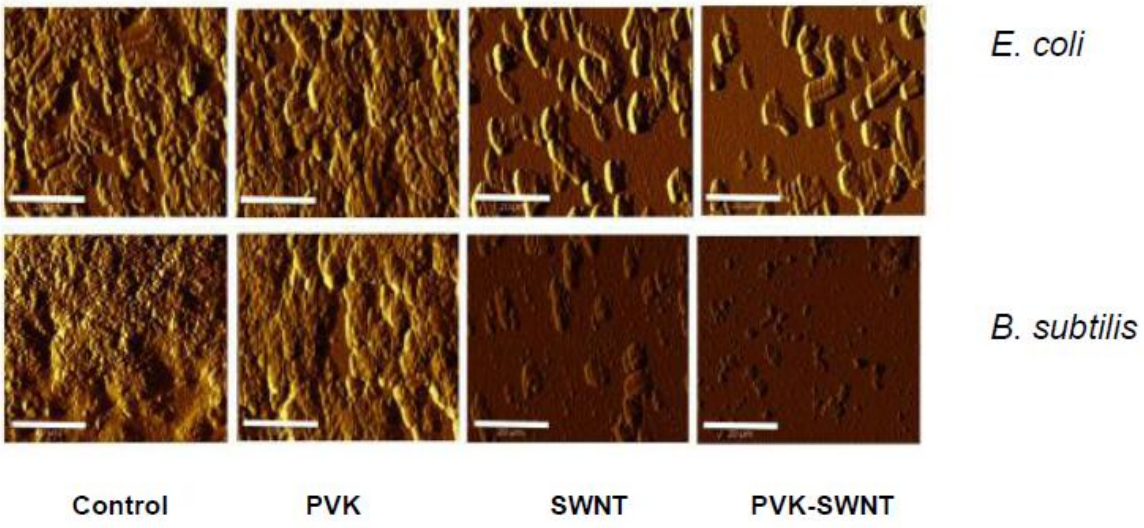

Figure 2.7. AFM images of biofilm formation on Control, PVK, SWNT and PVK-SWNT coated ITO surfaces (Scale: 20 µm).

2.4. Conclusion

Overall, this study shows that SWNT can be embedded into the electroactive polymer PVK to form stable PVK-SWNT nanocomposite dispersions and films. This mixture increased the dispersion and effective bacterial toxicity of SWNT into aqueous media and led to a homogeneous coating of PVK-SWNT on ITO surfaces via

electrodeposition. In both suspension and coated form, PVK-SWNT exhibited stronger antibacterial effects to *E. coli* and *B. subtilis* when compared to SWNT and PVK alone. PVK-SWNT, with only 3% SWNT (0.03 mg/ml of SWNT), exhibited similar or stronger antibacterial effects than 100% SWNT (1 mg/ml of SWNT). Our study demonstrated for the first time that by improving dispersibility of SWNT in solution, higher bacterial toxicity of SWNT can be achieved. These results also demonstrated that it is possible to obtain more economical SWNT antimicrobial coated surfaces by significantly reducing the need of higher loads of SWNT when embedding the SWNTs in the polymer PVK.

Chapter 3 Synthesis and Characterization of the Impacts of GO and the PVK –GO Nanocomposite on Pure Bacterial Cultures.

"Adapted with permission from (Santos, C. M.; Tria, M. C. R.; Vergara, R. A. M. V.; Ahmed, F.; Advincula, R. C.; Rodrigues, D. F., Antimicrobial graphene polymer (PVK-GO) nanocomposite films. *Chemical Communications* 2011**,** 47, (31), 8892-8894). Copyright (2011) American Chemical Society."

3.1. Rationale and Objectives

Biofilm formation on conducting materials (metal, metal alloys, metal oxides, and electrodes) has emerged as a significant problem in the long-term use of bioimplants, biosensors, and marine and industrial instrumentations [135, 154]. Strategies for controlling bacterial colonization have focused on improving and developing antimicrobial materials and designs to inhibit biofilm formation. Examples of antimicrobial agents previously used as surface coatings and showing reduced bacterial adhesion are mostly antibiotics and metal ions [66, 67]. However, problems related to the development of microbial resistance surface coating difficulties, and relatively high costs make these approaches unsuitable for long-term antimicrobial coatings [155].

The incorporation of graphene on surfaces is an alternative method to prevent bacterial colonization. This extremely thin nanomaterial has been reported to show promising antibacterial activity [52, 57]. Furthermore, compared to other antibacterial surfaces, it is relatively inexpensive and possesses very high mechanical stiffness and extraordinary electronic transport property [1]. Despite many advantages that it has to offer, the investigation of graphene as an antimicrobial coating film has not been well established. To our knowledge, most of the antibacterial investigations were conducted either in solution or as free-standing graphene sheets [52, 57]. In this present study, we investigate the antimicrobial properties of graphene nanocomposite coated surfaces. At

present, the major challenges of working with pristine graphene are its non-dispersibility in either aqueous or organic solvents, direct immobilization on surfaces and processability, which leads to the difficulty of working with pristine graphene alone. To address these issues, our group has developed a method of fabricating a more stable and easily dispersible graphene in a polymer matrix composed of graphene oxide (GO) and poly-*N*-vinyl carbazole (PVK). GO unlike its pristine counterpart contains unoxidized aromatic and aliphatic regions with phenolic, carboxyl, and epoxide groups that allows it to be easily dispersed in various solvents. PVK on the other hand forms a pi-pi stacking interaction with GO through the carbazole group that stabilizes the dispersion of the nanocomposite (NC) and creates a conducting polymer network (CPN) that can be immobilized and patterned on any conducting substrate via electrochemical methods [17, 149, 156]. In this work, we present the first report on the immobilization of graphene on conducting surface as an antimicrobial coating. Specifically, we deposited GO-PVK nanocomposite via electrodeposition on indium tin oxide (ITO). The antibacterial property of the electrodeposited GO-PVK films was then tested against *Escherichia coli* K12 MG1655 (*E. coli*).

3.2. Materials and Methods

3.2.1. Preparation of PVK-GO Nanocomposite film

The PVK-GO (97-3 wt%) nanocomposite was synthesized as the PVK-SWNT nanocomposite in previous chapter and was applied on bare ITO surface via electrodeposition. Briefly, the polymerizing solution was prepared by mixing 0.1 M TBAH (2 ml) in acetonitrile with PVK-GO (50 µl) at 97:3 (wt%) ratio. The PVK-GO

film was deposited on bare ITO by repeatedly scanning the potential between 0 to 1500 mv at a scan rate of 10 mv/s for 50 cycles. Ag and Pt wires were used as the reference and counter electrode, respectively. The deposited film was washed with acetonitrile (3X) to remove any unbound material from surface.

3.2.2. Characterization of nanocomposite coating

The morphology before and after electropolymerization of PVK/GO on ITO glass substrates were characterized by AFM. Atomic force microscopy (AFM) imaging was done under ambient conditions with a PicoSPM II (PicoPlus, Molecular Imaging - Agilent Technologies) in the Magnetic AC mode (MAC mode) using a magnetic field to drive a magnetically coated cantilever in the top-down configuration. Type II MAC levers with a spring constant of 2.8 nN/M with about 10 nm tip radius were used for all scans.

ITO surfaces coated with PVK and PVK-GO were characterized with Attenuated Total Reflectance Fourie Transformed Infrared (ATR FTIR). The ATR FTIR spectra were obtained on a Digilab FTS 7000 equipped with HgCdTe detector form 4000 to 600 (cm-1) wavenumbers. All spectra were taken with a nominal spectral resolution of 4 cm-1 in absorbance mode. All films were measured under ambient and dry conditions for several trials at different areas of the sample surfaces.

3.2.3. Measurement of Antimicrobial Effects of Nanocomposite Suspension

A single isolated *Escherichia coli* K12 MG1655 colony was inoculated in 5 ml Tryptic Soy Broth (TSB) overnight at 35 C. The bacterial culture was centrifuged at 10000 rpm and for 10 min and the bacterial pellets were resuspended in phosphate buffer

solution (PBS). The initial optical density of the suspension was adjusted to 0.5 at 600 nm, which corresoponds to a bacterial cell concentration of 10^7 colony forming units (CFU)/ml. Aliquots of 180 µl of bacterial suspension were placed in an eppendorf tube containing 20 µl of sample (GO, PVK-GO, PVK) at 1 mg/ml concentration in DI water. Control sample contained 20 µl of DI water instead of samples. The tubes were shaken at 50 rpm for 1 h at room temperature. The antimicrobial properties of GO, PVK-GO and PVK samples were evaluated by examining the bacterial growth curve via $O.D._{600}$ after 1h exposure to these materials. Briefly, the mixture of bacteria and samples were transferred in 5 ml TSB broth and incubated at 37 °C. Bacterial growth was monitored by measuring the $O.D._{600}$ every hour using spectrophotometer (Perkin Elmer). The OD curves were generated by plotting the OD values versus growth time. The fast or slow increase in OD during the incubation represents the ability of *E. coli* bacteria to survive and grow in presence of nonmaterial samples.

3.2.4. Measurements of Antimicrobial Effects of Nanocomposite Coated Surface

ITO substrates, individually coated with PVK, PVK-GO and GO were placed in different wells of a 12 well-plate (Falcon). To each well was added 1 ml of bacterial culture and then incubated at 37 C for 2 h. The samples were then removed carefully from solution and immediately stained with Live-Dead assay kit. The SYTO9 dye stains the total cell while the PI stains cell with compromised cell membranes. The samples were placed in microscope slide coved with cover slide and visualized with flurescence microscope (OLYMPUS). All acquired images were analyzed with CellSense Dimension

software. Percent dead cell was calculated as the ratio of total dead cells (PI stained) divided by the total cells (SYTO 9 stained).

3.3. Results and Discussions

3.3.1. Characterization

The preparation of the PVK-GO nanocomposite film was carried out by electrodeposition on the ITO surface. Figure 3.1 (a) shows the CV plot monitoring the immobilization of PVK-GO on the surface. The first oxidation peak was observed at 1.4 V, which was moved towards lower oxidation potential as the cycle increased. This lowering of potential is expected due to the formation of more pi-conjugated species upon the crosslinking of the carbazole pendant moieties of the vinyl backbone. The irreversible oxidation process could possibly be due to the reduced electron transfer kinetics caused by the presence of the graphene oxide. The homogeneity of the deposited film was determined via AFM (Figure 3.1, b). The electrodeposited PVK-GO surfaces revealed excellent well-defined film coverage with a root mean squared (rms) roughness value of 2.38 nm. The average grain size was about 160 nm typical of the grain size observed for the presence of PVK on the surface.

The ATR IR spectra for the PVK and GO-PVK-modified surfaces are depicted in Figure 3.1 (c). For the electropolymerized PVK, assignment of the main absorption peaks are as follows: 3100 cm^{-1} (aromatic C-H stretch), 2900- 3000 cm^{-1} (aliphatic C-H stretch from the polymer backbone), 1600 cm^{-1} (C=C stretching), 1226 cm^{-1} (C-N stretching of vinyl carbazole), 1100-1150 cm^{-1} (in plane –C-H aromatic), and 700-800 cm^{-1} (out of plane –C-H aromatic). While all these peaks were observed on the PVK-GO film, the

presence of GO on the surface was verified by the appearance of an intense peak at 1700 cm^{-1} assigned for the C=O stretch; and OH stretch the broad peak that extends from 3000-3500 cm^{-1} attributed to the OH functional groups from the carboxylic acid alcohol groups present in the GO [21, 157].

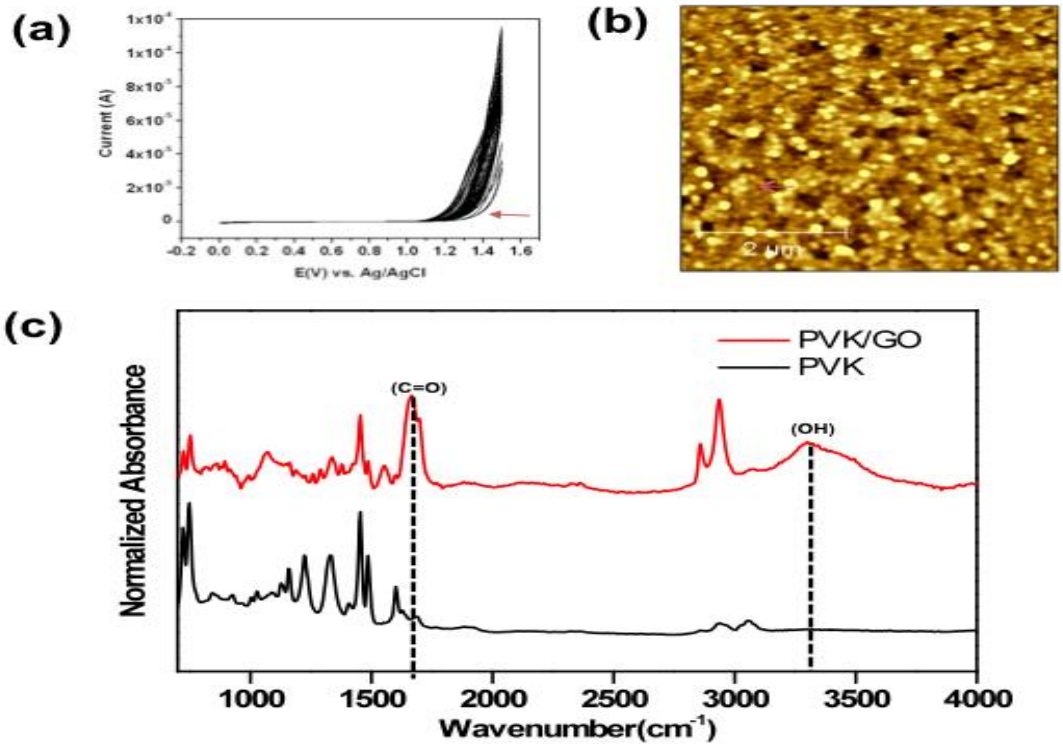

Figure 3.1. (a) Cyclic Voltamemmograms (CV) of the electropolymerized PVK-GO on ITO (b) AFM topography images of PVK-GO nanocomposites on ITO surface (c) ATR-FTIR spectra of the PVK and PVK-GO modified films.

3.3.2. Antimicrobial Effects of Nanocomposite Solution

The antibacterial property of the nanocomposite, GO-PVK, GO, and PVK were evaluated by incubating each of the solution with *E. coli* cells for 1h. The growth curves of bacterial-treated with GO-PVK nanocomposite, GO and PVK samples were examined

via optical density (OD) measurements, which corresponds to the number of live cells that are able to grow after 1h of exposure to the samples. In general, compared to the control, the samples containing GO were observed to be antibacterial. This activity was shown by the low OD values observed for all measured samples (Figure 3.2 a). To evaluate the antimicrobial effectiveness of the different nanomaterials, we measured for each of the growth curves the time required to reach 10^7 CFU/mL, which corresponds to an OD_{600} of 0.5.

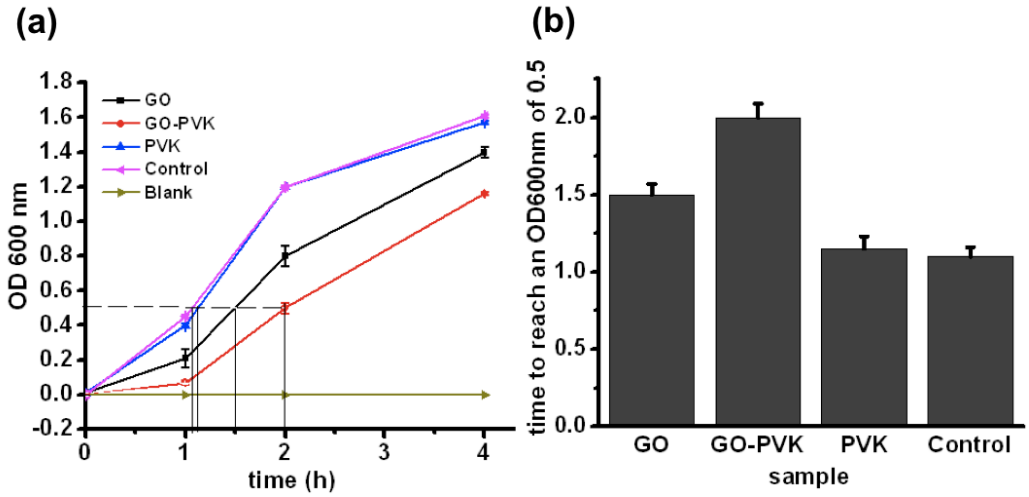

Figure 3.2. (a) Growth curves of *E. coli* exposed to GO, PVK and PVK-GO (b) The time required by the bacteria to reach an OD_{600} of 0.5 treated with samples.

Based on the results, all the GO-containing samples took longer time to reach OD of 0.5 as compared to the untreated samples (control) and the PVK samples (Figure 3.2.b). GO is already known to be toxic to bacteria; however, the addition of PVK resulted in an increased dispersion of GO in the solution, thereby resulting in an increased interaction with the bacteria and higher toxicity [158].

3.3.3 Antimicrobial Effects of Nanocomposite Coating

After testing the antibacterial properties of the composites in solution, we tested the effects of modified films of PVK, PVK-GO, and GO on *E. coli*. *In situ* live-dead staining of the bacterial organisms attached to the differently modified surfaces were performed to determine the ratio of dead bacteria versus the total number of bacteria. SYTO 9 dye was used to show both live and dead cells, while the dead bacteria with compromised membranes were stained only by propidium iodide (PI). Fluorescence images of the surface reveal that after incubation a more pronounced antibacterial activity was observed for the GO-modified surfaces than the unmodified and PVK films (Figure 3.3, a-d). In fact, the PVK-GO and GO-modified surfaces were successful in inactivating *E. coli* by approximately 90% and 84 %, respectively. This result showed that GO remained effective even after surface immobilization. It is worth noting that the addition of PVK did not hinder its efficacy but showed an enhanced bacterial toxicity than the GO alone. We infer that the improved dispersion caused by the presence of PVK led to the results observed. Although the mechanism of antibacterial toxicity is beyond the scope of this study, it is possible that GO has similar antimicrobial mechanisms as other carbon based nanomaterials such as carbon nanotubes, i.e. the direct contact of GO with bacteria can lead to cell inactivation [2].

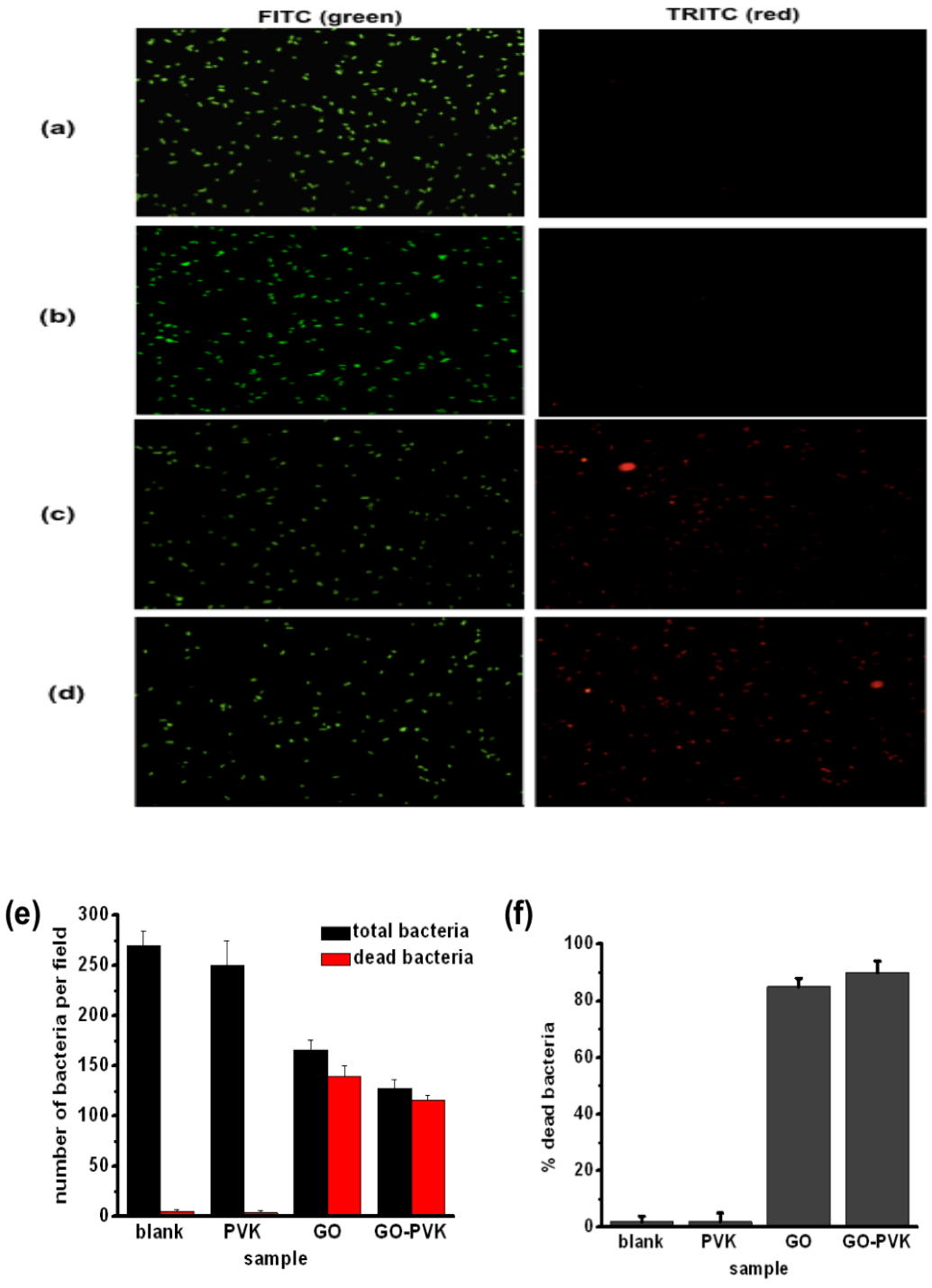

Figure 3.3. (a-d): Fluorescence images of the *E. coli* on (a) unmodified ITO, (b) electrodeposited PVK, (c) spin-coated GO, and (d) electrodeposited PVK-GO films. (e) Total number of bacteria (green) and dead bacteria (red) (f) Percentage of dead bacteria.

3.4. Conclusions

The antibacterial property of a PVK-GO nanocomposite and electropolymerized nanocomposite on ITO surface was studied. This robust antimicrobial coating can be applied on electrically conducting substrates. The inclusion of PVK allowed the immobilization of a well-defined and homogeneous film via electro-polymerization on the ITO surface. Antibacterial properties of the GO-containing films and solutions resulted in increased bacterial inactivation, relative to the control. Even with the presence of PVK, the nanocomposite maintained its bacterial toxicity. This result shows the potential of using the PVK-GO nanocomposite as an alternative antimicrobial coating for electrode surfaces that can be widely used in biomedical and industrial fields.

Chapter 4 Applications of PVK-SWNT Nanocomposites Coated Membranes for Water Treatment.

"Adapted with permission from (Ahmed, F.; Santos, C. M.; Mangadlao, J.; Advincula, R.; Rodrigues, D. F., Antimicrobial PVK:SWNT nanocomposite coated membrane for water purification: Performance and toxicity testing. *Water Research* **2013,** 47, (12), 3966-3975). Copyright (2013) Elsevier."

4.1. Rationale and Objectives

Membrane separation systems are used for drinking water treatment because of their potential to remove microorganisms [159]. The major issue of membrane operations is that they are often affected by biofouling phenomena (*e.g.*, bacterial adhesion) on the membrane surface [160]. Membrane biofouling is initiated by bacterial adhesion and growth on the membrane surface, which can eventually form a biofilm [159]. Hence, developing membranes with anti-bacterial property is certainly an attractive solution. The most common approach for developing anti-microbial membranes is the modification of commercial membrane surfaces with polymeric materials containing silver nanoparticles [155, 161]. Similarly, carbon based nanomaterials, like single-walled carbon nanotubes (SWNTs), have been reported to significantly reduce the bacterial and viral load in water due to its anti-microbial properties [2, 43, 96, 152].

Apart from anti-microbial properties, incorporation of SWNT into membranes has also been reported to improve membrane strength, thermal stability, and water flux [162]. The use of SWNTs to coat membranes is, however, still limited by high cost and poor dispersibility in aqueous solutions [123, 155, 163]. Though polymer nanocomposites have been used for surface modification of membranes, SWNT incorporated in the polyvinyl-*N*-carbazole (PVK) polymer has not yet been investigated for its application in water treatment. In our recent study with PVK-SWNT nanocomposite in suspension and

immobilized on solid surfaces, we demonstrated significant antimicrobial effects against both Gram-positive and Gram-negative bacteria [164]. PVK was selected as a base polymer because of its multiple aromatic groups that facilitate pi-pi interaction with carbon-based nanomaterials, making it a more compatible polymer with SWNT. Besides, PVK possesses excellent thermal, mechanical, and biocompatible properties and is easy and economical to prepare [165, 166]. Furthermore, the ratio of SWNT in the PVK-SWNT (97:3 wt% ratio PVK: SWNT) nanocomposite reduces the use of costly SWNT in the membrane preparation while showing excellent dispersion of SWNT in aqueous solution in the presence of PVK [167].

In this study, we investigated the antimicrobial properties of nitrocellulose membrane filters coated with PVK-SWNT (97:3 wt% ratios, PVK: SWNT). Highly purified and well characterized SWNT was used to synthesize the PVK-SWNT nanocomposite. Membrane surfaces were dip coated in PVK-SWNT suspension to create a film of PVK with a 3 wt% SWNT load. Antibacterial and virus removal properties of the membranes coated with PVK-SWNT was investigated with Gram-positive (*Bacillus subtilis*), Gram-negative (*Escherichia coli*) bacteria and the model virus MS2. Human cytotoxicity of PVK-SWNT nanocomposite was investigated with human fibroblast cells to assess suitability of this nanocomposite for drinking water treatment.

4.2. Materials and Methods

4.2.1. Coating of the filter membranes

PVK-SWNT nanocomposite was prepared following the procedure described in Chapter 2. Nitrocellulose membrane filters (0.45 µm, Milipore USA) were dip-coated with PVK (1mg/ml), SWNT (1mg/ml) and PVK-SWNT (1 mg/ml) suspensions in DI

water. After coating process, the filter membranes were carefully removed and dried overnight in a vacuum oven. Bare nitocellulose membranes were used as controls. Characterization of PVK, SWNT, and PVK-SWNT suspensions and coated membrane filters were conducted according to procedure described in Chapter 2 [164, 167].

4.2.2. Bacterial Culture

Freshly prepared suspensions of *Escherichia coli* MG 1655 and *Bacillus subtilis*-102 were used for all experiments in this study. In order to prepare fresh suspensions, single isolated colonies of *E. coli* and *B. subtilis* were inoculated in 5 ml of Tryptic Soya Broth (TSB) (Oxoid, England) and incubated overnight at 35 ^{0}C and 200 rpm (INNOVA 44, New Brunswick Scientific Co, USA). The bacterial culture was centrifuged at 10,000 rpm for 10 minutes. To remove any residual growth medium, cells were washed twice and re-suspended in phosphate buffer solution (PBS, 0.01M, pH=7.4) (Fisher Scientific, USA). The bacterial suspension was adjusted to give an optical density (OD) of 0.5 at 600 nm, which corresponds to a cell concentration of ~10^{7} CFU/ml.

4.2.3. Bacterial Cell Filtration

All the filtration apparatus were sterilized prior to use. The prepared membrane filters were washed for 15 min with ethanol (70%) and air dried for 24 h in a biological safety cabinet (LABGARD, NuAire Inc, USA) under laminar flow to evaporate any residual ethanol. All the filtration assays were conducted under a constant permeation rate (~57 L m^{-2} h^{-1}) using a peristaltic pump (Cole-Parmer, USA). The filtration experiment set up consisted of all glass filtration apparatus with 47 mm stainless steel

screen (Milipore, USA). The mode of filtration was dead-end, unless indicated otherwise. Prior to each filtration experiment, the filter surfaces were preconditioned by passing 10 ml of sterile PBS. For each membrane filter type (i.e., coated with SWNT, PVK-SWNT and non-coated), 2 ml of bacterial suspension in PBS at OD= 0.5 was passed through the membrane filter. Each membrane filter was tested at least in duplicate.

4.2.4. Bacterial Viability Assay

This test was performed to determine the percentage of inactivated bacterial cells retained on the surface of the membranes. The bacterial viability assay was performed using the LIVE/DEAD Baclight kit (Invitrogen, USA) to quantify the number of live and dead cells on the filter surfaces [2]. Immediately after the filtrations, the filter surfaces were stained with the LIVE/DEAD BacLight Bacterial Viability kit and were observed with a fluorescence microscope (OLYMPUS, Japan). SYTO 9 dye was used to stain the total number of cells, while propidium iodide (PI) was used to stain cells with compromised membranes. Five representative images at 40x magnification were taken for each sample and all the samples were tested in triplicate. Total cells and dead cells were counted with the Image-Pro Plus software (MediaCybernetics, USA). The percent of inactivated cells was determined from the ratio of the number of cells stained with PI divided by the number of cells stained with SYTO 9 plus PI. The results were averaged out and the standard deviations were calculated.

4.2.5. Bacterial Quantification in the Filtrate

The plate count method was used to enumerate viable bacteria in the filtrate [159]. The filtrates were collected and diluted in PBS through serial dilution. The dilutions were plated on Tryptic Soya Agar (TSA) (Oxoid, England) media and incubated overnight at 37^0 C. The total number of colony forming units (CFU) was enumerated. Each filtrate sample was plated in duplicate and standard deviations were calculated from the results.

4.2.6. Filter Agar Test

Viability and re-growth potential of the retained bacterial cells on the membrane surfaces were tested using the agar printing assay described elsewhere [159]. Immediately after filtration, the filter surfaces were flipped on a TSA plate facing down and incubated overnight at 37^0 C. Bacterial growth on the membrane perimeter was measured with a Mitutoyo 500-196-20 Digital micrometer Caliper (MSI Viking Gage, USA). Averages and standard deviations were calculated from triplicates.

4.2.7. Scanning electron microscopy (SEM) Imaging

SEM sample preparation and imaging was performed following the protocol described elsewhere [152]. Briefly, bacterial cells on the filter surfaces were fixed with 2% gluteraldehyde in 0.05M cacodyle buffer solution (Fisher Scientific, USA). The fixed cells were subsequently stained with 1% osmium tetraoxide (Sigma Aldrich Chemicals, USA) and dehydrated with increasing concentrations of ethanol (25%, 50%, 75%, 95% and 100%). SEM images were acquired using a LEO Gemini 1500 series microscope at

10 keV. Prior to imaging, the samples were mounted on carbon tape and coated with Au/Pd using a Denton Vacuum Desk II sputter coater.

4.2.8. Deoxyribonucleic Acid (DNA) Quantification Assay

This assay was performed to quantify the DNA concentration (ng/µl) in the filtrate that was released from damaged bacterial cells after filtration. The experimental procedure was adapted from another study [2]. Briefly, immediately after filtration, 2 µl of the filtrates were placed in a Take 3 Plate (for DNA quantification) in the Synergy MX (BioTek, USA). Sterile PBS without bacteria and DNA were used as blanks. Average DNA concentrations and standard deviations were calculated from duplicate filtrate samples.

4.2.9. Viral Culture and Quantification

MS2 bacteriophage was selected to test viral removal by these new membranes. MS2 bacteriophage and its host *E. coli* 15597 were obtained from the American Tissue Culture Collection (ATCC). The stock solution of MS2 was prepared as described elsewhere [168]. Stock solutions of MS2 in PBS ($4.5x10^{11}$ PFU/ml) were used for the filtration experiments. The concentrations of bacteriophages were determined before and after each filtration experiment. The membrane filters were prepared and preconditioned as described in *Section* "Bacteria Cell Filtration". A solution of 2 ml of the MS2 was filtered through the membrane filter at constant permeation rate (~57 L m^{-2} h^{-1}). Filtrate was collected on sterile 2 ml tubes and viral concentrations were determined with the PFU method [168]. Briefly, each serial dilution in PBS of the filtrate was mixed with the *E. coli* host and molten soft agar (0.7% TSA), then poured on TSA plates. The plates

were incubated overnight at 35 °C and the plaque forming units were quantified. All the virus experiments were done in a biological safety cabinet. Each filter was tested in duplicate and the standard deviations were calculated.

4.2.10. Human Cytotoxicity Evaluation

Cytotoxicity test of PVK-SWNT, SWNT, and PVK solutions were performed against NIH 3T3 Fibroblast cells using CellTiter 96 AQ_{ueous} (Promega) [169]. The NIH 3T3 Fibroblasts were a gift from Dr. Albee Messing of the University of Wisconsin-Madison and were cultured at 37 °C in a growth media containing 86% of Dulbecco's modified Eagle's medium, 10% fetal bovine serum (FBS), 1% penicillin-streptomycin, 1% 4-(2- hydroxyethyl)-1-piperazineethanesulfonic acid in 1 M HEPES, 1% L-glutamine, and 1% minimum essential medium (MEM) in 10 mM nonessential amino acids solution (100×; GibcoBRL). Fibroblast cells of passages 129 and 132 were harvested from culture flasks by 10-12 min incubation with 0.25% trypsin and were resuspended in the growth media. Assay kits containing 3- (4,5-dimethylthiazol-2-yl)-5-(3-carboxymethoxyphenyl)-2-(4-sulfophenyl)- 2*H*-tetrazolium, inner salt (MTS) and an electron coupling reagent, phenazine methosulfate (PMS) were used. Briefly, cells were seeded onto a 96-well plate with a seeding density of $2.5x10^4$ cells/ 100 µL and incubated at 37° C and 5% CO_2 in humidified air for 24 h. The cell culture medium was then aspirated from the wells and the plates containing cells were gently rinsed with Dulbecco's Modified Eagle Medium (DMEM) to remove any non-adherent cells. Next, 100 µl of nanomaterials (PVK, SWNT and PVK-SWNT) were added onto each well containing cells and incubated for 24 h at 37° C with 5% CO_2. After the incubation, the

nanomaterials dispersed in solutions were aspirated and the wells were rinsed 3 times with DMEM. The adherent cells were evaluated for their viability using MTS assay as described by the manufacturer (Promega, Madison, WI, USA). Briefly, MTS and PMS detection reagents were mixed, using a ratio of MTS/PMS 20:1. This procedure was done immediately before to addition to the cell culture media (DMEM) in which a 1:5 ratio of detection reagents to cell culture medium was used. Then the aspirated wells containing the samples were incubated for 2 h at 37 °C in a 5% CO_2 atmosphere. A well containing only the culture medium (i.e. DMEM) was used as a "medium only" control. The untreated cell suspension was used as a negative control. For the positive control, 4% paraformaldehyde in PBS buffer was added to the cells grown on the plate. The absorbance of the formazan was read using a Synergy MX Microtiter plate reader (BioTek, VT) at 495 nm.

4.3. Results and Discussions

4.3.1. Filter membrane Characterization

Prior to membrane fabrication, the PVK-SWNT and PVK sample solutions were characterized using UV-Vis. Figure 4.1 shows the UV-visible spectra for the pure SWNTs. As expected no absorption peaks at the visible region of the electro-magnetic spectrum were observed. However for the pure PVK solution, main signature bands occurring at 331 and 345 nm were observed. These peaks are attributed to the π-π* and n-π* optical transitions in pendant carbazole moieties of PVK [170]. It can be seen from the spectra that the main absorption peaks for pure PVK still prominent in the PVK-SWNT nanocomposite, but the intensity was slightly reduced due to the presence of the SWNT.

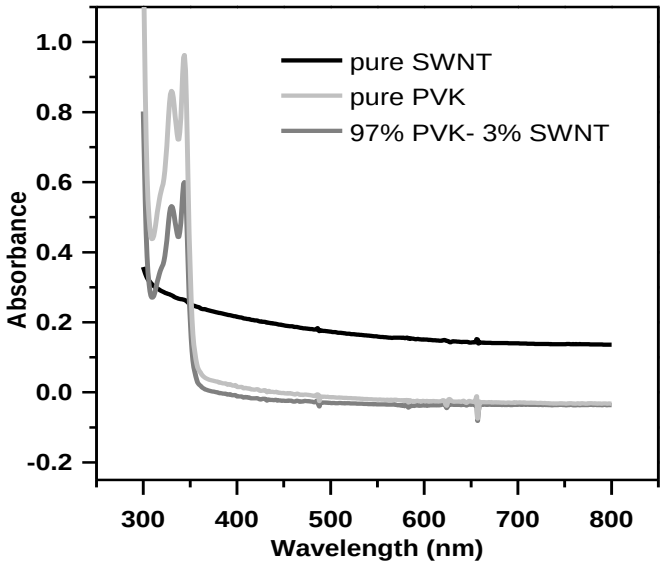

Figure 4.1. UV-vis spectra of the pure SWNT, PVK and PVK-SWNT nanocomposite solutions.

FTIR was also used to determine the functional groups present on the modified filter surfaces. Figure 4.2 shows the IR spectra of the nitrocellulose filter membrane with the following peak assignments: 832 cm^{-1} (NO stretch), 1651 cm^{-1} (asymmetric NO_2 stretch), 1282 cm^{-1} (symmetric NO_2 stretch), 1060 cm^{-1} (asymmetric CO stretch) and a weak band at 1746 cm-1 (CO stretch) [171]. Similar peaks were observed for the PVK-SWNT membranes corresponding to olefinic C-H bending (822-837 cm^{-1}), C-N stretching (1012-1273 cm^{-1}) and C=C stretching (1635-1645 cm^{-1}), except for the weak band at 1746 cm^{-1} found in bare nitrocellulose filter (inset). The disappearance of this band as well as the significant increase of absorbance intensity in modified membranes suggests successful coating of the filter with PVK-SWNT.

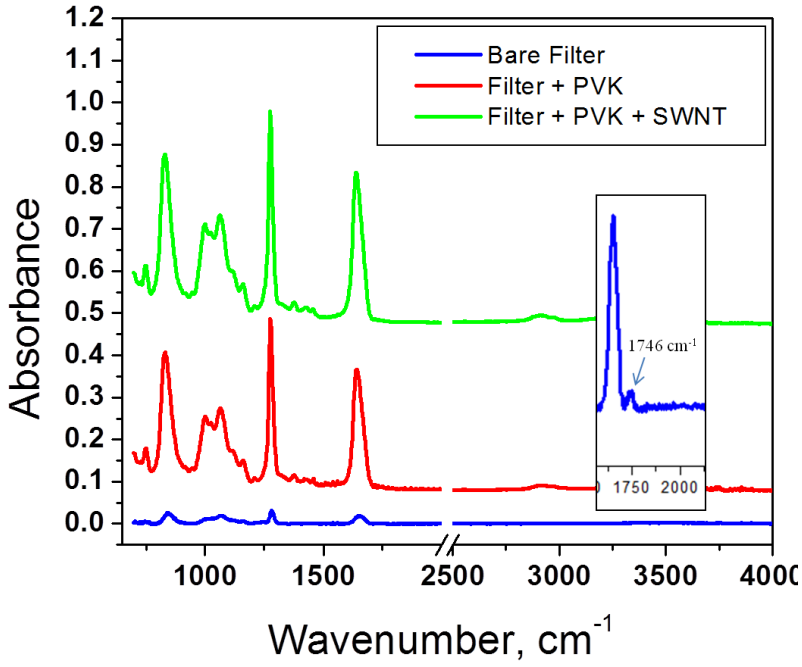

Figure 4.2. FTIR spectra of the unmodified, PVK-modified and PVK-SWNT modified nitrocellulose membranes.

The successful modification of the filter was characterized using XPS (Figure 4.3). Narrow scan in the N 1s region of the unmodified filter membrane showed an intense peak at ~408 eV coming from N=O of the nitrocellulose membrane. Upon addition of PVK-SWNT, a new peak centered at ~399 eV appeared, indicative of the N-C coming from the carbazole moieties of PVK. Furthermore, the C 1s scan of the PVK-SWNT showed higher peak intensity in the C-C region (284.5 eV) as compared to the PVK and unmodified membranes due to the incorporation of C-C containing SWNT. To estimate the amount of SWNT loaded on the filter membrane, the peak area ratios from the N-C and C-C peaks of the PVK-SWNT and PVK were used. Using this method, the amount of SWNT was estimated to be ~3 wt %. This value is similar to the solution mixture ratios of PVK-SWNT used to prepare the modified filter.

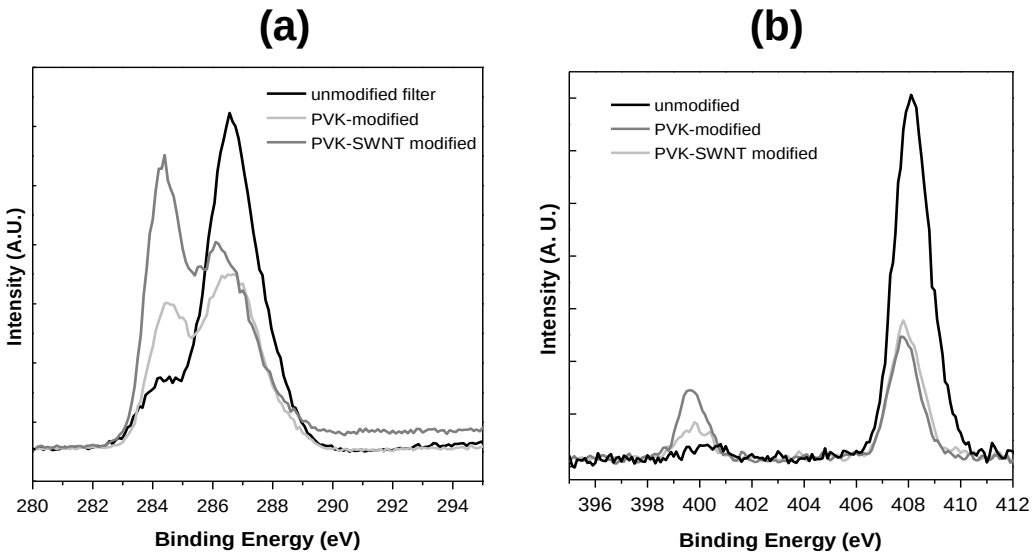

Figure 4.3. XPS spectra of the unmodified, PVK-modified, and PVK-SWNT modified nitrocellulose membranes. (a) C 1s and (b) N 1s regions.

The morphology of all the membranes were evaluated using SEM. Figure 4.4a depicts the SEM image of the unmodified nitrocellulose membrane, which revealed a layered and mat-like porous surface. The SWNT and PVK-SWNT-modified filters, on the other hand, formed a denser coating on the surfaces that were seen over several layers. Furthermore, the uniform aspect of the surfaces throughout the membranes demonstrates successful and homogeneous coating of the nitrocellulose membrane surfaces with SWNT and PVK-SWNT (Figure 4.4, b & c).

(a) **(b)** **(c)**

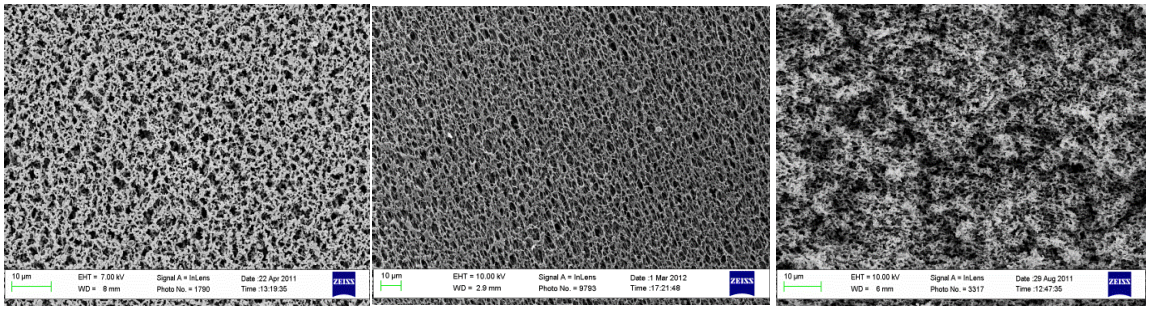

Figure 4.4. SEM images of membrane morphologies: (a) bare nitrocellulose membrane; (b) SWNT coated membrane; (c) PVK-SWNT coated membrane. Scale: 10 µm.

4.3.2. Antibacterial property of the coated membranes

The LIVE/DEAD assay was performed to determine bacterial viability after interaction with the nanomaterials during filtration. Fluorescence microscopy was used to assess the loss of bacterial viability. SYTO 9 dye (green dye) was used to stain both live and dead cells while propidium iodide (PI) (red dye) was used to stain the cells with compromised membranes. Figure 4.5 (a, b) shows representative fluorescence images of the *E. coli* and *B. subtilis* cells on the filter surfaces. Results show that in the absence of the nanomaterials (control), bacterial inactivation was <10% (Figure 4.5, c). While, ~90 % and ~81 % of the *E. coli* cells were inactivated after being retained on the PVK-SWNT and SWNT coated membranes, respectively. Similarly, ~90 % and ~40 % of the *B. subtilis* cells were inactivated after retained on PVK-SWNT and SWNT coated membranes, respectively. In similar studies with SWNT coated membranes, 80-90 % *E coli* inactivation was observed [96, 152]. No noticeable toxicity effects (inactivation < 10%) of PVK coated membranes were observed on either *E. coli* or *B. subtilis*. This suggests that toxicity observed on PVK-SWNT coated membranes were either due to the presence of SWNT or synergistic effects of PVK-SWNT, but not due to the presence of

PVK. In the case of 100% SWNT coated membranes (Figure 4.5, c), the toxic effect of these membranes on *B. subtilis* were considerably smaller than on *E. coli*. However, these findings are similar to many other studies where *E. coli* and *B. subtilis* exhibited different tolerance levels towards SWNT. These finds were explained as differences in cell wall structure, the protective effect of the outer membrane surface properties, ability to form spores and/or unique repair mechanisms of different microorganisms [43, 155, 172, 173].

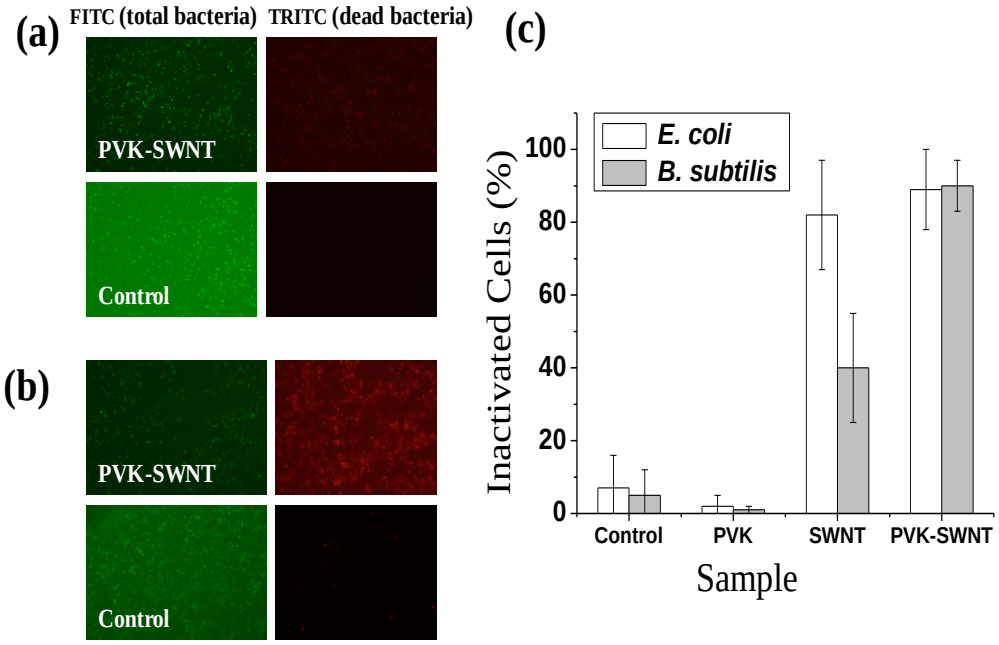

Figure 4.5. Viability assay for bacteria retained on membrane filters: (a) *E. coli* retained on PVK-SWNT coated filter and on bare filter (control); (b) *B. subtilis* retained on PVK-SWNT coated filter and on bare filter (control). (c) % Inactivated cells.

The results demonstrated that PVK-SWNT nanocomposite with only 3% SWNT content achieved similar or better cell inactivation than 100% SWNT coated membranes. These results can be explained by the better dispersion and debundling of SWNT in the

presence of PVK, which would increase the probability of SWNT to be in contact with bacterial cells[152]. Though the exact mechanism of SWNT-bacterial interaction has not been completely elucidated yet, several studies suggested physical disruption of bacterial membrane and oxidative stress as the major mechanisms [152, 153, 155, 174]. Therefore, the cells in contact with this nanomaterial were probably inactivated by one or both mechanisms.

4.3.3. Intracellular DNA Release

Although the membrane damage test (LIVE-DEAD) is a strong indicator of cell damage, not all damaged membranes will lead to bacterial cell death. Current literature describes that the release of large quantities of intracellular material from cells, only occurs when bacterial cell walls and cellular membranes suffer irreparable damages [2]. In many SWNT cytotoxicity studies, cell membrane damage has been reported as one of the mechanisms for bacterial toxicity. This mechanism is verified by measuring the efflux of cytoplasmic material (e.g. DNA) in the filtrate. In Figure 4.6, the filtration of both *E. coli* and *B. subtilis* yielded higher DNA concentrations in the filtrate of SWNT and PVK-SWNT coated membranes than uncoated and PVK coated membranes. In the case of SWNT coated membranes, ~2 fold and ~1 fold increase in DNA efflux compared to the control were observed for *E. coli* and *B. subtilis,* respectively. While for PVK-SWNT coated membranes, ~4 fold and ~2.5 fold increase in DNA efflux were observed for *E. coli* and *B. subtilis,* respectively. In similar studies, release of intercellular DNA was observed to be as high as 5 fold for *E. coli* as a result of the bacterial interaction with SWNT and subsequent membrane damage [2, 152]. In the case of PVK-SWNT coated

membranes, the SWNTs were highly dispersed, which increased the chances of cell interaction with the open ends of nanotubes and led to cellular damage. Similar results were also described on studies with coated surfaces with SWNTs and other polymers [153, 155, 164].

We believe that the measured DNA concentration in the filtrate of SWNT and PVK-SWNT coated membranes should have been much higher than what we are reporting, since DNA tends to adsorb to SWNT surfaces [2]. This high efflux of DNA suggests considerable bacterial cell membrane damage and potential cell death.

In Figure 4.6, the DNA efflux from *B. subtili*s cells (Gram-positive) was lower than from *E. coli* cells (Gram-negative), which could be explained by the thicker peptidoglycan cell-wall found in Gram-positive bacteria. This thick peptidoglycan cell-wall would make it harder for nanomaterials to cause considerable cell membrane damage [175, 176].

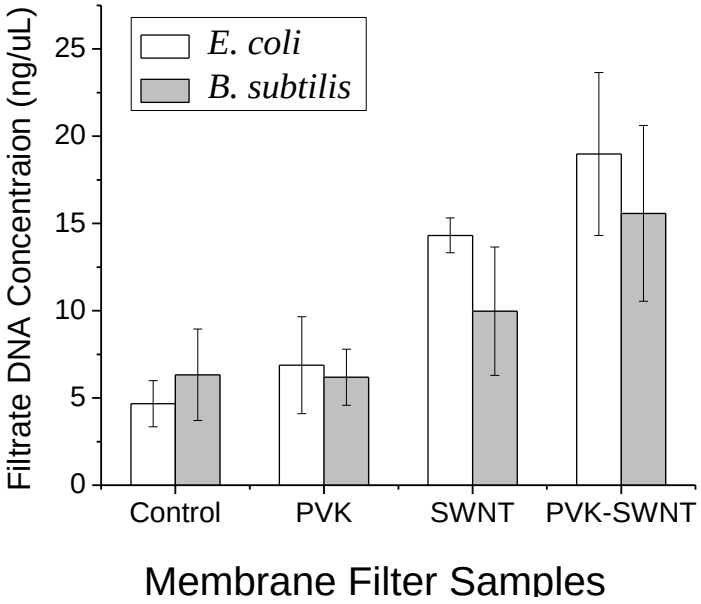

Figure 4.6. Efflux of cytoplasmic material (DNA, ng/µL) in the filtrate after filtration of *E. coli* and *B. subtilis* through PVK, SWNT and PVK-SWNT coated membrane filters and non-coated filters (control).

4.3.4. Filter Agar Printing Test

Recent studies have shown that *E. coli* can endure and repair low to moderately damaged cell membranes [2, 177]. The main goal of this test was to confirm the results from the DNA release assay and determine at what extent the damaged bacterial cells retained on the membrane filter could recover from the cellular damage and grow after the exposure to the nanomaterial. In the results of the LIVE/DEAD and DNA release assays, the control and PVK coated membrane filters presented very few bacterial cells with compromised cellular membranes as opposed to SWNT and PVK-SWNT coated membrane filters. Similarly, in the agar printing assay (Figure 4.7), much higher bacterial growth was observed on the control and PVK-coated membranes than on the other coated membranes. SWNT membranes presented ~73% and ~66% growth inhibition for *E. coli*

and *B. subtilis*, respectively, when compared to the control. Similar inhibition was also observed for PVK-SWNT membranes (~70% for *E. coli* and ~65% for *B. subtilis*). These results suggest that bacteria retained on the membrane filters significantly lose their potential for re-growth. Bacterial re-growth and biofilm formation have been demonstrated in many studies to cause great problems in membrane operations [178]; these results show that this new coating has the potential to solve such problems.

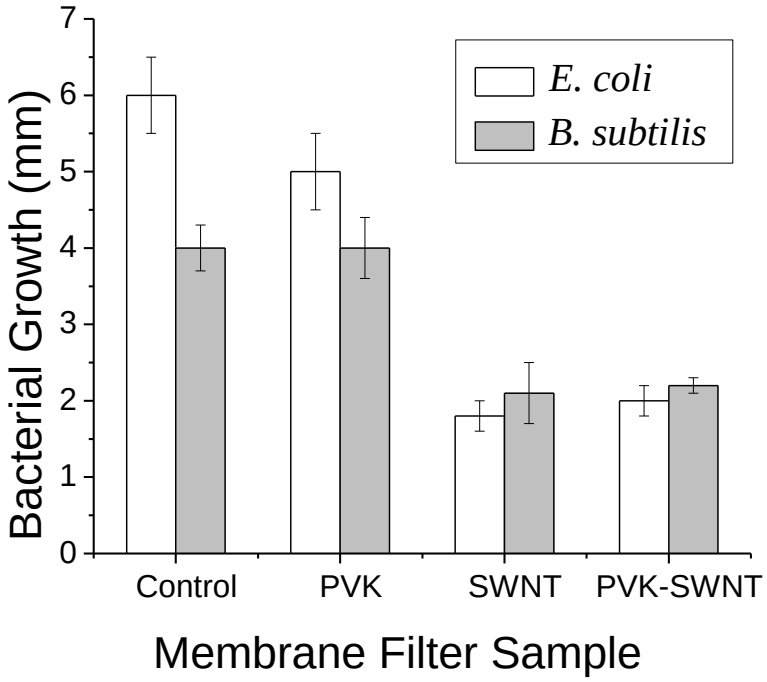

Figure 4.7. Agar printing assay to determine the growth behavior of bacteria retained on membrane coated with PVK, SWNT, PVK-SWNT and bare membrane (Control).

4.3.5. Bacterial Morphology on the Filters

The SEM images of *E. coli* (Figure 4.8) showed bacterial cells disrupted and shrunk on both SWNT and PVK-SWNT filter surfaces. This result corroborates our results of the Live/Dead assay, intracellular DNA release, and the filter agar printing test.

Similar bacterial damage was also observed for *B. subtillis* after filtration on the PVK-SWNT and SWNT modified membranes.

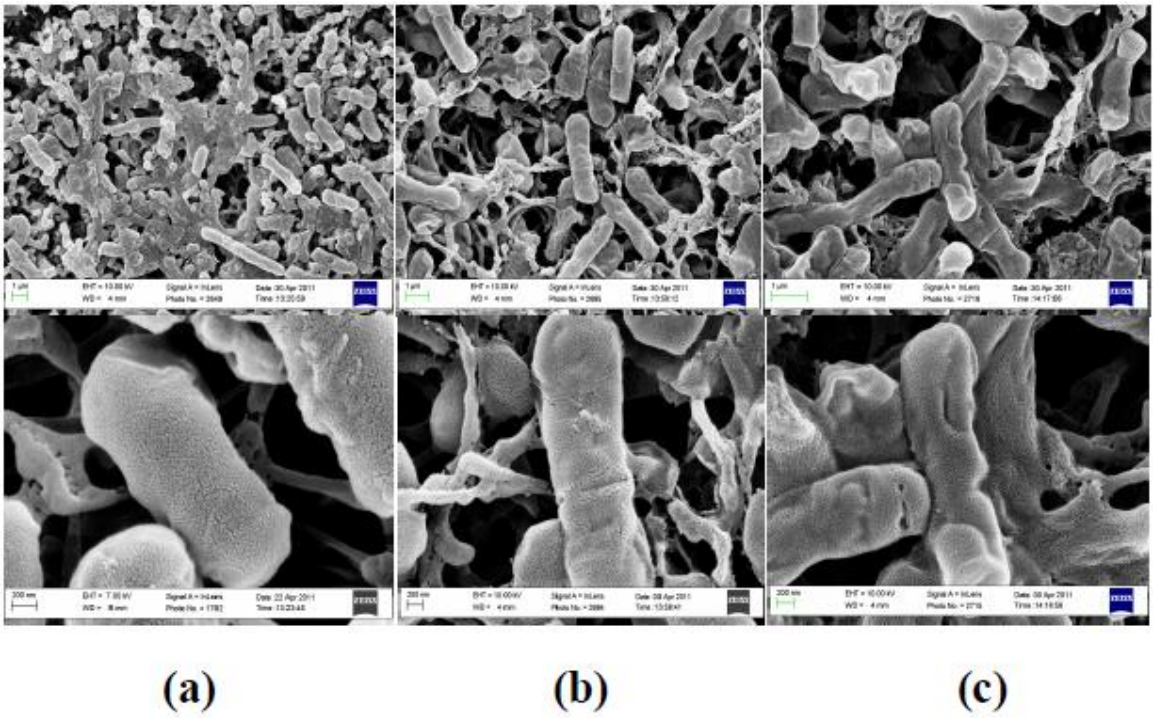

Figure 4.8. SEM images ɔf filters with retained bacterial (*E. coli*) cells on (a) unmodified membrane (control), (b) SWNT coated membrane, and (c) PVK-SWNT coated membrane. Scale: 1 µm (top), 200 µm (bottom).

4.3.6. Bacterial Removal Property

In theory, membrane filters with smaller pore size than the size of bacterial cells are expected to retain all cells by a sieving mechanism. Studies, however, have shown that bacterial cells can entrain through membrane pores due to high filtration rates, solution chemistry, and lack of membrane surface uniformity [100, 179]. Our study demonstrated that both SWNT and PVK-SWNT coated filters had ~ 4 log higher bacterial removal than the control filters (Figure 4.9). This bacterial removal might be a combined effect of cell retention and inactivation by SWNT while passing through the

membranes. The small pore size (0.45 μm) of the nitrocellulose membranes, the added thickness of SWNT and PVK-SWNT layers to the membrane, and the strong affinity of the bacterial cells to SWNT surfaces increased the efficiency of the filters by cell inactivation, sieving, and depth filtration mechanisms [96, 100, 168]. The similar log removal of 100% SWNT coated membranes and PVK-SWNT coated membranes with only 3% SWNT load could be attributed to a more homogeneous dispersion of SWNTs on the membrane surface in the presence of PVK, and hence more SWNT open ends to inactivate bacterial cells.

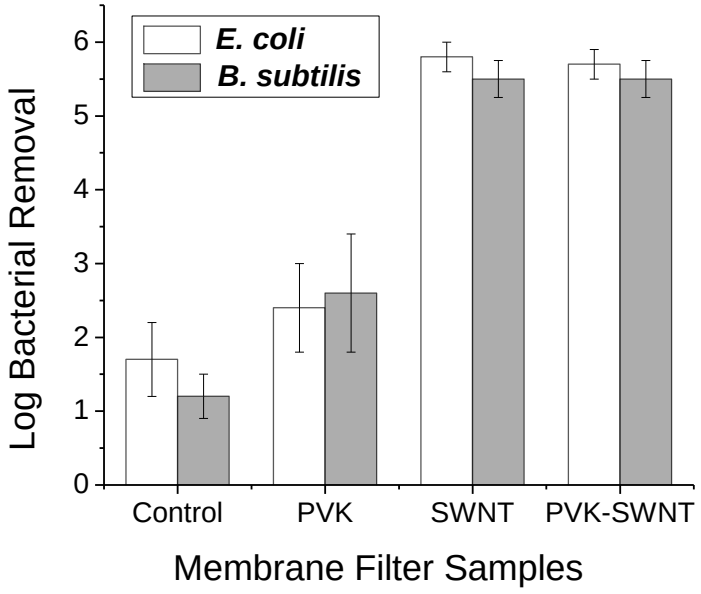

Figure 4.9. *E. coli* and *B. subtilis* (10^7 CFU/ml) log removal after filtration at constant permeation rate through bare membrane (control) and through PVK, SWNT and PVK-SWNT coated membranes.

4.3.7. Virus Removal Property

MS2 bacteriophage was used to investigate the removal efficiency of nanometer-sized viral particles. The bacteriophages were filtered through bare membranes (control),

and through PVK, SWNT, and PVK-SWNT coated membranes. As expected, the log removal of MS2 for both control and PVK coated membranes were very poor (<1 log), due to the very small size of the virus (~27-34 nm) compared to the membrane pore size (0.45 μm) (Figure 4.10). On the other hand, the log viral removal was ~3 and ~2.2 for SWNT and PVK-SWNT coated membranes, respectively. The mechanism of virus removal on SWNT coated membranes has been demonstrated to be by depth filtration [168]. A higher virus removal (~3 logs) by 100% SWNT coated membranes than PVK-SWNT (with 3% of SWNT) coated membranes can be attributed to a larger amount of SWNT in the 100% SWNT membranes. The higher the SWNT concentration on the membrane, the larger will be the surface area available for the virus particles to adsorb. Studies have shown that SWNT loads of 0.5 mg/cm^2 achieve more than 4 log virus removal. Furthermore, a linear relationship was established between the effluent virus concentration and SWNT load on the membrane surface [168].

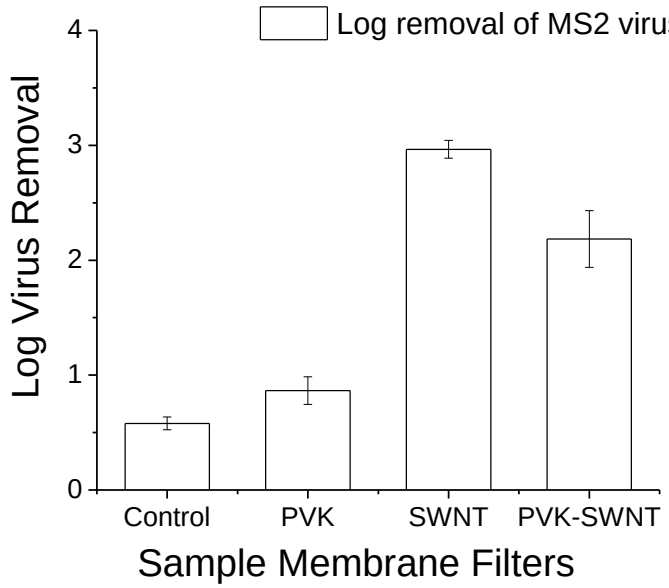

Figure 4.10. Log removal of MS2 virus ($4.5x10^{11}$ PFU/ml) after filtration at constant permeation rate through bare membrane (control) and through PVK, SWNT, and PVK-SWNT coated membranes.

4.3.8. Human Cytotoxicity Test

During the filtration process, some SWNT particles may detach from the membrane surface and end up in the drinking water. Certain concentrations of SWNTs have been shown to be toxic to humans. For instance, pure SWNT/MWNT was described to damage the plasma membrane of mammalian cells and to induce considerable toxicity [74, 180]. Therefore, it is essential to investigate the human cytoxicity of the SWNT concentrations used in the filters in this study to assess their suitability for drinking water treatment. Fibroblast cells are part of human connective tissue and play an important role in wound healing; therefore they are often used in *in vitro* studies. These cells can easily get exposed by SWNT entering the human body through physical contact or ingestion [181].

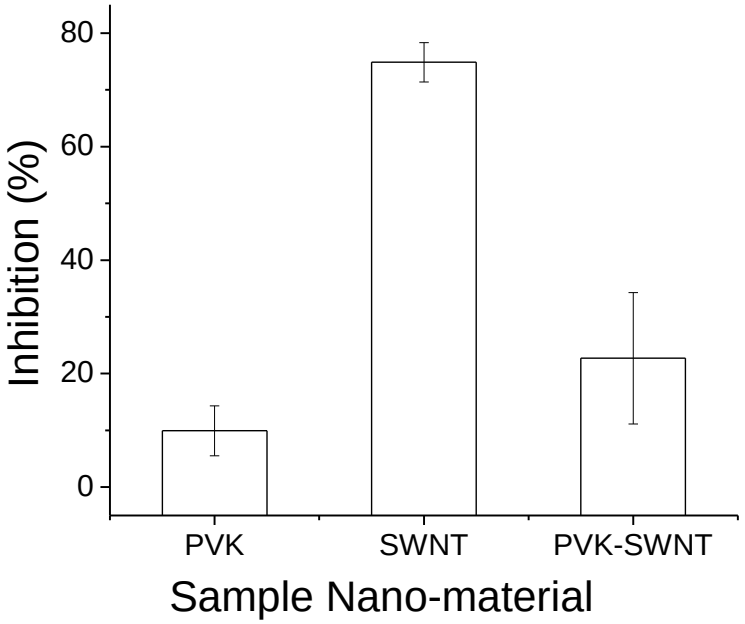

Figure 4.11. Cytotoxicity of the PVK-SWNT (1 mg/ml), SWNT (1mg/ml), and PVK (1mg/ml) solutions against NIH-3T3 Fibroblasts.

The exposure of fibroblast cells to SWNTs showed that the concentration of SWNT plays an important role in the toxic behavior of SWNT towards human cells (Figure 4.11). In SWNT samples, with a concentration of 1mg/ml, ~75% cytotoxicity was observed in the human cells. In the PVK-SWNT suspension with a SWNT concentration of 0.03 mg/ml was observed only ~20% toxicity. PVK, on the other hand, that functions as dispersant, displayed minimal cytotoxic effects (~10%). Previous studies with other human cells, such as the human umbilical vein endothelial cells, demonstrated that a SWNT mixture with the phosphorycholine polymer exhibited a cytotoxicity of only ~8-10%, while SWNT/MWNT suspended with polyethylene glycol (PEG) showed no considerable toxicity to mammalian cells [7, 176, 180]. The PEG and other polymers mixed with SWNT/MWNT were reported to be able to penetrate mammalian cells

without damaging the plasma membrane, and their accumulation did not show significant toxic effect on cell cycle [74] . Hence, it seems that in the event of some leaching from the PVK-SWNT coated membranes, the SWNT used in this study will not exhibit considerable toxicity towards human fibroblast cells. However, the effects of SWNT exposure to other human cell types and effects of chronic exposure need to be further investigated before such material can be widely used for water treatment.

4.4. Conclusion

In this study, we demonstrated that membrane (nitrocellulose) coated with SWNT and PVK-SWNT nanocomposite can effectively remove and inactivate bacterial cells during filtration. The PVK-SWNT (97:3 wt% ratio PVK: SWNT) coated membranes achieved similar or improved bactericidal effects than 100% SWNT coated membrane. Log removal of MS2 virus was lower in PVK-SWNT filters compared to 100% SWNT filters due to smaller loads of SWNT in the nanocomposite, which reduced adsorption sites for the virus. The log removal efficiency (both bacteria and virus) could be further investigated by increasing the thickness of PVK:SWNT and SWNT coating. Again, substantial reduction of bacterial re-growth of the retained bacteria on the new membranes and the high concentrations of intracellular material efflux (DNA, ng/µL) in the filtrate are suggestive of irreversible bacterial cell membrane damage and bacterial death as a possible mechanism of bacterial inactivation by both SWNT and PVK-SWNT membranes. These observations are promising in terms of controlling biofouling problem during membrane filter operations. Cytotoxicity tests on human fibroblast cells demonstrated that PVK-SWNT (97:3 wt% ratio PVK: SWNT) are considerably less toxic

than pure SWNT (100%), which makes the application of this nanocomposite for water treatment very promising. PVK:SWNT coating is also significantly economical as use of costly SWNT was greatly reduced. Although SWNT and PVK-SWNT membranes tested in this study showed impressive removal of pure bacterial culture, further study should be conducted with natural water where many other factors like natural organic material (NOM), complex microbial communities and solution chemistry can influence the membrane filter performance.

Chapter 5 Applications of Carbon-based nanomaterials (Graphene, Graphene Oxide and Single-Walled Carbon Nanotube) for the Removal of a Biofouling Agent (Protein) from Aqueous Solution

5.1. Rationale and Objectives

Proteins are major components of naturally occurring organic matter (NOM) and are known to cause biofouling during membrane filtration of surface and wastewater [30, 182,183]. Excess NOM and protein are also reported to deteriorate effluent quality and increase the production of harmful disinfection by-products during the chlorination process [184]. Traditionally, activated carbon is used in water treatment plants to remove organic pollutants, including proteins, from surface water and wastewater. However, the protein adsorption capacity of activated carbon is relatively low; for high removal requirements, more efficient and innovative adsorbents should be considered [86].

In recent years, carbonaceous nanomaterials such as single-walled carbon nanotubes (SWNT), graphene (G), and graphene oxide (GO) have received significant attention for their utility as absorbents [30, 87, 185, 186]. These nanomaterials are promising replacements for other conventional adsorbents like activated carbon, due to exceptionally high specific surface area available for adsorption [185]. Among the three nanomaterials evaluated in this study, SWNT has been most extensively examined for adsorption applications. Several studies have reported that SWNT possess good adsorption capacity for many organic and inorganic pollutants present in aqueous phases [186-188]. Ongoing research suggests SWNT could be a better candidate for removal of contaminants in aqueous solutions than conventional adsorbents [85]. Although G and

GO have not been studied as extensively as SWNT, several studies have shown promising results for their application as adsorbents; G and GO nanoparticles and their nanocomposites can successfully remove various contaminants like antibiotics, heavy metals and synthetics dyes from aqueous solutions [87, 185, 189, 190]. However, to date, there has been no systematic study of these nanomaterials for removal of fouling compounds, like proteins, for water treatment applications. So far, protein related studies of these nanomaterials have been limited to bio-conjugate formations with proteins and other biomolecules for biomedical and biosensing applications [191-196]. Hence, there is a need to investigate protein adsorption characteristics of G, GO, and SWNT and the effects of different water chemistries on their adsorption capacities for the development of more suitable water treatment technologies.

In this study, the adsorption capacities of G, GO, and SWNT were investigated with respect to protein removal from aqueous solutions. Lysozyme was used as the model protein. Lysozyme is an extensively studied protein and its physicochemical characteristics (structure, charge distribution, hydrophilicity/hydrophobicity) are well known in different solution chemistries. To account for various environmental factors related to water treatment, adsorption experiments were conducted at several pHs and salt concentrations. Experimental results were fit to Langmuir, Freundlich and Tenkin models to better understand the adsorption capacity and adsorption isotherm parameters of this protein to the nanomaterials. The investigation was further extended to wastewater from local treatment plants to determine the efficacy of these three nanomaterials for removing proteins from a system with complex water chemistry.

5.2. Materials and Methods

5.2.1. Synthesis of Nanomaterials and Preparation of Stock Solution

In this study, three carbon-based nanomaterials, i.e., graphene (G), graphene oxide (GO), and single-walled carbon nanotubes (SWNT) were tested for adsorption of protein in aqueous solution. Briefly, G nanoparticles (XG Sciences, MI) were suspended in deionized (DI) water to make a stock solution of 2 mg/mL [5]. The prepared stock solution was sonicated for 30 min before the adsorption tests. GO was synthesized from the graphite flakes (Alfa Aesar, USA) following the modified Hummers method using all reagent grade chemicals (Sigma-Aldich and Fisher Scientific, USA) [197]. Briefly, graphite flakes were digested with $NaNO_3$ and concentrated H_2SO_4, followed by oxidation with $KMnO_4$ and H_2O_2. The pH of the solution was neutralized to 7.0 and GO was collected as a pellet after centrifuging the neutralized solution. An appropriate mass of GO was suspended in DI water to make a stock solution of 2 mg/mL. SWNT were purchased from Cheap Tubes Inc. (Vermont, US) and the stock suspension was prepared in DI water (2 mg/mL) according to previously published methods [40, 174]. The SWNT stock solution was homogenized using a bath sonicator for 15 minutes before use in the adsorption experiments.

5.2.2. Adsorption Capacity Measurement

Lysozyme (Sigma-Aldich, USA) was used as a model protein for all the adsorption experiments. A 1 mg/mL stock solution of lysozyme was prepared in DI water. To study the effects of different initial protein concentrations on adsorption capacity of a fixed mass of nanoparticles, 0.5 mg/mL of nanomaterial was incubated with

varying concentrations of protein (0.2, 0.4, 0.6, 0.8 and 1 mg/mL). The protein stock solution was diluted with DI water, and 0.375 mL was added from each concentration to 2 mL Eppendorf tubes. 0.125 mL of the nanomaterial solution was then added to the tubes. As a control, 0.125 mL of DI water was added to one set of tubes in place of nanomaterial. Preliminary experiments indicated that all three nanomaterials reach absorptive equilibrium after 3 h; therefore, the mixed suspensions of protein and nanomaterial were incubated for 3 h at room temperature while being shaken at 200 rpm. After incubation, the sample tubes were centrifuged at 15,000 rpm to separate the nanomaterial from the suspension. Protein concentration in the supernatant was quantified by Take 3 Plate (for lysozyme quantification, Wavelength 280/260) in the Synergy MX (BioTek, USA). DI water without protein or nanomaterial was used as a blank. Each experiment was performed in triplicate and standard deviations were calculated. The adsorption capacity of the nanomaterials were calculated according to the equation [87]

$$qe = (Ci - Ce)V/m \quad (1)$$

where q_e = equilibrium adsorption capacity (mg protein/g nanomaterial); Ci = initial protein concentration; Ce= equilibrium protein concentration; and m = mass of nanomaterial (g).

To better explain lysozyme adsorption phenomena on the nanomaterials, the adsorption tests data were fitted into Langmuir, Freundlich and Temkin models. Mathematical representations of the models are as:

Langmuir model

$$\frac{1}{q_e} = \frac{1}{q_m} + \frac{1}{K_L q_m Ce} \quad (2)$$

q_m = Theoretical maximum adsorption capacity of per unit of adsorbent (mg/g)

K_L = Langmuir constant

Freundlich model

$$\ln q_e = \ln K_F + \frac{1}{n} \ln C_e \quad (3)$$

K_F = Freundlich constant, n= Linearity index

Temkin model

$$q_e = K_T \ln C_e + K_T \ln f \quad (4)$$

K_T = Temkin constant, f = Temkin isotherm equilibrium binding constant (L/g)

Langmuir is the simplest model, and assumes a single layer of adsorbed molecules on the surfaces [87]. The Freundlich model is an empirical model used for adsorption studies while the Temkin model is used for accounting for electrostatic interactions between charged surfaces [87, 198].

5.2.3. Effects of Solution pH on Protein Adsorption

Effects of pH on protein adsorption capacity of nanomaterials were evaluated. For this and all subsequent lysozyme adsorption experiments, the protein and nanomaterial mass ratio was kept constant at 1:2. Aliquots of lysozyme solution were adjusted to pH 2, 4, 6, 8, and 10 with addition of either HCl or NaOH. 0.400 mL of the pH-adjusted

lysozyme solutions were added to a set of 2mL Eppendorf tubes, and 0.100 mL of nanomaterial stock solution were added to the tubes. As a control, 0.100 mL of DI water was added to one set of tubes in place of nanomaterial. The suspensions were incubated for 3 h at room temperature while being shaken at 200 rpm, then centrifuged at 15,000 rpm. Protein concentration was quantified by Take 3 Plate. Each experiment was performed in triplicate to calculate average and standard deviations values.

5.2.4. Effects of Solution Ionic Strength on Protein Adsorption

The effects of salt concentration on the protein adsorption capacity of nanomaterials were evaluated for both monovalent (Na^+) and divalent (Ca^{2+}) ions. Stock solutions 0.250 mg/mL lysozyme, 0.250 mg/mL lysozyme in 1 M NaCl, and 0.250 mg/mL lysozyme in 1 M $CaCl_2$ were prepared in DI water. The solution containing lysozyme only was used to dilute the ionic strength of the protein and salt solutions; protein solution with salt concentrations of 0.0, 0.2, 0.4, 0.6, 0.8 and 1 M were prepared. 0.400 mL was taken from these protein solutions and placed into a set of 2 mL Eppendorf tubes, and 0.100 mL of nanomaterial solution was added to each. As a control, 0.100 mL of DI water was added to one set of tubes in place of nanomaterial. The suspensions were incubated for 3 h at room temperature while being shaken at 200 rpm, then centrifuged at 15,000 rpm. Protein concentration was quantified by Take 3 Plate. Average protein adsorption with standard deviation by each nanomaterial was calculated from triplicate experiments.

5.2.5. Zeta Potential Measurement

To better explain the protein adsorption behavior of GO and SWNT in the presence of divalent Ca^{2+} ion, surface charge measurements were performed with zeta potential. Zeta potential measurements were done for GO and SWNT particles after protein adsorption at 0 and 0.2 M strength of Ca^{2+} with Zeta potential/Particle sizer NICOMP 380 ZLS (Particle Sizing System, USA). Briefly, after 3 h of incubation, samples were diluted in DI water (for 0 M sample) and 0.2 M Ca^{2+} solution (for 0.2 M Ca^{2+} samples) to a ratio of 1:40. 1.5 ml of the diluted solutions of respective samples was transferred to cuvettes for Zeta potential measurements. All the experiments were done in triplicate to measure average and standard deviation values.

5.2.6. Protein adsorption from Environmental Sample (Wastewater)

The protein adsorption capacity of nanomaterials in a medium with complex water chemistry was investigated by measuring the adsorption of total protein present in wastewater. As nanomaterial may be present in environmental samples like wastewater at varying concentrations, dose dependent adsorption capacities of nanomaterials were investigated. Fresh activated sludge samples were collected three times from Sims South Bayou Wastewater Treatment Plant (Houston, TX) as wastewater samples. The average characterization values of the wastewater utilized in this study is presented in Table 5.1. Appropriate volumes of nanomaterial stock solutions were mixed with wastewater samples to give final concentrations of 10, 20, 50, 100, 200 and 300 mg/L to evaluate a dose dependent adsorption behavior of the nanomaterials. A 20 ml volume of activated sludge samples with different doses of nanomaterials were incubated in Conical tubes

(Corning, USA) for 3 h at room temperature at 200 rpm. Incubated suspension was filtered through 0.22 µm membrane filter and the filtrate was further centrifuged to remove any suspended nanomaterial or organics. Supernatants were used for protein quantification. A control was set with no added nanomaterial. Triplicate experiments were performed for measuring average protein adsorption from wastewater by each nanomaterial.

Table 5.1. Characterization of Wastewater

Total suspended solids, TSS (mg/L)	2666.6±942.8
Total Protein (mg/L)	130±2.12
pH	7.3±0.37

5.2.7. Characterization of Nanomaterials

All three nanomaterials (G, GO and, SWNT) used in this study were characterized. Further characterization was conducted in the presence of protein and divalent Ca^{2+} salt. Characterization was done with Attenuated Total Reflection Infrared Spectroscopy (ATR-IR) and X-ray Photoelectron Spectroscopy (XPS) analysis. Briefly for ATR-IR analysis, bare nanomaterials, nanomaterials with protein, and nanomaterial with protein and Ca^{2+} were deposited on PVDF membrane via vacuum filtration. All three samples were subjected to ATR-IR spectral analysis on a Nicolet iS Mid Infrared FT-IR Spectrometer (Thermo Fischer Scientific) equipped with a ZnSe crystal. Data was obtained through Omnic 8 Software (Thermo Fischer Scientific). For XPS analysis,

samples were deposited on either zirconium coated silicon wafers (SWNT) or gold wafers (G and GO). This analysis was carried out on a PHI 5700 X-ray photoelecton spectrometer, which was equipped with a monochromatic Al K X-ray source (h = 1486.7 eV). The X-rays were incident at 90° relative to the axis of a hemispherical energy analyzer. Spectra were taken at high and low resolutions, with pass energies of 23.5 eV and 187.85 eV, with photoelectron take off angle and analyzer spot diameter held constant at 45° from the surface and 1.1 mm. The survey spectrum was from 0-1400 eV, and high resolution spectra were collected for photoelectrons emitted from C1s, O1s, N1s, Ca1s, and Cl1s. Spectra were collected under a base pressure of $1x10^{-8}$ torr and at room temperature. Calibration of electron binding energies was performed with respect to the C1s line at 284.5 eV (C-C). All data was processed using the manufacturer's PHI Multipak software (version 5.0A). The high resolution spectra were first analyzed via background subtraction using the Shirley routine, and then fit to non-linear mixed Gaussian-Lorentzian functions.

5.3. Results and Discussion

5.3.1. Adsorption Capacity Measurement

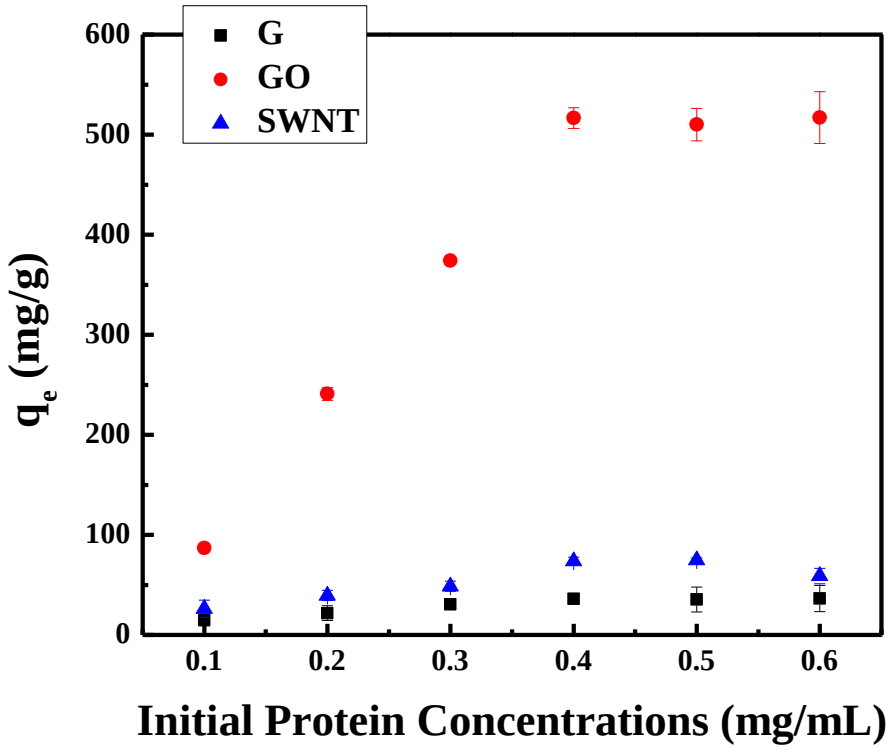

Figure 5.1. Adsorption capacity of G, GO, and SWNT at different initial protein concentrations. The nanomaterial concentration was held constant at 0.5 mg/mL in all samples.

Protein adsorption capacity of G, GO, and SWNT was evaluated at different lysozyme concentrations in aqueous solution. Overall, GO showed the highest capacity for lysozyme adsorption for all concentrations. The largest increase in protein adsorption (~500 mg/g) was observed from initial concentration of 0.1 mg/mL to 0.4 mg/L (Figure 5.1). Saturation of the binding sites in GO was observed in protein concentrations above 0.4 mg/mL. Lysozyme adsorption by G and SWNT nanomaterials followed an adsorption pattern similar to that observed for GO, however the rate of protein adsorption was significantly lower (<100 mg/g). The two most common forces involved in protein

adsorption on surfaces are electrostatic interaction and van der Waals forces [199]. The relatively high protein adsorption on GO can be explained as a result of electrostatic attraction between protein molecules and functional groups present on GO surfaces as observed with other chemicals such as antibiotics, heavy metals, etc [87, 190]. Lysozyme molecules contain both negative and positive sites, however at pH 7.0, it has a net positive charge [200]. The higher adsorption of GO could be attributed to the abundance of functional groups (-OH and –COOH) on its surface (at pH =7) which cause an attractive electrostatic force [87]. The opposite charges of lysozyme and GO generated a high adsorption rate [198, 201]. In similar studies, the amount of protein adsorbed was found to be dependent on the electrostatic force, which depends on the number of functional groups present on the surface rather than the total surface charge [201]. Another cause for greater affinity of lysozyme for GO could be their hydrophilic nature which facilitated mutual interaction [200]. On the other hand, lysozyme adsorption on non-functionalized G and SWNT could be attributed to van der Waals force and some electrostatic attraction as observed in a similar study [194].

5.3.2. Effects of pH on lysozyme adsorption to nanomaterials.

Variation of solution chemistry, especially pH, has been reported to affect protein adsorption on surfaces [199, 202-204]. The electrostatic state of the protein depends on the solution pH [201]. The adsorption behavior of lysozyme on GO, SWNT and G was therefore evaluated by varying pH values below the isoelectric point of lysozyme, i.e., pH 11 [200]. In this study, GO and SWNT exhibited moderately reduced lysozyme adsorption with increasing pH (Figure 5.2). On the other hand, no noticeable effect of pH

change was observed on the lysozyme adsorption capacity of G. The highest amount of protein adsorption by GO and SWNT (~370 and 70 mg/g, respectively) occurred at pH 4.0, the lowest pH tested.

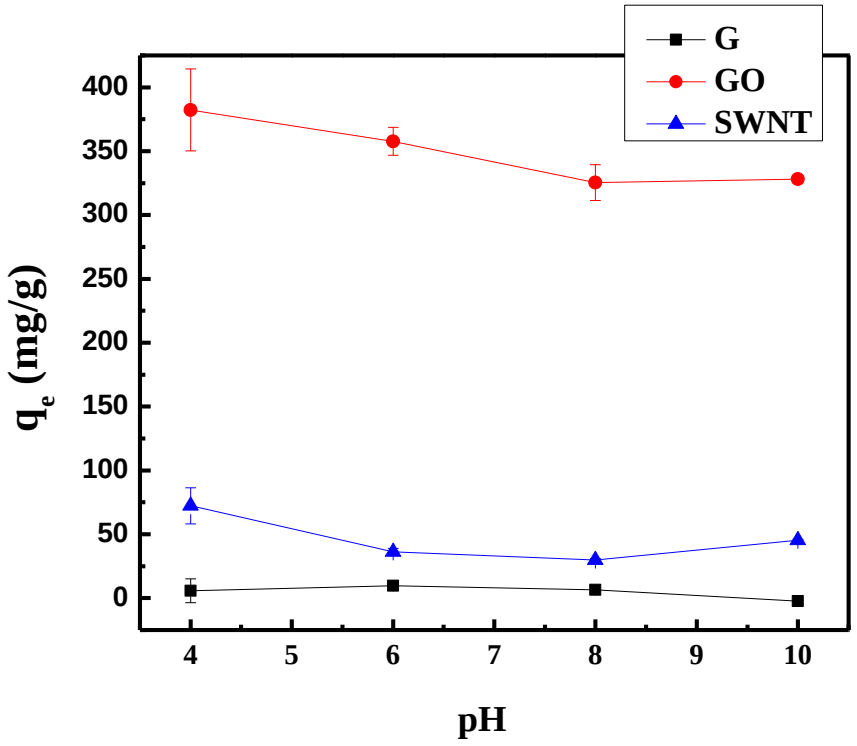

Figure 5.2. Effects of pH on the adsorption capacity of G, GO, and SWNT. The nanomaterial concentration was 0.4 mg/mL and the protein concentration was 0.2 mg/mL.

Gradual decrease in adsorption capacity was observed for both GO and SWNT from pH 4 to 10. GO's surface contains both –OH and –COOH groups while the protein contains $–NH_2$ group. Increase of pH has shown to facilitate the deprotonation of these groups and weakening their electron accepting capacity, resulting in reduced electrostatic attraction and protein adsorption [87]. Overall, in this study, small to negligible effects of

solution pH change on lysozyme adsorption capacity of G, GO and SWNT were observed.

5.3.3. Effects of salt concentrations on lysozyme adsorption to nanomaterials.

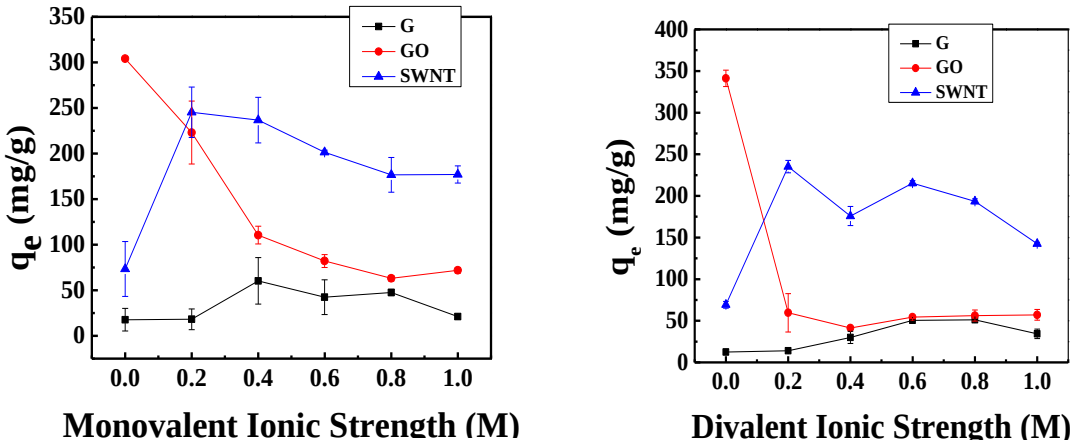

Figure 5.3. Effects of (a) monovalent (Na^{1+}) and (b) Di-valent (Ca^{2+}) ionic strength on the adsorption capacity of G, GO, and SWNT. The nanomaterial concentration was 0.4 mg/mL and the protein concentration was 0.2 mg/mL.

The presence of dissolved salt ions is known to affect protein adsorption behavior of adsorbents [199, 201]. Ions can affect the interfacial interaction of protein and adsorbent surface and hence the electrostatic phenomena [205]. To consider ionic effects, the adsorption capacities of lysozyme by G, GO, and SWNT were evaluated in presence of dissolved mono- (NaCl) and divalent ($CaCl_2$) salts. With the introduction of dissolved ions (Na^{1+} and Ca^{2+}) in the solution, GO exhibited a sharp decrease in lysozyme adsorption capacity. The largest reductions in adsorbed lysozyme, ~200 and 300 mg/g,

were observed at ionic concentrations of 0.4 M Na^{1+} and 0.2 M Ca^{2+}, respectively (Figure 5.3 a & b). Such reduction of adsorbed protein in the presence of ions was also observed in other studies with lysozyme on negatively charged surfaces like GO, as the result of double layer interactions on both particles [205]. The positive cations balance the negative charges on GO, reducing the interaction strength between GO and the protein; cations are selectively bound due to the relative bulkiness of the protein. Beyond 0.4 M salt concentrations, no change in protein adsorption was observed with further concentration increase (0.4 M to 1.0 M). Interestingly, SWNT exhibited an opposite trend in protein adsorption behavior when compared to GO. With introduction of both Na^{1+} and Ca^{2+}, a sharp increase in adsorbed protein (~200 mg/g) was observed. Cations are known to form cation-pi bonds on carbonaceous nanomaterials like SWNT, creating positive surface charge [87]. It is probable that these positive sites bind with negative sites in the protein and cause increased protein adsorption. However, no increase in protein adsorption to SWNT was observed when the ionic strength was increased beyond 0.2 M, suggesting saturation of adsorption sites. For G, slightly increased lysozyme adsorption was observed with increased ionic strength (Na^{1+} and Ca^{2+}).

5.3.4. Characterization and analysis of protein adsorption

IR spectra of G, GO and SWNT are presented for samples containing protein and protein with salt (Figure 5.4). Pristine graphene exhibited no functional groups at all, and so had a smooth spectrum (Figure 5.4a). The samples containing only graphene and graphene with protein are nearly identical. The spectrum of the sample containing graphene, protein, and salt had small peaks at around 1626 cm^{-1} and 3388 cm^{-1},

corresponding to amide and amino groups, respectively [206]. The relative weakness of these peaks indicated a low amount of protein adsorbed to the nanomaterial. The spectrum of the pristine GO sample corresponds well with other spectra from the literature (Figure 5.4b). In the presence of lysozyme, the major change in the spectrum was the replacement of the broad –OH peak from around 3000 – 3600 cm^{-1} with a narrower –NH peak from 3300 – 3500 cm^{-1}, indicating the hydroxyl groups on the surface of the GO were masked by the sorbed protein [207].

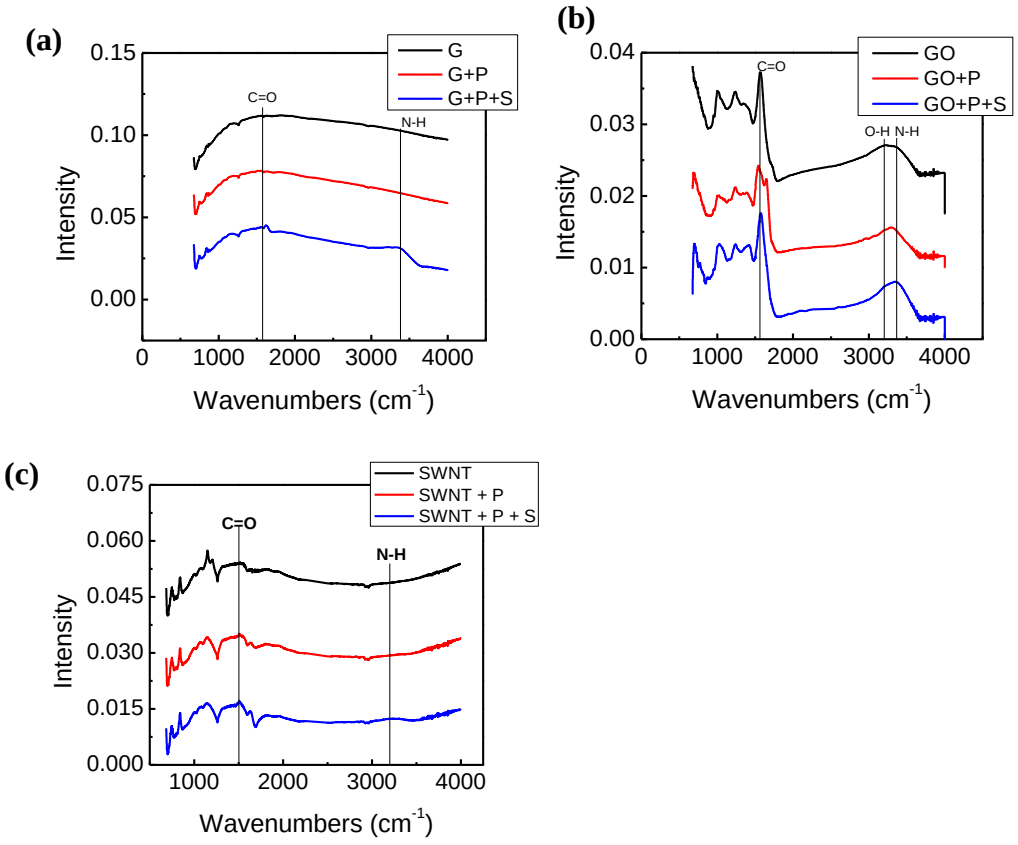

Figure 5.4. Infrared spectra of (a) G, (b) GO and (c) SWNT in DI water solution, protein solution, and protein-salt solution. In the legends, P indicates the presence of protein in the trial and S indicates the presence of $CaCl_2$ salt.

In the sample containing GO, protein, and salt, this peak widens again, indicating a smaller amount of protein on the GO's surface. Similar to graphene, bare SWNT had no functional groups and therefore showed a smooth spectrum (Figure 5.4c). The sample containing SWNT and protein were again almost identical to that containing SWNT only, which indicated that there was a negligible amount of protein bound to the SWNT. The sample containing SWNT, protein, and salt had peaks at 1628 and 3619 cm^{-1}, corresponding respectively to the amide and amine groups of lysozyme. Robustness of these peaks indicated significant adsorption of protein by SWNT.

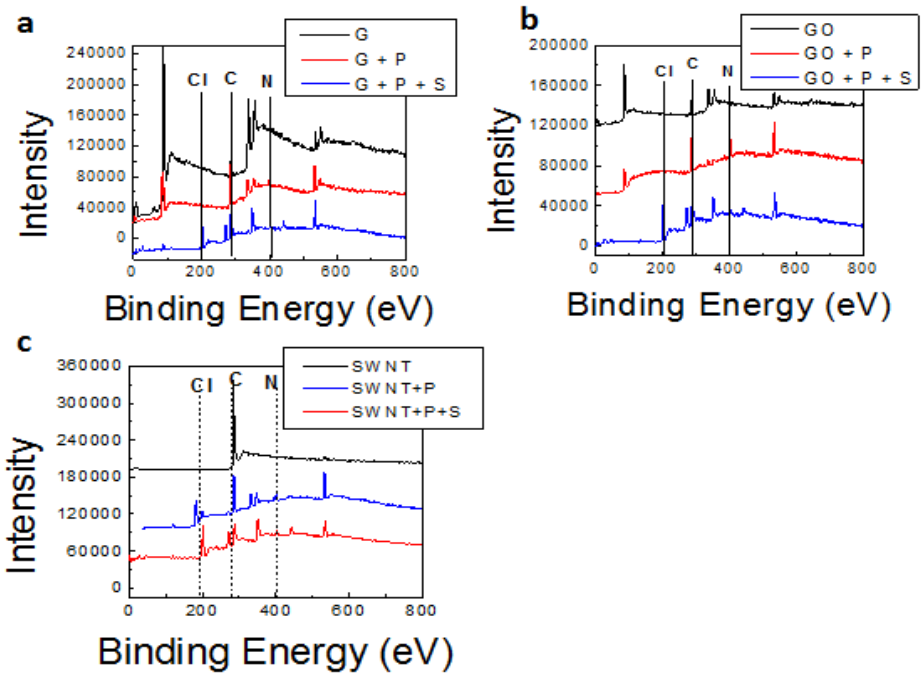

Figure 5.5. XPS of (a) G, (b) GO and (c) SWNT in DI water solution, protein solution, and protein-salt solution. Samples were prepared on PVDF filters by gravity filtration, and allowed to dry at room temperature. P, protein; S, salt.

XPS was used to further confirm the presence of adsorbed protein on nanomaterials. Figure 5.5 shows the scans of the nanomaterials in the presence of the protein and protein in the presence of salts. Using the XPS spectra, three distinct elements were used to identify the presence of the nanomaterial, protein, and salt. The elements were selected based on the most abundant or distinct element given in each material. Specifically, the C1s peak at ~285 eV was used to identify the carbon-based nanomaterials, N1s peak at ~400 eV was assigned for the presence of the protein, and ~C12p peak at ~199 eV. XPS spectra for all nanomaterials depicts resulted in the appearance of the N1s peak at 400 eV, which confirms the presence of the protein. This peak was not observed for the pristine samples. Upon addition of the salt, an additional peak at ~199 eV designated as Cl2p due to the salt was observed for all nanomaterial samples. It is worth noting that even in the presence of the salt, protein in the sample indicated by the peak at ~400 eV was still present. This confirms that even after the addition of the salt, protein was not removed from the nanomaterials.

5.3.5. Zeta potential measurements

GO and SWNT exhibited opposing lysozyme adsorption patterns in the presence of salts, both mono- and divalent (Figure 5.3); e.g., with addition of 0.2 M of Ca^{2+}, lysozyme adsorption was reduced by ~300 mg/g on GO while increasing by ~250 mg/g on SWNT surfaces. To further verify the influence of Ca^{2+} ion presence on adsorption behavior, zeta potential measurements were performed on GO and SWNT nanoparticles after protein adsorption at 0 and 0.2 M Ca^{2+} (Figure 5.6). The highest zeta potential value was for GO in 0.0 M $CaCl_2$, which correlated well with high protein adsorption as

observed in Figure 5.3b. Lysozyme carries a net positive charge, while GO carries a negative charge at this pH, which facilitated high protein adsorption on GO surface in the absence of ions.

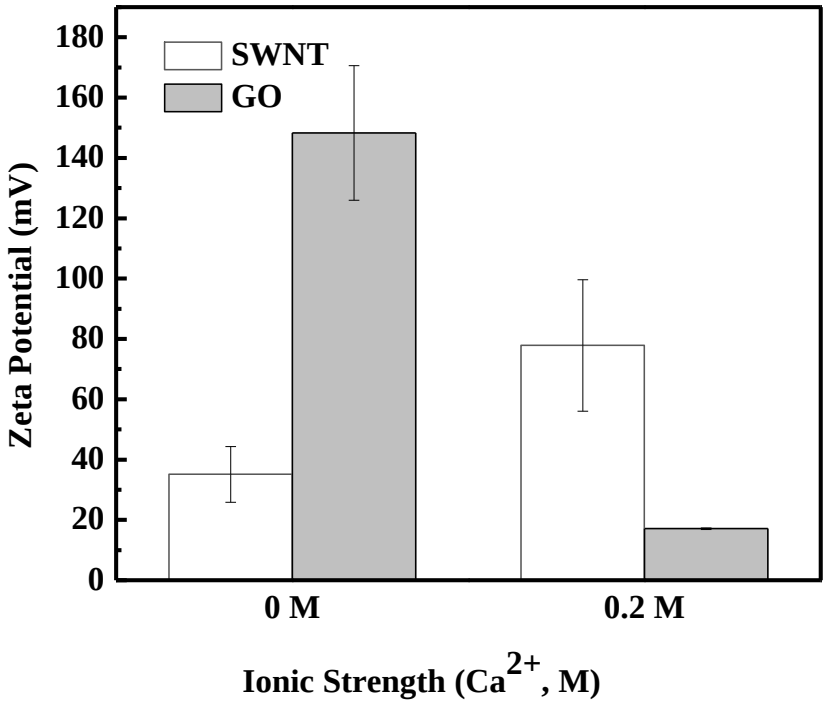

Figure 5.6. Zeta potential values of GO and SWNT nanoparticles in the presence of lysozyme at different concentrations of Ca^{2+} (0 and 0.2 M). The nanomaterial concentration was 0.4 mg/mL and the protein concentration was 0.2 mg/mL.

On the other hand, in the presence of 0.2 M Ca^{2+}, Zeta potential dropped to ~20 mV in GO samples as the amount of protein adsorption was significantly reduced (Figure 5.3b). Similarly, net surface charge on SWNT surface was found to be strongly correlated with the amount of adsorbed lysozyme. In the presence of 0.2 M Ca^{2+}, Zeta potential values in the SWNT samples increased from ~30 mV to ~80 mV which confirmed the

increased protein adsorption observed previously (Figure 5.3b). Overall, the differences in adsorbed protein correlate well with change of total surface potential on both GO and SWNT surfaces.

5.3.6 Adsorption isotherms of lysozyme.

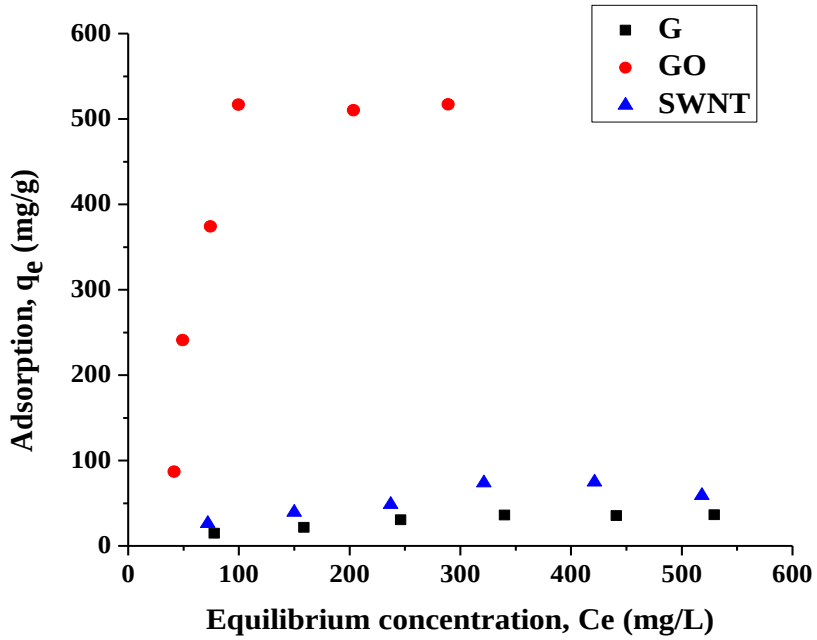

Figure 5.7. Adsorption isotherm of lysozyme on G, GO and SWNT nanomaterials. The nanomaterial concentration was 0.5 mg/mL in all samples. All samples were incubated for 3 h at room temperature.

The adsorption isotherms of lysozyme on G, GO, and SWNT surfaces are presented in Figure 5.7. Overall, with increasing equilibrium lysozyme concentration, increasing adsorbed lysozyme was observed on all three nanomaterials. However, GO exhibited the highest capacity for lysozyme adsorption among the three nanomaterials at all concentrations of lysozyme. To better explain lysozyme adsorption phenomena on the nanomaterials, the adsorption tests data were fit to Langmuir, Freundlich, and Temkin

models. and the calculated fitting parameters for lysozyme are presented in Figure 5.8 and Table 5.2.

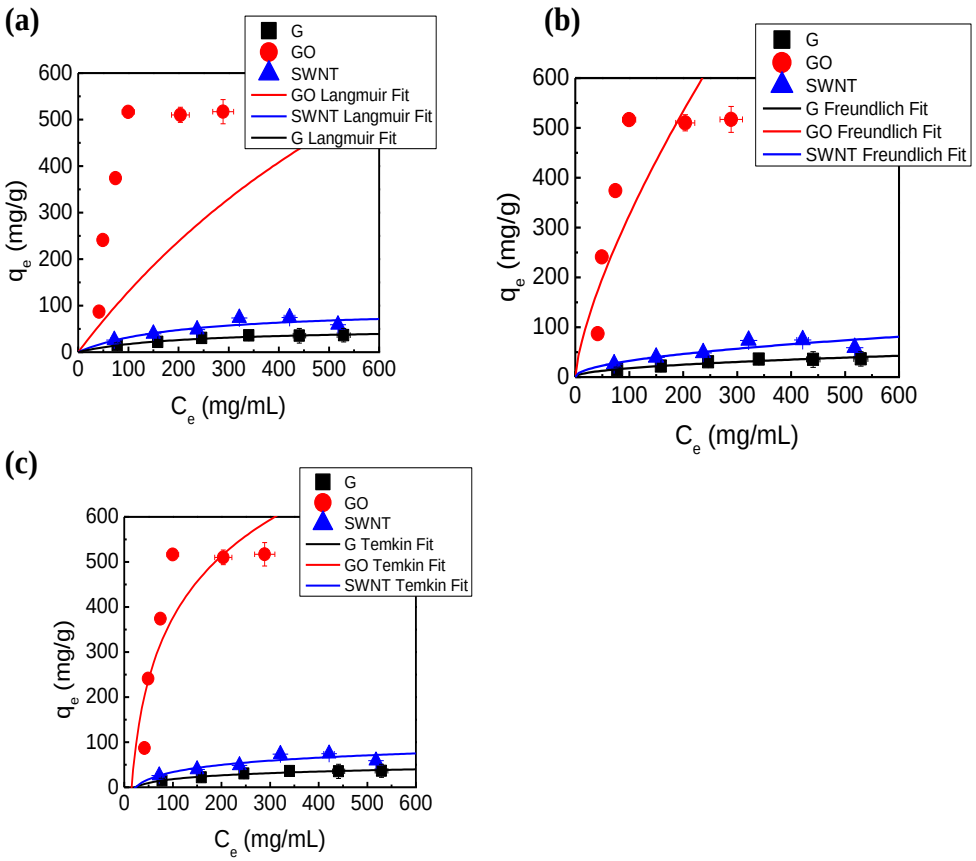

Figure 5.8. Model fitting of lysozyme adsorption on G, GO and SWNT using (a) Langmuir (b) Freundlich (c) Temkin. The nanomaterial concentration was 0.5 mg/mL in all samples. All samples were incubated for 3 h at room temperature.

The Langmuir model was found to be the best fit for lysozyme adsorption on G and SWNT (R^2 =0.98 t and 0.94, respectively). On the other hand, it was not a good fit for lysozyme adsorption on GO (R^2 = 0.66); however, the fitting parameter of q_m (1428.57 mg/g) was indicative of relatively high adsorption capacity of GO (Experimental q_m~500 mg/g). Similarly in case of Freundlich model, it was observed that lysozyme adsorption on G and SWNT could be fitted better compared to that for GO

(based on R^2 values in Table 5.2). However, the fitted Freundlich constants (K_F) for G, GO and SWNT are in good approximation with Freundlich constants reported in similar studies with lysozyme adsorption to hybrid adsorbents [198]. In case of Temkin model, the higher values of K_T (198.97 and 23.099 on GO and SWNT, respectively) suggest electrostatic interaction as a possible mechanism of lysozyme adsorption on GO and SWNT. Abundance of –OH and –COOH groups on GO surface facilitates its electrostatic bonding with lysozyme. Similarly, along with pi-pi interactions, electrostatic bonding on defected sites on SWNT has been reported as a significant mechanism of lysozyme adsorption on SWNT [194].

Table 5.2. Fitting parameters of Langmuir, Freundlich and Temkin models for adsorption of lysozyme on G, GO and SWNT.

	Langmuir Parameters			**Freundlich Parameters**			**Temkin Parameter**	
	R^2	q_m (mg/g)	K_L (L/mg)	R^2	K_F (L/mg)	n	R^2	K_T
G	0.983	52.083	0.005	0.945	2.003	2.032	0.949	12.15
GO	0.656	1428.571	0.001	0.616	1.099	1.396	0.741	198.97
SWNT	0.943	95.238	0.005	0.849	7.788	1.964	0.767	23.099

5.3.7. Application of G, GO and SWNT as adsorbent for wastewater treatment.

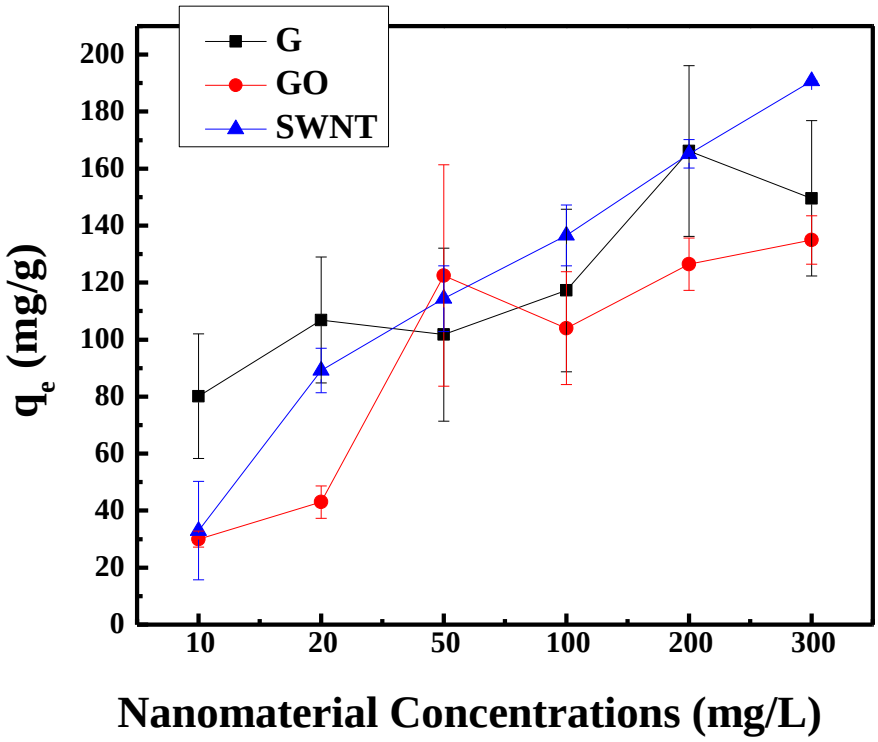

Figure 5.9. Effects of nanomaterial exposure on adsorption of proteins present in wastewater. Wastewater samples were incubated by varying concentrations of G, GO, and SWNT for 3 h at room temperature at 200 rpm.

The results show that G, GO, and SWNT can remove lysozyme in DI water solution under different solution chemistries, indicating that they can be applied for adsorption. However, natural aquatic systems generally contain a wide variety of proteins and often other types of natural organic matter that can influence adsorption by these nanomaterials [86]. The presence of multiple proteins mixed with other organic matter may influence the adsorption capacity of any adsorbent. Therefore, dose-dependent adsorption capacities of G, GO, and SWNT to total protein present in wastewater were also investigated (Figure 5.9). Overall, with increase in nanomaterial dose, increased

adsorption of natural proteins present in wastewater was observed for G, GO and SWNT. Protein removal capacities (~ 120-160 mg/g at 250 mg/L) of these three nanomaterials from wastewater were considerably higher than the previously reported protein removal capacity (26.6 mg/g at 250 mg/L) of activated carbon from wastewater [86]. These results suggest that G, GO, and SWNT are significantly more efficient than the traditional adsorbent, activated carbon, for removing organic fouling agents like protein. Although in pure lysozyme solution GO exhibited the highest adsorption capacity, in wastewater the adsorption capacities were not very different among the three nanomaterials. This could be due to the complex nature of wastewater proteins, NOMs and other solution chemistry factors. Further studies could be performed to investigate the effects of wastewater composition and chemistry on the adsorption behavior of these adsorbents.

5.4. Conclusions

In this study, we investigated the protein adsorption capacities of three widely used carbonaceous nanomaterials: G, GO, and SWNT. Overall, GO exhibited the highest adsorption capacity (~500 mg protein/g nanomaterial) for lysozyme among the three tested nanomaterials at equilibrium. This could be attributed to the presence of –OH and –COOH functional groups which facilitated electrostatic attraction with lysozyme. The effects of varying solution chemistry were investigated by varying pH conditions and the concentrations of mono- and divalent salts. No significant effects of changing solution pH on the lysozyme adsorption were observed for the three nanomaterials. However, the presence of mono- and divalent ions significantly affected the adsorption of lysozyme to GO and SWNT. At a salt concentration of 0.2 M, a sharp decrease and increase in

lysozyme adsorption were observed for GO and SWNT, respectively. All three nanomaterials were found to be significantly more efficient in removing total proteins present in wastewater samples compared to activated carbon reported in literature.

Chapter 6 Environmental Impact of GO on Wastewater Microbial Community Using Culture Dependent Methods

"Adapted with permission from (Ahmed, F.; Rodrigues, D. F., Investigation of acute effects of graphene oxide on wastewater microbial community: A case study. *Journal of Hazardous Materials* 2013, 256–257, (0), 33-39). Copyright (2013) Elsevier."

6.1. Rationale and Objectives

Graphene oxide (GO) is the functionalized form of graphene containing epoxy, hydroxyl, and carboxyl groups [57, 208]. GO possesses excellent electrochemical properties, hence, it has wide applications in electronics, biosensors, pipes, semiconductor, and packaging in both pure and nanocomposite forms [209, 210]. Due to the potential wide utilization of this nanomaterial, it is expected that wastes containing this nanomaterial will be generated and end up in landfills and wastewater treatment plants. A typical wastewater treatment plant utilizes the functions of diverse groups of microorganisms for degradation of organic matter, remediation of toxic or carcinogenic compounds and removal of excess nutrients (nitrogen and phosphorus) to reduce the pollution of receiving waters [211]. However, contaminants in the wastewater influent may adversely affect the functions of these microorganisms. In recent years, disposal and fate of nanomaterials in aquatic systems have become a matter of concern; however very few studies are available on this topic. One study recently demonstrated that high loads (219 mg/L) of single walled carbon nanotubes (SWNT) can differentially impact various microbial communities in activated sludge processes and adversely affect treatment efficiency [212].

In the case of GO, no studies so far have investigated the effects of GO on the wastewater processes. However, the fact that SWNT, like GO, is also made of graphene

and presents adverse effects to activated sludge processes, it is reasonable to hypothesize that GO will also present toxic effects to the wastewater microbial community. Additionally, several studies have reported that better dispersion and longer contact time of carbon-based nanomaterials with pure bacterial cultures increase their antimicrobial effects [2, 43, 172, 174]. When comparing GO to SWNTs, GO presents stronger hydrophilic nature and is more stably dispersed in aqueous solution than SWNTs. Hence these properties can potentially enhance the contact of GO with microbial communities and produce stronger adverse effects to the wastewater treatment process than SWNTs.

Furthermore, in recent studies investigating the antibacterial properties of GO to pure bacterial cultures, it was demonstrated that GO is toxic to pure bacterial cultures (Gram-positive and Gram-negative) on both planktonic and biofilm stages [38, 52, 213]. In these studies, depending on the concentrations (~40-80 mg/L), significant levels of inactivation (~60-80%) were observed in pure cultures [52, 213, 214]. So far, all these studies on the antimicrobial properties of GO were done using microorganisms in pure cultures under controlled laboratory conditions. However, natural and engineered aquatic systems are more complex than the simplified system used in these studies in terms of microbial community, solution chemistry, nanomaterial aggregation, and presence of suspended particles and natural organic matter. Therefore, more complex environments need to be investigated to determine the real impact of GO to the environment and its effect on the normal functions of the ecosystem [38, 52].

The global market for graphene-based products, such as graphene, is projected to increase in 5 years in 51.7% and reach a global market of $122.9 M in 2017 and $986.7 M in 2022 [4]. Therefore, wastewater treatment plants can potentially experience an acute

exposure to this nanomaterial, i.e. short term exposure to high GO concentrations (ppm level). The objective of this study is to evaluate the effects of acute exposure of wastewater microbial communities to GO, using batch scale tests. The short term effects of GO on wastewater microbial communities were evaluated in terms of metabolic activity and bacterial inactivation. The effects of GO on wastewater process performance were evaluated through bacterial removal of organic carbon (Biochemical Oxygen Demand, BOD), removal of nutrients (ammonia nitrogen, NH_3-N and phosphate, PO_4^-), effluent quality (turbidity), and sludge quality (dewatering properties).

6.2. Materials and Methods

6.2.1. GO Preparation and Characterization

GO was prepared by the modified Hummers method [197]. All chemicals were reagent grade and were purchased from Sigma-Aldrich and Fisher Scientific, USA. Briefly, graphite flakes (Alfa Aesar, USA) were allowed to react with $NaNO_3$ and concentrated H_2SO_4 for 30 min in an ice bath. Later, oxidation was carried out by adding $KMnO_4$ and incubating at 35 °C for 12 h. Further oxidation was carried out by adding H_2O_2 at 90 °C in oil bath. The resultant mixture was sieved out with 425 and 250 µm US Standard Testing Sieves to remove any remaining graphite flakes. The resultant solution was centrifuged repeatedly with base and acid washing steps to neutralize pH to 7.0. The GO pellet was collected and washed with methanol and dried for 3 days in a vacuum oven. Then, the dried GO pellets were suspended in deionized water (DI) to prepare GO stock solutions with a concentration of 500 mg/L and were homogenously dispersed by probe sonication (5 min) (Tekmar, USA) and bath sonication (24 h). Prior to the toxicity assays, the stock solution was vortexed for a few seconds.

The characterization of the prepared GO was carried out using atomic force microscopy (AFM) to examine morphology and X-ray photoelectron spectroscopy (XPS) to determine the functional groups. The topographical measurement of the nanomaterial was done under ambient conditions with a PicoSPM II (PicoPlus, Molecular Imaging-Agilent Technologies) using the intermittent contact mode. The GO sample used for AFM measurement was a spin coated GO film onto indium tin oxide (ITO) substrate.

XPS measurements were performed using a PHI 5700 X-ray photoelectron spectrometer equipped with a monochromatic Al K X-ray source (h=1486.7 eV) incident at 90° relative to the axis of a hemispherical energy analyzer. The spectrometer was operated both at high and low resolutions with pass energies of 23.5 eV and 187.85 eV, a photoelectron take off angle of 45 ° from the surface, and an analyzer spot diameter of 1.1 mm. The survey spectra were collected from 0 to 1400 eV, and high resolution spectra were obtained for photoelectrons emitted from C1s and O1s. All spectra were collected at room temperature with a base pressure of 1 x10 $^{-8}$ torr. Electron binding energies were calibrated with respect to the C1s line at 284.5 eV (C-C). A PHI Multipak software (version 5.0A) was used for all data processing. The high resolution data were analyzed first by background subtraction using the Shirley routine and a subsequent non-linear fitting to mixed Gaussian-Lorentzian functions.

6.2.2. Wastewater Sample Collection and Preparation

Activated sludge samples were collected from the aeration tank of Sims South Bayou Wastewater Treatment Plant (Houston, TX). This treatment plant uses conventional activated sludge process with no enhanced phosphorus or nitrogen removal

process. Briefly, fresh activated sludge samples were collected and transported to the laboratory inside a styrofoam container filled with ice packs to maintain the samples at 4^{o}C. The collection and preparation of the wastewater samples were adapted from a previous study [10]. Briefly, activated sludge samples were aerated for 1 h and 20 ml was transferred to conical tubes (Corning, USA), which were used as batch reactors. Appropriate volumes of the GO stock solution were calculated and added in each reactor to attain final concentrations of 10, 20, 50, 100, 200 and 300 mg/L of GO. The GO concentrations selected for this study were based on a preliminary metabolic assay study with the activated sludge (data not shown) and on previous studies investigating acute effects of heavy metals and other nanoparticles in activated sludge. In these studies, the concentrations used were between 1 to 3000 mg/L [212, 215-217]. The incubation was carried out at room temperature in a shaker at 200 rpm (New Brunswick Scientific, USA). To evaluate short term toxic effects, the incubation time was ~5 h according to previous similar studies [212, 216]. All the tests were performed in triplicates and a paired t-test statistical analysis was performed. The physiochemical characteristics of the wastewater were measured according to the Standard methods and presented in Table 6.1 [211].

Table 6.1. Physico-chemical characteristics of the activated sludge samples.

Total suspended solids, TSS (mg/L)	2666.6±942.8
Dissolved oxygen, DO (mg/L)	9.81±0.83
pH	7.3±0.37
Ammonia-nitrogen, NH_3-N (mg/L)	1.46±0.35
Phosphate, PO_4^- (mg/L)	5.3±0.56

6.2.3. Bacterial Metabolic activity and Viability Assay

The microbial metabolic activity assay was performed with the activated sludge after interaction with GO according to previously reported procedure [218]. Briefly, 100 µL of incubated activated sludge samples were transferred in a 96-well flat bottom plate (Corning, USA). A volume of 60 µL of C_{12}-resazurin (Vybrant Cell Metabolic Assay kit, Molecular Probe, USA) was added to each well. The mixtures in the 96-well plates were incubated for 15 minutes at 37 °C in the dark. In the presence of metabolic active cells, C_{12} resazurin is reduced to red fluorescent C_{12}-resofurin. The production of C_{12}-resofurin by the activated sludge was quantified with a Synergy MIX Microtiter plate reader (BioTek, USA) at 530/587 nm wavelength. Bacterial viability test was done according to the heterotrophic plate count agar methodology described in the Standard Methods [211].

6.2.4. Organic carbon degradation test

A Biochemical Oxygen Demand (BOD_5) test was performed according to the Standard Methods to investigate the bacterial capacity to degrade organic carbon in presence of GO [211]. Briefly, after 5 h incubation, 15 ml of samples from each reactor were placed and mixed in 300 ml BOD bottles. A DO probe with stirrer (YSI Incorporated) was used to read the initial DO and final DO (after 5 d incubation).

6.2.5. Removal of nutrients (Nitrogen and Phosphorus)

Removal of Nitrogen was measured by determining the conversion of ammonia (NH_3-N) to nitrate (NO_3^-) (nitrification process), while removal of phosphorus was measured in terms of phosphate (PO_4^{3-}) bacterial uptake. Soluble ammonia-nitrogen

(NH_3-N), NO_3^- and PO_4^{3-} were measured from the incubated samples according to previously described methods [211, 219]. Since nitrification is a slow process (~20 h), GO and activated sludge samples were incubated for 20 h prior to ammonia and nitrate final concentration measurements. These tests were done as follows: 5 ml of the control and the incubated activated sludge samples with GO were filtered through 0.22 µm membrane filters to remove the suspended flocs and 1 ml of the filtrate was diluted with DI water for ammonia, nitrate and phosphate quantifications. Colorimetric methods were used to quantify NH_3-N, NO_3^- and PO_4^- in the filtrate with a DR3900 spectrophotometer (Hach, USA). NH_3-N, NO_3^- and PO_4^{3-} were measured by the salicylic acid method (method 8155, Hach), cadmium reduction method (method 8039, Hach) and the ascorbic acid method (method 8048, Hach), respectively.

6.2.6. Effluent quality and sludge dewatering property

To determine the effluent quality and sludge dewatering ability, turbidity of the supernatant (nephelometric turbidity unit, NTU) and capillary suction time (CST) were measured, respectively, after the settling of the activated sludge. Both the NTU and CST were measured according to the Standard Methods [211]. Briefly, after 5 h incubation with GO, batch reactors with activated sludge samples were left to settle for a period of 2 h, which is the average residence time in the clarifier. The supernatant was removed carefully for turbidity measurement, while the settled sludge was used for CST measurement. Briefly, for the CST measurement, a stainless steel tube with inner radius of 1.5 inch was placed on a coarse type filter paper (Whatman, UK) and a 5 inch radius circle was drawn around the tube on the filter. Settled sludge (2 ml) samples were quickly

released inside the tube and the time to wet the filter from radius 1.5 to 5 inch was recorded as CST.

6.2.7. Scanning electron microscopy (SEM) and Fluorescence imaging

To observe the interaction of activated sludge flocs and microorganisms with GO, SEM and fluorescence microscopy were conducted [10, 174, 176]. Briefly, for the SEM samples, at the end of 5 h incubation, 0.5 ml of solution was taken from each reactor and fixed with 2% gluteraldehyde in 0.05M cacodyle buffer solution (Fisher Scientific, USA). Fixed samples were serially dehydrated with increasing concentrations of ethanol (25%, 50%, 75%, 95% and 100%). SEM images were acquired at 10 Kev accelerated voltage with JSM 6010LA (Jeol, USA). For fluorescence imaging, 0.2 ml of each sample was stained with 0.2 µl of green dye (SYTO9, Invitrogen, USA) and images were taken with a fluorescence microscope (OLYMPUS, Japan). For each sample, 10 representative images were recorded. GO dispersion in DI water was imaged under bright field condition with a fluorescence microscope (OLYMPUS, Japan).

6.2.8. Reactive Oxygen Species (ROS) production and oxidative stress

Dose dependent ROS production by GO was reported in previous studies [59]. ROS are known to cause oxidative stress in cells, hence ROS production by GO in wastewater was investigated [2, 59, 220]. ROS production was quantified as oxidation of glutathione (GSH) according to Ellman's Assay method described elsewhere [220]. GSH is a thiol containing polypeptide present in prokaryotic and eukaryotic cells which is known to protect the cells from stress caused by ROS [59, 220, 221]. Oxidation of GSH

in aqueous solution in presence of nanomaterials is an indirect measure of ROS production. Briefly, various GO concentrations in filtered wastewater were spiked with GSH in bicarbonate buffer solution in a 12 well-plate. Then, the plate was incubated for 2 h in dark to prevent any photochemical reaction. After the incubation period, the Ellman's reagent, 5,5-dithio-bis-(2-nitrobenzoic acid) (DTNB), was added and the resultant yellow solution was filtered with a 0.22 µm filter to remove GO from the solution. DTNB reacts with aqueous GSH which can be quantified colorimetrically. A volume of 200 µL of the solution was placed in a 96-well plate and quantified at 412 nm wavelength with the Synergy MIX Microtiter plate reader (BioTek, USA). The negative control did not contain GO, whereas in the positive control contained 1 mM of H_2O_2 for oxidation of the GSH.

6.3. Results and Discussions

6.3.1. Characterization of GO

Digital image of the GO in aqueous solution is shown in Figure 6.1 (a). A typical GO solution has a brownish color and is well dispersed in aqueous solution as opposed to pristine graphene in water, which is black and non-dispersible in water. Figure 6.1 (b) shows a representative atomic force microscopy (AFM) image of the spin coated graphene oxide dispersion on an indium tin oxide (ITO) surface. The AFM analysis revealed that the average interlayer spacing of exfoliated GO obtained in this work was ~ 1 nm (Figure 6.1c), indicating that exfoliation of graphite down to individual GO nanosheets was successfully achieved.

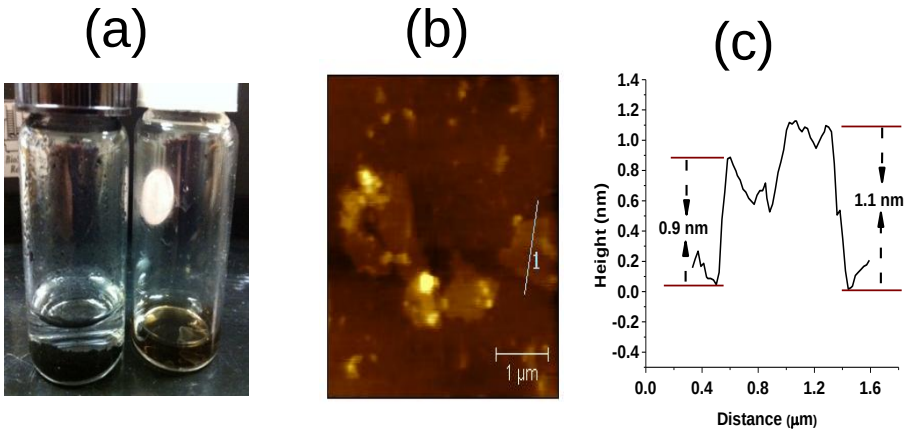

Figure 6.1. (a) Digital images of graphene oxide in water. (b) AFM image of spin coated GO on ITO substrate. (c) Height profile of the GO (labeled as 1 in Figure b).

6.3.2. Effects on Bacterial Metabolic Activity and Viability

The acute toxicity effects of GO was first evaluated through the metabolic activity assay of the wastewater bacterial community in the presence of different concentrations of the nanomaterial. In this assay, only viable bacteria are able to reduce non-fluorescent resazurin to red-fluorescent resofurin [218]. The results of this assay showed that, at all GO concentrations tested, significant inhibition of the wastewater microbial community metabolic activity (~20-70%) was observed (Figure 6.2). Additionally, the results show that the toxicity of the nanomaterial is concentration dependent, since at higher GO concentrations (100-300 mg/L), significantly higher inhibition of bacterial metabolic activity (~50-70%) was observed. The GO concentration at 300 mg/L showed statistically significant inhibition of metabolic activity compared to the other GO concentrations. These results agree with several toxicity studies with bacterial pure cultures, where significant inhibition of the bacterial metabolic activity was observed in the presence of GO and other carbon-based nanomaterials (e.g. carbon nanotubes and fullerenes) [2, 38, 52, 53].

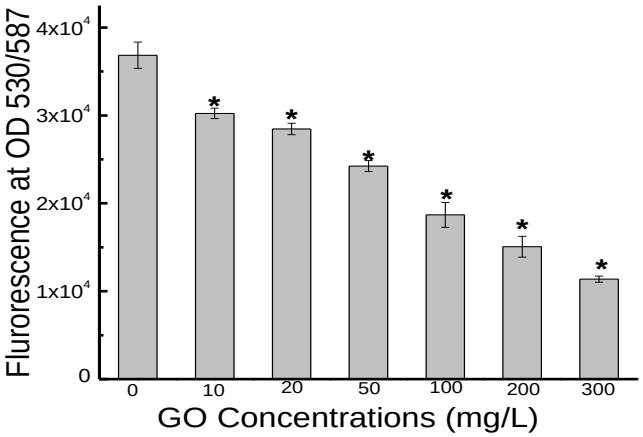

Figure 6.2. Metabolic activity of the bacteria in activated sludge after 5 h incubation with different concentrations of GO. * refers to statistically significant different results between control and the corresponding sample.

The antibacterial effect of GO in wastewater was further verified by the plate count method. The results from the plate counts corroborated the metabolic activity assay, since the increase in GO concentrations resulted in reduced numbers of viable bacteria (Figure 6.3).

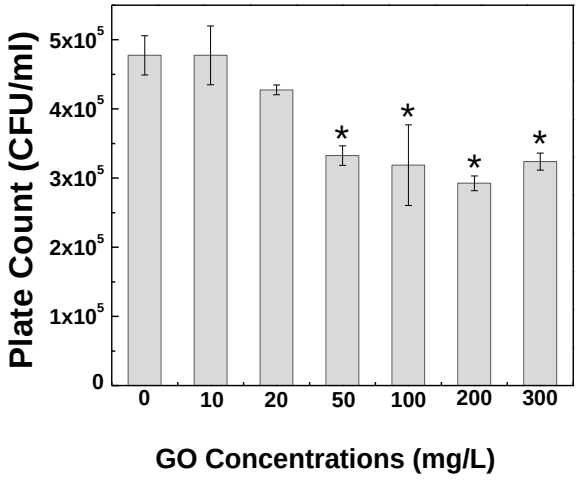

Figure 6.3. Enumeration of total viable bacterial cells (CFU/ml) in activated sludge after 5 h incubation with different concentrations of GO. * refers to statistically significant different results between control and the corresponding sample.

The significant reduction of metabolic activity (~50-70%) at GO concentrations of 100-300 mg/L, resulted in ~35% bacterial growth inhibition. This difference in the bacterial growth inhibition compared to bacterial metabolic activity was previously observed in antibacterial studies with other carbon-based nanomaterials [2]. This difference was explained by the fact that bacterial cells will, under unfavorable conditions, reduce their metabolic activity and resume growth when switched to favorable conditions (i.e., addition of nutrients or removal of an inhibitor), like a bacteriostatic agent [2, 177]. This reduced bacterial metabolic activity and viability results suggest that GO can potentially inhibit the essential biological functions of bacteria in the activated sludge process.

6.3.3. Inhibition of Biodegradation of Organic Carbon

In order to verify the acute effect of GO in the wastewater treatment process, a standard BOD_5 test was conducted to determine the ability of microorganisms to remove the organic matter in the wastewater under aerobic conditions. The results showed > 50% reduction in the BOD_5 at all concentrations of GO (Figure 6.4). These results can be explained by the lower bacterial metabolic activity observed in the metabolic activity assay (Figure 6.2). During the BOD_5 tests, the lower metabolic activity of microorganisms in the presence of the nanomaterials led to reduced oxygen consumption by aerobic microorganisms during the metabolization of the organic waste in the wastewater, hence leading to a reduction in the BOD_5 values. It is noteworthy that the different GO concentrations in the activated sludge did not show considerable variation in

their effect on the BOD values, which suggests that the minimum concentration to inhibit degradation of organic matter is around 10 mg/L. In a similar study with multi-walled carbon nanotubes (MWNT), ~50 % BOD reduction was observed at various concentrations. However, with MWNT, the concentrations used were much higher (1440 to 3240 mg/L) than the GO concentrations used in this study [222].

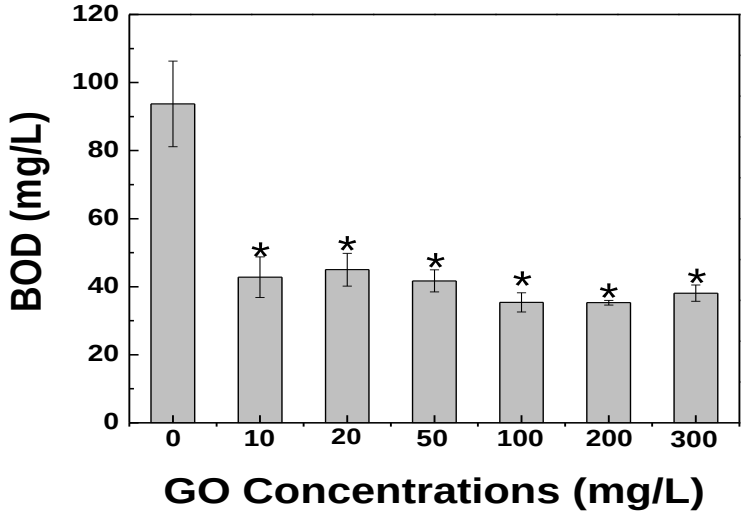

Figure 6.4. 5-day BOD results of the activated sludge samples with different concentrations of GO. * refers to statistically significant different results between control and the corresponding sample.

6.3.4. Effects of GO on the Biological Process of Nitrogen Removal and Phosphorus Accumulation

Nitrogen (as NH_3-N) and phosphorus (as PO_4^{3-}) are two major nutrients that must be removed from the influent during wastewater treatment. The microbial communities in the activated sludge responsible for removing nitrogen and phosphorus are ammonia oxidizing bacteria (AOB) and polyphosphate accumulating organisms (PAO), respectively. Details of the chemical processes of nitrogen and phosphorus removal are described in the Supporting Information section. Briefly, in a functional activated sludge

process, ammonia is converted to nitrate, through the aerobic process of nitrification. In our study, with increasing GO concentrations, we observed ammonia accumulation due to reduced conversion of ammonia to nitrate (Figure 6.5), which suggests inhibition of nitrifying bacteria in the activated sludge sample in the presence of GO.

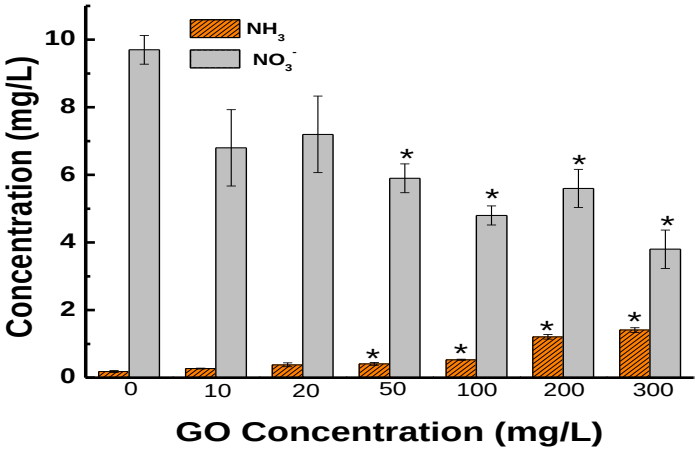

Figure 6.5. Concentrations of NH_3-N and NO_3^-, measured in activated sludge samples incubated with different GO concentrations. * refers to statistically significant different results between control and the corresponding sample.

Another important microbial community in the wastewater treatment process is the PAO community, which is responsible for removing phosphorus nutrients from the wastewater. In the wastewater process, phosphorus exists as PO_4^- which gets accumulated by PAO and hence removed from the wastewater.

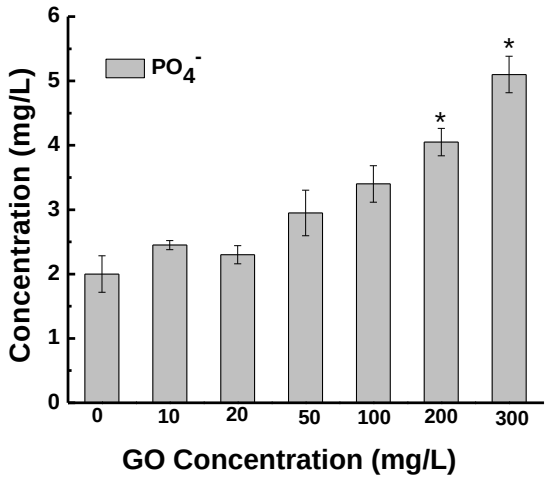

Figure 6.6. Concentrations of PO_4^{3-}, measured in activated sludge samples incubated with different GO concentrations. * refers to statistically significant different results between control and the corresponding sample.

In our results (Figure 6.6), significant effects of GO on the PAO microbial community were observed at higher concentrations of GO (200 – 300 mg/L). At these high concentrations, the activity of PAO was inhibited since PO_4^- concentrations in the wastewater did not decrease over time as observed in the control samples.

Therefore, these results suggest that acute exposure of the wastewater microbial community to GO, especially at higher concentrations (~100-300 mg/L), can inhibit the activated sludge microbial community functions, such as ammonia degrading and phosphate accumulating microbial communities.

6.3.5. ROS Production and Oxidative Stress

Several studies have shown that carbonaceous nanomaterials like GO can produce chemically reactive species in aqueous solution and can adversely impact microbial and eukaryotic cell structures [59, 220, 221, 223]. In our study, significantly higher ROS production was found at high concentrations of GO in the wastewater samples when

compared to the control samples (Figure 6.7). Previous studies with GO in aqueous solution demonstrated ROS production was a dose dependent phenomena [59]. The increased loss of GSH at higher concentrations of GO samples (200 and 300 mg/L) suggests that ROS production could be contributing to the increasing toxicity observed (~60-70%, Figure 6.2) to the microbial community at those concentrations. Although we did not determine the exact toxicity mechanism generated by the ROS on the wastewater microbial community, other studies suggest that ROS can cause severe damages to bacterial DNA, proteins and cell membranes as a cause for GO toxicity [8, 11, 16].

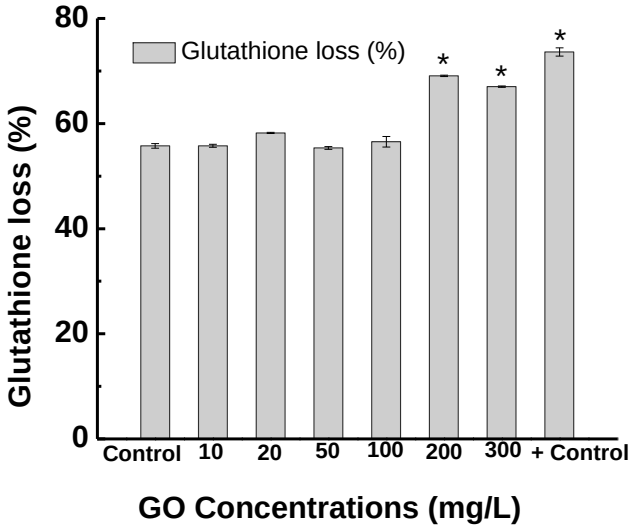

Figure 6.7. Loss of Glutathion as an indicator of ROS production. * refers to statistically significant different results between control and the corresponding sample.

6.3.6. Effects of GO on Sludge Settling and Dewatering

In a typical activated sludge process, turbidity of the effluent is an indicative of the effectiveness of the treatment process and successful removal of organic matter from the wastewater. High turbidity carries two implications in the disinfection process before the discharge into receiving waters. First, higher turbidity signifies higher organic matter

content in the water. To treat such wastewater, higher concentrations of disinfecting agent (chlorine) will be required, since organic matter can reduce the availability of free chlorine for microbial disinfection [224]. Secondly, the presence of organic matter increases formation of carcinogenic disinfection by-products (DBP), since chlorine reacts with organic matter to produce DBP [184]. Therefore it is important to determine the effect of GO on the turbidity of the effluent. In a typical wastewater treatment plant, turbidity of the supernatant of the settled sludge in a clarifier unit is routinely measured to monitor the effectiveness of the treatment process. We performed similar settling tests in the batch reactors to observe any potential effects of GO on the turbidity of the supernatants.

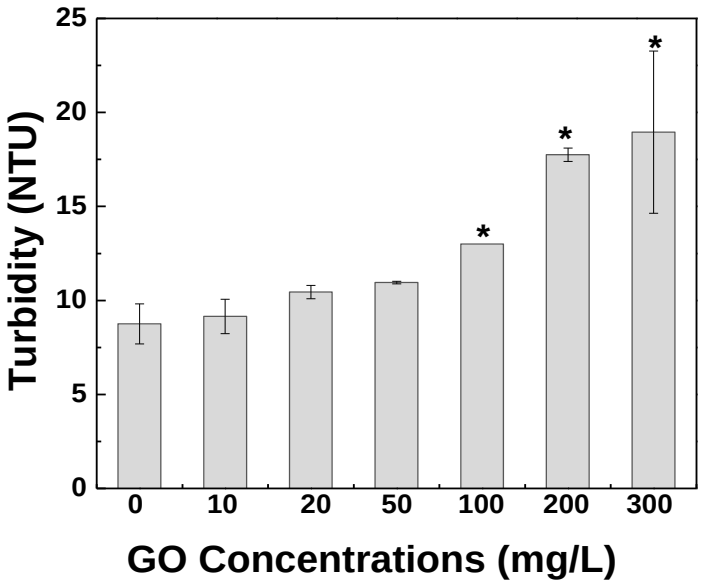

Figure 6.8. Turbidity (NTU) of the supernatant of activated sludge samples after 2 h settling period.* refers to statistically significant different results between control and the corresponding sample. Control sample does not contain any nanomaterial.

The results of the sludge settling test showed that with the increase in GO concentrations, the turbidity of the effluent steadily increased (Figure 6.8). Microscopic analysis of the supernatant revealed that increased turbidity is attributed to the presence of both suspended GO and attached organic matters onto GO surfaces. Overall it was observed that the addition of GO to the wastewater effluent increased the final effluent turbidity.

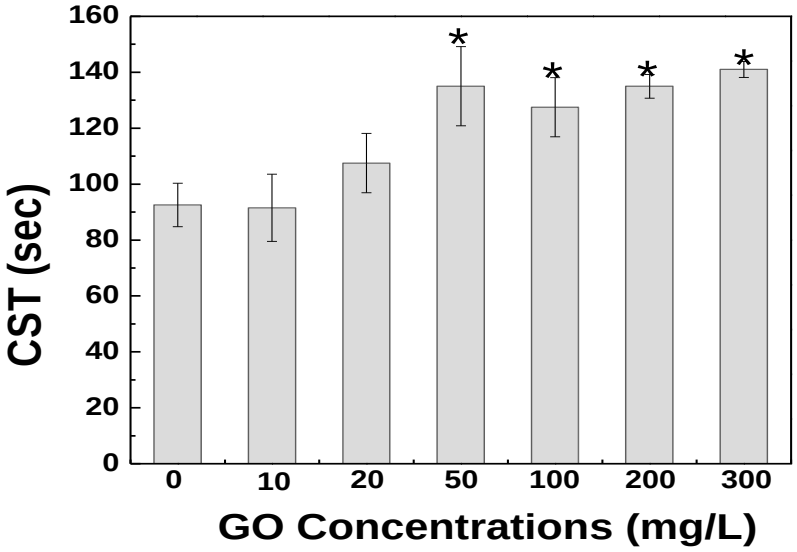

Figure 6.9. Capillary suction time (CST) required for dewatering of settled activated sludge samples after 2 h settling period. * refers to statistically significant different results between control and the corresponding sample.

The sludge dewatering, or removing water from the sludge, is the final process in the wastewater treatment. The dewatering of sludge is very important since dewatered solids are cheaper and easier to incinerate, produce less offensive smells, and reduce volume and disposal costs in landfills [225]. The typical values of municipal sludge dewatering is variable (CST>100 sec) and is highly dependent on the sludge composition

and treatment steps (addition of polymer or other thickeners). In the present study, the results of the dewatering tests showed that with increasing GO concentrations, the dewatering capacity of the activated sludge is significantly reduced, since the capillary suction time (CST) increased. Increase of dewatering time was observed to be ~45% at GO concentrations of 50 mg/L and above compared to controls (Figure 6.9). The possible cause for this phenomenon could be a combination of both chemical reactivity and antimicrobial characteristics of GO. However these potential mechanisms need to be further investigated.

6.3.7. Interaction of GO and Activated Sludge

The fluorescence images from the sludge samples incubated with GO shows that GO nanosheets accumulated inside the floc matrix (Figure 6.10.c). SEM images show adsorption of bacteria and other microorganisms to the GO nanosheets (Figure 6.10.f). Several studies suggested that the accumulation of nanomaterial in activated sludge flocs could result into longer retention of GO in the treatment system and therefore pose chronic toxicity [10]. Future studies are needed to better understand the effects of GO accumulation in the activated sludge flocs as well as the potential chronic toxicity of this nanomaterial to the microbial community.

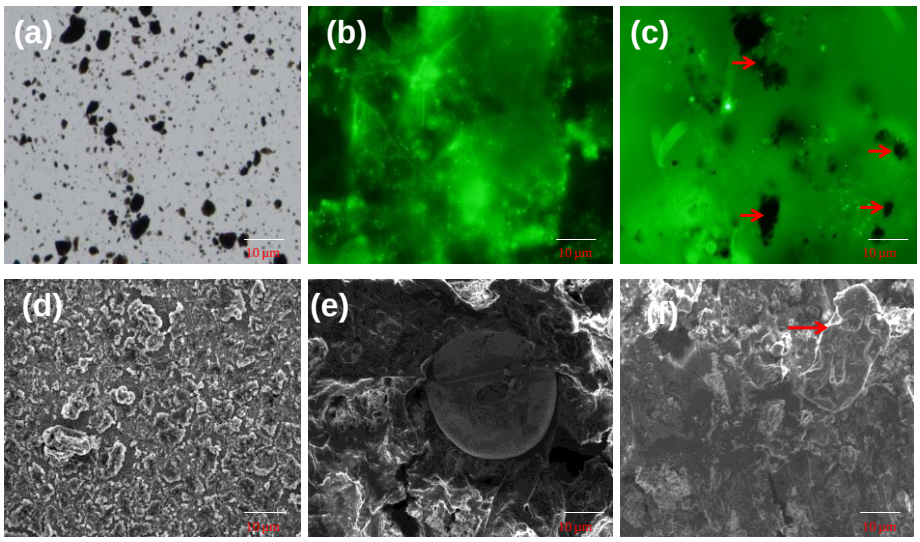

Figure 6.10. (a) Bright field image of aqueous suspension of GO; fluorescence image of (b) control activated sludge and (c) activated sludge with GO. SEM image of (d) aqueous suspension of GO, (e) control, and (f) activated sludge with GO. Red arrow shows GO sheets.

6.4. Conclusion

This study shows that acute exposure of activated sludge to GO can impact the wastewater microbial communities. Bacterial metabolic activity was significantly compromised in the presence of GO, which indicates that GO has the potential to hinder the essential microbial functions needed in activated sludge processes, such as removal of organic matter and other nutrients from the wastewater. The presence of GO in the activated sludge led to reduced BOD_5 values and low nitrogen and phosphorus removal by the biological treatment process, which can potentially lead to excess of organic matter, nitrogen and phosphorus, respectively, discharge into receiving waters from the treatment plants. Furthermore, GO also negatively impacted the effluent quality and

sludge dewaterbility, which can cause regulatory violations and increased disposal cost of sludge, respectively. As applications and disposal of engineered nanomaterials, such as GO, are in rapid rise, these findings suggest that further studies, especially on the chronic exposure of this nanomaterials to the wastewater microbial community is needed. Both acute and chronic microbial exposures to GO are essential for a complete understanding of the effects of GO to the wastewater treatment process and prevention of their adverse effects to the treatment performance.

Summary and Future Directions

The present study determined that SWNT and GO can be successfully embedded into PVK to form stable nanocomposite suspensions and coatings. The presence of PVK in the nanocomposite allowed the dispersion of the nanomaterials and immobilization of a homogeneous film. The PVK-SWNT and PVK-GO nanocomposites exhibited significant toxicity towards bacteria in planktonic and biofilm stages. The principal mechanism of bacterial inhibition was found to be due to the cell membrane damage in the presence of SWNT and GO nanoparticles. These findings show the potential use of PVK-SWNT and PVK-GO nanocomposites for antimicrobial coatings in biomedical applications. The application of the antimicrobial nanocomposites was further investigated for drinking water treatment. Nitrocellulose membranes coated with PVK-SWNT effectively removed and inactivated bacterial cells and prevented biofilm growth. Due to the small load of SWNT (3 wt%), PVK-SWNT exhibited significantly less cytotoxicity to mammalian cells, which shows great promises for possible applications in drinking water treatment.

Again, a systematic study to investigate the capacity of carbon-based nanomaterials (G, GO and SWNT) to remove biofouling agent (protein) was performed for water treatment purposes. GO showed the highest adsorption capacity for the model protein, lysozyme (~500 mg protein/g of nanomaterial), which could be attributed to the strong electrostatic interaction between the negatively charged GO and the positive sites in the protein structure. However, adsorption properties of SWNT and GO were found to be highly dependent on the solution chemistry i.e., ionic strength. Interestingly, all three

nanomaterials were found to be significantly more efficient in removing total proteins present in wastewater samples compared to activated carbon. The preliminary results obtained from this study could be utilized for developing efficient nanomaterial based adsorbents for water purification applications. On the other hand, environmental implications of nanomaterial (GO) were found to be significant. In case of acute exposure, GO was found to significantly compromise the metabolic activities of the microbial communities in activated sludge; hence adversely impact their biological functions to degrade organic carbon, nitrogen and phosphorus. The antimicrobial mechanism of GO to wastewater bacteria was found to be adsorption to bacterial cells and production of reactive oxygen species (ROS).

Future Directions:

1. The antimicrobial properties of PVK-SWNT and PVK-GO nanocomposite coatings need to be tested under different environmental conditions with diverse group of microorganisms.

2. The bacterial removal and inactivation properties of the PVK-SWNT coated membranes should be tested with natural waters collected from rivers, lakes or other drinking water sources. Since, it is expected that the presence of high load of organic matter, varying pH and salinity will affect the efficiency of nanocomposite coated membranes.

3. The adsorption study of SWNT and GO with lysozyme can be further extended to other types of proteins. Different protein structures and surface charge distributions on protein surfaces may affect the interaction mechanism with the nanomaterials. A better

understanding of the protein-nanomaterial interaction mechanism will be helpful to design more efficient nanomaterial-based adsorbents for water treatment.

4. To better understand the effects of nanomaterials on diverse microbial communities, culture independent methods, e.g., DNA microarray, can be utilized. By analysing the gene expression of the microbial community, we may get a better understating about the inhibitory effects of GO on various bacterial communities. This will help to identify a safe environmental concentration of nanomaterials to better regulate their disposal.

References

[1] V. Singh, D. Joung, L. Zhai, S. Das, S.I. Khondaker, S. Seal, Graphene based materials: Past, present and future, *Progress in Materials Science*, 56 (2011) 1178-1271.

[2] S. Kang, M. Herzberg, D.F. Rodrigues, M. Elimelech, Antibacterial Effects of Carbon Nanotubes: Size Does Matter!, *Langmuir*, 24 (2008) 6409-6413.

[3] S. Kang, M.S. Mauter, M. Elimelech, Microbial cytotoxicity of carbon based nanomaterials: Implication of river water and wastewater effluent., *Environmental Science and Technoogy*, 43 (2009) 2648-2653.

[4] D.Y. Lyon, P.J.J. Alvarez, Fullerene Water Suspension (nC60) Exerts Antibacterial Effects via ROS-Independent Protein Oxidation, *Environmental Science and Technology*., 42 (2008) 8127-8132.

[5] I.E. Mejias Carpio, C.M. Santos, X. Wei, D.F. Rodrigues, Toxicity of a polymer-graphene oxide composite against bacterial planktonic cells, biofilms, and mammalian cells, *Nanoscale*, 4 (2012) 4746-4756.

[6] H. Pelicano, D. Carney, P. Huang, ROS stress in cancer cells and therapeutic implications, *Drug Resistance Updates*, 7 (2004) 97-110.

[7] F.-M. Xu, J.-P. Xu, J. Ji, J.-C. Shen, A novel biomimetic polymer as amphiphilic surfactant for soluble and biocompatible carbon nanotubes (CNTs), *Colloids and Surfaces B: Biointerfaces*, 67 (2008) 67-72.

[8] W. Miao, G. Shim, S. Lee, S. Lee, Y.S. Choe, Y.-K. Oh, Safety and tumor tissue accumulation of pegylated graphene oxide nanosheets for co-delivery of anticancer drug and photosensitizer, *Biomaterials*, 34 (2013) 3402-3410.

[9] A.M. Pinto, I.C. Gonçalves, F.D. Magalhães, Graphene-based materials biocompatibility: a review, *Colloids and Surfaces B: Biointerface,* 104 (2013) 229-238.

[10] L.A. Luongo, X. Zhang, Toxicity of carbon nanotubes to the activated sludge process, *Journal of Hazardous Materials*, 178 (2010) 356-362.

[11] V.N. Popov, Carbon nanotubes: properties and application, *Materials Science and Engineering: Reports,* 43 (2004) 61-102.

[12] M. Paradise, T. Goswami, Carbon nanotubes – Production and industrial applications, *Materials & Design*, 28 (2007) 1477-1489.

[13] M.S. Dresselhaus, A. Jorio, A.G. Souza Filho, G. Dresselhaus, R. Saito, Raman spectroscopy on one isolated carbon nanotube, *Physica B: Condensed Matter*, 323 (2002) 15-20.

[14] W.K. Maser, P. Bernier, J.M. Lambert, O. Stephan, P.M. Ajayan, C. Colliex, V. Brotons, J.M. Planeix, B. Coq, P. Molinié, S. Lefrant, Elaboration and characterization of various carbon nanostructures, *Synthetic Metals*, 81 (1996) 243-250.

[15] J.H. Lehman, M. Terrones, E. Mansfield, K.E. Hurst, V. Meunier, Evaluating the characteristics of multiwall carbon nanotubes, *Carbon*, 49 (2011) 2581-2602.

[16] P.M. Ajayan, Carbon nanotubes: Novel architecture in nanometer space, *Progress in Crystal Growth and Characterization of Materials*, 34 (1997) 37-51.

[17] T.M. Fulghum, P. Taranekar, R.C. Advincula, Grafting Hole-Transport Precursor Polymer Brushes on ITO Electrodes: Surface-Initiated Polymerization and Conjugated Polymer Network Formation of PVK, *Macromolecules* (Washington, DC, U. S.), 41 (2008) 5681-5687.

[18] X. Ling, Y. Wei, L. Zou, S. Xu, The effect of different order of purification treatments on the purity of multiwalled carbon nanotubes, *Applied Surface Science*, 276 (2013) 159-166.

[19] M. Terrones, A.R. Botello-Méndez, J. Campos-Delgado, F. López-Urías, Y.I. Vega-Cantú, F.J. Rodríguez-Macías, A.L. Elías, E. Muñoz-Sandoval, A.G. Cano-Márquez, J.-C. Charlier, H. Terrones, Graphene and graphite nanoribbons: Morphology, properties, synthesis, defects and applications, *Nano Today*, 5 (2010) 351-372.

[20] Z. Spitalsky, D. Tasis, K. Papagelis, C. Galiotis, Carbon nanotube–polymer composites: Chemistry, processing, mechanical and electrical properties, *Progress in Polymer Science*, 35 (2010) 357-401.

[21] S. Stankovich, D.A. Dikin, R.D. Piner, K.A. Kohlhaas, A. Kleinhammes, Y. Jia, Y. Wu, S.T. Nguyen, R.S. Ruoff, Synthesis of graphene-based nanosheets via chemical reduction of exfoliated graphite oxide, *Carbon*, 45 (2007) 1558-1565.

[22] R.S. Dey, C.R. Raj, Redox-Functionalized Graphene Oxide Architecture for the Development of Amperometric Biosensing Platform, *ACS Applied Materials & Interfaces*, 5 (2013) 4791-4798.

[23] J. Duan, S. Shao, L. Ya, L. Wang, P. Jiang, B. Liu, Polylactide/graphite nanosheets/MWCNTs nanocomposites with enhanced mechanical, thermal and electrical properties, *Iran Polym J*, 21 (2012) 109-120.

[24] H. Kim, Y. Miura, C.W. Macosko, Graphene/Polyurethane Nanocomposites for Improved Gas Barrier and Electrical Conductivity, *Chemistry of Materials*, 22 (2010) 3441-3450.

[25] H. Kim, C.W. Macosko, Processing-property relationships of polycarbonate/graphene composites, *Polymer*, 50 (2009) 3797-3809.

[26] H. Kim, A.A. Abdala, C.W. Macosko, Graphene/Polymer Nanocomposites, Macromolecules, 43 (2010) 6515-6530.

[27] J.M. Lambert, P.M. Ajayan, P. Bernier, Synthesis of single and multi-shell carbon nanotubes, *Synthetic Metals*, 70 (1995) 1475-1476.

[28] Y.-w. Ma, Z.-r. Liu, B.-l. Wang, L. Zhu, J.-p. Yang, X.-a. Li, Preparation of graphene-supported Pt-Co nanoparticles and their use in oxygen reduction reactions, *New Carbon Materials*, 27 (2012) 250-257.

[29] K.K.U. Venkata, D. Shuguang, C.M. Martha, B.S. Geoffrey, Application of carbon nanotube technology for removal of contaminants in drinking water: A review, *Science of the Total Environmt*, 408 (2009) 1–13.

[30] S. Zhang, T. Shao, T. Karanfil, The effects of dissolved natural organic matter on the adsorption of synthetic organic chemicals by activated carbons and carbon nanotubes, *Water Research*, 45 (2011) 1378-1386.

[31] N.B. Saleh, L.D. Pfefferle, M. Elimelech, Aggregation Kinetics of Multiwalled Carbon Nanotubes in Aquatic Systems: Measurements and Environmental Implications, *Environmental Science & Technology*, 42 (2008) 7963-7969.

[32] M.S. Mauter, M. Elimelech, Environmental Applications of Carbon-Based Nanomaterials, *Environmental Science & Technology*, 42 (2008) 5843-5859.

[33] J. Du, S. Wang, H. You, X. Zhao, Understanding the toxicity of carbon nanotubes in the environment is crucial to the control of nanomaterials in producing and processing

and the assessment of health risk for human: A review, *Environmental Toxicology and Pharmacology*, 36 (2013) 451-462.

[34] B. Kang, D.C. Yu, S.Q. Chang, D. Chen, Y.D. Dai, Y.T. Ding, Intracellular uptake, trafficking and subcellular distribution of folate conjugated single walled carbon nanotubes within living cells, *Nanotechnology*, 19 (2008) -.

[35] E. Murugan, G. Vimala, Effective functionalization of multiwalled carbon nanotube with amphiphilic poly(propyleneimine) dendrimer carrying silver nanoparticles for better dispersability and antimicrobial activity, *Journal of Colloid and Interface Science*, 357 (2011) 354-365.

[36] S. Aslan, Z.L. Codruta, S. Kang, M. Elimelech, L.D. Pfefferle, R.V.T. Paul, Antimicrobial biomaterials based on carbon nanotubes dispersed in poly(lactic-co-glycolic acid), *Nanoscale*, 2 (2010) 1789–1794.

[37] K.L. Aillon, Y. Xie, N. El-Gendy, C.J. Berkland, M.L. Forrest, Effects of nanomaterial physicochemical properties on in vivo toxicity, *Advanced Drug Delivery Reviews*, 61 (2009) 457-466.

[38] S. Liu, T.H. Zeng, M. Hofmann, E. Burcombe, J. Wei, R. Jiang, J. Kong, Y. Chen, Antibacterial Activity of Graphite, Graphite Oxide, Graphene Oxide, and Reduced Graphene Oxide: Membrane and Oxidative Stress, *ACS Nano*, 5 (2011) 6971-6980.

[39] D.Y. Lyon, L. Brunet, G.W. Hinkal, M.R. Wiesner, P.J.J. Alvarez, Antibacterial activity of fullerene water suspensions (nC(60)) is not due to ROS-mediated damage, *Nano Lett*, 8 (2008) 1539–1543.

[40] F. Ahmed, C.M. Santos, R.A.M.V. Vergara, M.C.R. Tria, R. Advincula, D.F. Rodrigues, Antimicrobial Applications of Electroactive PVK-SWNT Nanocomposites, *Environmental Science & Technology*, (2012).

[41] D. Rodrigues, M. Elimelech, Toxic Effects of Single-Walled Carbon Nanotubes in the Development of E. coli Biofilm, *Environmental. Science & Technology*, 44 (2010) 4583–4589.

[42] D.F. Rodrigues, D.P. Jaisi, M. Elimelech, Toxicity of Functionalized Single-Walled Carbon Nanotubes on Soil Microbial Communities: Implications for Nutrient Cycling in Soil, *Environmental Science & Technology*, 47 (2012) 625-633.

[43] S. Kang, M.S. Mauter, M. Elimelech, Microbial Cytotoxicity of Carbon-Based Nanomaterials: Implications for River Water and Wastewater Effluent, *Environmental Science & Technology*, 43 (2009) 2648-2653.

[44] D. Lyon, J.D. Fortner, C.M. Sayes, V.L. Colvin, J.B. Hughes, Bacterial cell association and antimicrobial activity of a C-60 water suspension, Environ. Toxicol. Chem, 24 (2005) 2757–2762.

[45] T. Akasaka, F. Watari, Capture of bacteria by flexible carbon nanotubes, *Acta. Biomater*, 5 (2009) 607–612.

[46] S. Kang, S.M. Mauter, M. Elimelech, Physiochemical determinants of multiwalled carbon nanotube bacterial cytotoxicity., *Environmental. Science & Technology*, 42 (2008b) 7528–7534.

[47] R.J. Narayan, C.J. Berry, R.L. Brigmon, Structural and biological properties of carbon nanotube composite films, *Materials Science and Engineering*, 123 B (2005) 123–129.

[48] D. Nepal, S. Balasubramanian, A.L. Simonian, V.A. Davis, Strong antimicrobial coatings: single walled carbon nanotubes armored with biopolymers, *Nano. Letter*, 8(7) (2008) 1896–1902.

[49] Y. Zhu, T. Ran, Y. Li, J. Guo, W. Li, Dependence of cytotoxicity of multi walled carbon nanotubes on the culture medium, *Nanotechnology*, 17 (2006) 4668–4674.

[50] S. Liu, L. Wei, L. Hao, N. Fang, M.-W. Chang, R. Xu, Y. Yang, Y. Chen, Sharper and faster "nano darts" kill more bacteria: A study of antibacterial activity of individually dispersed pristine single-walled carbon nanotubes, *Acs Nano*, 3 (2009) 3891-3902.

[51] X. Wang, X. Liu, H. Han, Evaluation of antibacterial effects of carbon nanomaterials against copper-resistant Ralstonia solanacearum, *Colloids and Surfaces B: Biointerfaces*, 103 (2013) 136-142.

[52] W. Hu, C. Peng, W. Luo, M. Lv, X. Li, D. Li, Q. Huang, C. Fan, Graphene-Based Antibacterial Paper, *Acs Nano*, 4 (2010) 4317-4323.

[53] C.D. Vecitis, K.R. Zodrow, S. Kang, M. Elimelech, Electronic-Structure-Dependent Bacterial Cytotoxicity of Single-Walled Carbon Nanotubes, *ACS Nano*, 4 (2010) 5471-5479.

[54] A.A. Shvedova, Castranova, V., Kisin, E.R., Schwegler-Berry, D., Murray, A.R., Gandelsman, V.Z., Maynard, A., Baron, P., Exposure to carbon nanotube material: assessment of nanotube cytotoxicity using human keratinocyte cells, *J. Toxicol. Environ. Health*, 66 (2003) 1909–1926.

[55] A.A. Shvedova, A. Pietroiusti, B. Fadeel, V.E. Kagan, Mechanisms of carbon nanotube-induced toxicity: Focus on oxidative stress, *Toxicology and Applied Pharmacology*, 261 (2012) 121-133.

[56] N. Yanamala, V.E. Kagan, A.A. Shvedova, Molecular modeling in structural nano-toxicology: Interactions of nano-particles with nano-machinery of cells, *Advanced Drug Delivery Reviews*.

[57] O. Akhavan, E. Ghaderi, Toxicity of Graphene and Graphene Oxide Nanowalls Against Bacteria, *ACS Nano*, 4 (2010) 5731-5736.

[58] J. Boczkowski, S. Lanone, Respiratory toxicities of nanomaterials — A focus on carbon nanotubes, *Advanced Drug Delivery Reviews*, 64 (2012) 1694-1699.

[59] Y. Chang, S.-T. Yang, J.-H. Liu, E. Dong, Y. Wang, A. Cao, Y. Liu, H. Wang, In vitro toxicity evaluation of graphene oxide on A549 cells, *Toxicology Letters*, 200 (2011) 201-210.

[60] N.A. Monteiro-Riviere, R.J. Nemanich, A.O. Inman, Y.Y. Wang, J.E. Riviere, Multi-walled carbon nanotube interactions with human epidermal keratinocytes, *Toxicology Letters*, 155 (2005) 377-384.

[61] J. Muller, F. Huaux, N. Moreau, P. Misson, J.-F. Heilier, M. Delos, M. Arras, A. Fonseca, J.B. Nagy, D. Lison, Respiratory toxicity of multi-wall carbon nanotubes, *Toxicology and Applied Pharmacology*, 207 (2005) 221-231.

[62] G. Jia, H. Wang, L. Yan, X. Wang, R. Pei, T. Yan, Y. Zhao, X. Guo, Cytotoxicity of Carbon Nanomaterials: Single-Wall Nanotube, Multi-Wall Nanotube, and Fullerene, *Environmental Science & Technology*, 39 (2005) 1378-1383.

[63] Y. Zhang, S.F. Ali, E. Dervishi, Y. Xu, Z. Li, D. Casciano, A.S. Biris, Cytotoxicity Effects of Graphene and Single-Wall Carbon Nanotubes in Neural Phaeochromocytoma-Derived PC12 Cells, *ACS Nano*, 4 (2010) 3181-3186.

[64] C. Zhou, M.D. Weir, K. Zhang, D. Deng, L. Cheng, H.H.K. Xu, Synthesis of new antibacterial quaternary ammonium monomer for incorporation into CaP nanocomposite, *Dental Materials*.

[65] M.S. Tamboli, M.V. Kulkarni, R.H. Patil, W.N. Gade, S.C. Navale, B.B. Kale, Nanowires of silver–polyaniline nanocomposite synthesized via in situ polymerization and its novel functionality as an antibacterial agent, *Colloids and Surfaces B: Biointerfaces*, 92 (2012) 35-41.

[66] H. Münstedt, C.R. Kumar, Silver ion release antimicrobial polyamide/silver composites, *Biomaterials*, 26 (2005) 2081–2088.

[67] C. Radheshkumar, H. Munstedt, Antimicrobial polymers from polypropylene/silver composites-Ag release measurement by anode stripping voltammetry, *React Funct Polym* 66 (2006) 780–788.

[68] Z. Liu, J.T. Robinson, X. Sun, H. Dai, PEGylated Nanographene Oxide for Delivery of Water-Insoluble Cancer Drugs, *Journal of the American Chemical Society,* 130 (2008) 10876-10877.

[69] K. Yang, J. Wan, S. Zhang, Y. Zhang, S.-T. Lee, Z. Liu, In Vivo Pharmacokinetics, Long-Term Biodistribution, and Toxicology of PEGylated Graphene in Mice, *ACS Nano,* 5 (2010) 516-522.

[70] L. Feng, Y. Chen, J. Ren, X. Qu, A graphene functionalized electrochemical aptasensor for selective label-free detection of cancer cells, *Biomaterials,* 32 (2011) 2930-2937.

[71] J.-H. Kim, Y.-S. Kim, K. Park, E. Kang, S. Lee, H.Y. Nam, K. Kim, J.H. Park, D.Y. Chi, R.-W. Park, I.-S. Kim, K. Choi, I. Chan Kwon, Self-assembled glycol chitosan

nanoparticles for the sustained and prolonged delivery of antiangiogenic small peptide drugs in cancer therapy, *Biomaterials*, 29 (2008) 1920-1930.

[72] G. Qu, X. Wang, Q. Liu, R. Liu, N. Yin, J. Ma, L. Chen, J. He, S. Liu, G. Jiang, The ex vivo and in vivo biological performances of graphene oxide and the impact of surfactant on graphene oxide's biocompatibility, *Journal of Environmental Sciences*, 25 (2013) 873-881.

[73] K.J. Gilmore, S.E. Moulton, G.G. Wallace, Incorporation of carbon nanotubes into the biomedical polymer poly(styrene-β-isobutylene-β-styrene), *Carbon*, 45 (2007) 402-410.

[74] X. Chen, H.J. Schluesener, Mode of dye loading affects staining outcomes of fluorescent dyes in astrocytes exposed to multiwalled carbon nanotubes, *Carbon*, 48 (2010) 730-743.

[75] S. Park, N. Mohanty, J.W. Suk, A. Nagaraja, J. An, R.D. Piner, W. Cai, D.R. Dreyer, V. Berry, R.S. Ruoff, Biocompatible, Robust Free-Standing Paper Composed of a TWEEN/Graphene Composite, *Advanced Materials*, 22 (2010) 1736-1740.

[76] S. Aslan, M. Deneufchatel, S. Hashmi, N. Li, L.D. Pfefferle, M. Elimelech, E. Pauthe, P.R. Van Tassel, Carbon nanotube-based antimicrobial biomaterials formed via layer-by-layer assembly with polypeptides, *Journal of Colloid and Interface Science*, 388 (2012) 268-273.

[77] M.J. Focazio, D.W. Kolpin, K.K. Barnes, E.T. Furlong, M.T. Meyer, S.D. Zaugg, L.B. Barber, M.E. Thurman, A national reconnaissance for pharmaceuticals and other organic wastewater contaminants in the United States — II) Untreated drinking water sources, *Science of The Total Environment*, 402 (2008) 201-216.

[78] V.K.K. Upadhyayula, S. Deng, M.C. Mitchell, G.B. Smith, Application of carbon nanotube technology for removal of contaminants in drinking water: A review, *Science of The Total Environment*, 408 (2009) 1-13.

[79] O.S. Amuda, A.A. Giwa, I.A. Bello, Removal of heavy metal from industrial wastewater using modified activated coconut shell carbon, *Biochemical Engineering Journal*, 36 (2007) 174-181.

[80] H. Treviño-Cordero, L.G. Juárez-Aguilar, D.I. Mendoza-Castillo, V. Hernández-Montoya, A. Bonilla-Petriciolet, M.A. Montes-Morán, Synthesis and adsorption properties of activated carbons from biomass of Prunus domestica and Jacaranda mimosifolia for the removal of heavy metals and dyes from water, *Industrial Crops and Products*, 42 (2013) 315-323.

[81] Q. Li, S. Mahendra, D.Y. Lyon, L. Brunet, M.V. Liga, D. Li, P.J.J. Alvarez, Antimicrobial nanomaterials for water disinfection and microbial control: Potential applications and implications, *Water Research*, 42 (2008) 4591-4602.

[82] S. Chowdhury, P. Champagne, P.J. McLellan, Models for predicting disinfection byproduct (DBP) formation in drinking waters: A chronological review, *Science of The Total Environment*, 407 (2009) 4189-4206.

[83] X. Yang, C. Shang, W. Lee, P. Westerhoff, C. Fan, Correlations between organic matter properties and DBP formation during chloramination, *Water Research*, 42 (2008) 2329-2339.

[84] P.C. Chiang, Y.W. Ko, C.H. Liang, E.E. Chang, Modeling an ozone bubble column for predicting its disinfection efficiency and control of DBP formation, *Chemosphere*, 39 (1999) 55-70.

[85] C. Lu, F. Su, Adsorption of natural organic matter by carbon nanotubes, *Separation and Purification Technology*, 58 (2007) 113-121.

[86] N. Dizge, B. Tansel, Multiparametric investigation of competitive and noncompetitive sorption characteristics of SMP fractions (carbohydrate and protein) on activated carbon, *Journal of Hazardous Materials*, 185 (2011) 996-1004.

[87] Y. Gao, Y. Li, L. Zhang, H. Huang, J. Hu, S.M. Shah, X. Su, Adsorption and removal of tetracycline antibiotics from aqueous solution by graphene oxide, *Journal of Colloid and Interface Science*, 368 (2012) 540-546.

[88] D. Zhang, H. Niu, X. Zhang, Z. Meng, Y. Cai, Strong adsorption of chlorotetracycline on magnetite nanoparticles, *Journal of Hazardous Materials*, 192 (2011) 1088-1093.

[89] A. Ghauch, A. Tuqan, H.A. Assi, Antibiotic removal from water: Elimination of amoxicillin and ampicillin by microscale and nanoscale iron particles, *Environmental Pollution*, 157 (2009) 1626-1635.

[90] I. Michael, L. Rizzo, C.S. McArdell, C.M. Manaia, C. Merlin, T. Schwartz, C. Dagot, D. Fatta-Kassinos, Urban wastewater treatment plants as hotspots for the release of antibiotics in the environment: A review, *Water Research*, 47 (2013) 957-995.

[91] A.M. Comerton, R.C. Andrews, D.M. Bagley, P. Yang, Membrane adsorption of endocrine disrupting compounds and pharmaceutically active compounds, *Journal of Membrane Science*, 303 (2007) 267-277.

[92] J.P. Ruparelia, S.P. Duttagupta, A.K. Chatterjee, S. Mukherji, Potential of carbon nanomaterials for removal of heavy metals from water, *Desalination*, 232 (2008) 145-156.

[93] V.C. Srivastava, I.D. Mall, I.M. Mishra, Optimization of parameters for adsorption of metal ions onto rice husk ash using Taguchi's experimental design methodology, *Chemical Engineering Journal*, 140 (2008) 136-144.

[94] T.A. Kurniawan, G.Y.S. Chan, W.-h. Lo, S. Babel, Comparisons of low-cost adsorbents for treating wastewaters laden with heavy metals, *Science of The Total Environment*, 366 (2006) 409-426.

[95] T.A. Kurniawan, W.-h. Lo, G.Y.S. Chan, Radicals-catalyzed oxidation reactions for degradation of recalcitrant compounds from landfill leachate, *Chemical Engineering Journal*, 125 (2006) 35-57.

[96] A.S. Brady-Estévez, S. Kang, M. Elimelech, A Single-Walled-Carbon-Nanotube Filter for Removal of Viral and Bacterial Pathogens, *Small*, 4 (2008) 481-484.

[97] D. Shuguang, V.K.K. Upadhyayula, G.B. Smith, M.C. Mitchell, Adsorption Equilibrium and Kinetics of Microorganisms on Single-Wall Carbon Nanotubes, *Sensors Journal*, IEEE, 8 (2008) 954-962.

[98] V.K.K. Upadhyayula, S. Deng, G.B. Smith, M.C. Mitchell, Adsorption of Bacillus subtilis on single-walled carbon nanotube aggregates, activated carbon and NanoCeram™, *Water Research*, 43 (2009) 148-156.

[99] S.T. Mostafavi, M.R. Mehrnia, A.M. Rashidi, Preparation of nanofilter from carbon nanotubes for application in virus removal from water, *Desalination*, 238 (2009) 271-280.

[100] A.S. Brady-Estévez, T.H. Nguyen, L. Gutierrez, M. Elimelech, Impact of solution chemistry on viral removal by a single-walled carbon nanotube filter, *Water Research*, 44 (2010) 3773-3780.

[101] A. Matilainen, N. Vieno, T. Tuhkanen, Efficiency of the activated carbon filtration in the natural organic matter removal, *Environment International*, 32 (2006) 324-331.

[102] M.H.S. Anna S. Brady-Estevez, Chad D. Vecitis,Navid B. Saleh, Menachem Elimelech, Multiwalled Carbon Nanotube Filter: Improving Viral Removal at Low Pressure, *Langmuir Article*, 26 (2010) 14975-14982.

[103] W. Cheng, S.A. Dastgheib, T. Karanfil, Adsorption of dissolved natural organic matter by modified activated carbons, *Water Research*, 39 (2005) 2281-2290.

[104] S.A. Dastgheib, T. Karanfil, W. Cheng, Tailoring activated carbons for enhanced removal of natural organic matter from natural waters, *Carbon*, 42 (2004) 547-557.

[105] F. Wang, J. Yao, H. Chen, Z. Yi, B. Xing, Sorption of humic acid to functionalized multi-walled carbon nanotubes, *Environmental Pollution*, 180 (2013) 1-6.

[106] F. Li, A. Yuasa, K. Ebie, Y. Azuma, T. Hagishita, Y. Matsui, Factors affecting the adsorption capacity of dissolved organic matter onto activated carbon: modified isotherm analysis, *Water Research*, 36 (2002) 4592-4604.

[107] P.A. Quinlivan, L. Li, D.R.U. Knappe, Effects of activated carbon characteristics on the simultaneous adsorption of aqueous organic micropollutants and natural organic matter, *Water Research*, 39 (2005) 1663-1673.

[108] C. Lu, C. Liu, G.P. Rao, Comparisons of sorbent cost for the removal of Ni2+ from aqueous solution by carbon nanotubes and granular activated carbon, *Journal of Hazardous Materials*, 151 (2008) 239-246.

[109] Y.-H. Li, Z. Di, J. Ding, D. Wu, Z. Luan, Y. Zhu, Adsorption thermodynamic, kinetic and desorption studies of Pb2+ on carbon nanotubes, *Water Research*, 39 (2005) 605-609.

[110] C. Lu, H. Chiu, C. Liu, Removal of Zinc(II) from Aqueous Solution by Purified Carbon Nanotubes: Kinetics and Equilibrium Studies, *Industrial & Engineering Chemistry Research,* 45 (2006) 2850-2855.

[111] G.P. Rao, C. Lu, F. Su, Sorption of divalent metal ions from aqueous solution by carbon nanotubes: A review, *Separation and Purification Technology*, 58 (2007) 224-231.

[112] X. Ren, C. Chen, M. Nagatsu, X. Wang, Carbon nanotubes as adsorbents in environmental pollution management: A review, *Chemical Engineering Journal*, 170 (2011) 395-410.

[113] H. Wang, A. Zhou, F. Peng, H. Yu, J. Yang, Mechanism study on adsorption of acidified multiwalled carbon nanotubes to Pb(II), *Journal of Colloid and Interface Science,* 316 (2007) 277-283.

[114] S. Wang, H. Sun, H.M. Ang, M.O. Tadé, Adsorptive remediation of environmental pollutants using novel graphene-based nanomaterials, *Chemical Engineering Journal*, 226 (2013) 336-347.

[115] G. Zhao, J. Li, X. Ren, C. Chen, X. Wang, Few-Layered Graphene Oxide Nanosheets As Superior Sorbents for Heavy Metal Ion Pollution Management, *Environmental Science & Technology,* 45 (2011) 10454-10462.

[116] N. Zhang, H. Qiu, Y. Si, W. Wang, J. Gao, Fabrication of highly porous biodegradable monoliths strengthened by graphene oxide and their adsorption of metal ions, *Carbon,* 49 (2011) 827-837.

[117] L. Liu, C. Li, C. Bao, Q. Jia, P. Xiao, X. Liu, Q. Zhang, Preparation and characterization of chitosan/graphene oxide composites for the adsorption of Au(III) and Pd(II), *Talanta,* 93 (2012) 350-357.

[118] Y.-H. Li, S. Wang, Z. Luan, J. Ding, C. Xu, D. Wu, Adsorption of cadmium(II) from aqueous solution by surface oxidized carbon nanotubes, *Carbon,* 41 (2003) 1057-1062.

[119] A. A.Hirsch, Functionalization of Single-Walled Carbon Nanotubes, *Chem. Ind. Ed,* 41 (2002).

[120] C. Chen, X. Wang, Adsorption of Ni(II) from Aqueous Solution Using Oxidized Multiwall Carbon Nanotubes, *Industrial & Engineering Chemistry Research,* 45 (2006) 9144-9149.

[121] C.-H. Wu, Studies of the equilibrium and thermodynamics of the adsorption of Cu2+ onto as-produced and modified carbon nanotubes, *Journal of Colloid and Interface Science,* 311 (2007) 338-346.

[122] Y.-H. Li, J. Ding, Z. Luan, Z. Di, Y. Zhu, C. Xu, D. Wu, B. Wei, Competitive adsorption of Pb2+, Cu2+ and Cd2+ ions from aqueous solutions by multiwalled carbon nanotubes, *Carbon,* 41 (2003) 2787-2792.

[123] V.K.K. Upadhyayula, V. Gadhamshetty, Appreciating the role of carbon nanotube composites in preventing biofouling and promoting biofilms on material surfaces in environmental engineering: A review, *Biotechnology Advances,* 28 (2010) 802-816.

[124] S. Aslan, C.Z. Loebick, S. Kang, M. Elimelech, L.D. Pfefferle, P.R. Van Tassel, Antimicrobial biomaterials based on carbon nanotubes dispersed in poly(lactic-co-glycolic acid), *Nanoscale*, 2 (2010) 1789-1794.

[125] L. Q, S. Mahendra, D.Y. Lyon, L. Brunet, M.V. Liga, D. Li, P.J.J. Alvarez, Antimicrobial nanomaterials for water disinfection and microbial control: Potential applications and implications, *water. Research,* 42 (2008) 4 5 9 1 – 4 6 0 2.

[126] L. Dumée, J. Lee, K. Sears, B. Tardy, M. Duke, S. Gray, Fabrication of thin film composite poly(amide)-carbon-nanotube supported membranes for enhanced performance in osmotically driven desalination systems, *Journal of Membrane Science,* 427 (2013) 422-430.

[127] J.R. McCutcheon, R.L. McGinnis, M. Elimelech, Desalination by ammonia–carbon dioxide forward osmosis: Influence of draw and feed solution concentrations on process performance, *Journal of Membrane Science,* 278 (2006) 114-123.

[128] H. Cong, J. Zhang, M. Radosz, Y. Shen, Carbon nanotube composite membranes of brominated poly(2,6-diphenyl-1,4-phenylene oxide) for gas separation, *Journal of Membrane Science,* 294 (2007) 178-185.

[129] V. Vatanpour, S.S. Madaeni, R. Moradian, S. Zinadini, B. Astinchap, Fabrication and characterization of novel antifouling nanofiltration membrane prepared from oxidized multiwalled carbon nanotube/polyethersulfone nanocomposite, *Journal of Membrane Science,* 375 (2011) 284-294.

[130] X. Wang, X. Chen, K. Yoon, D. Fang, B.S. Hsiao, B. Chu, High Flux Filtration Medium Based on Nanofibrous Substrate with Hydrophilic Nanocomposite Coating, *Environmental Science & Technology*, 39 (2005) 7684-7691.

[131] J.-H. Choi, J. Jegal, W.-N. Kim, Fabrication and characterization of multi-walled carbon nanotubes/polymer blend membranes, *Journal of Membrane Science,* 284 (2006) 406-415.

[132] S. Roy, S.A. Ntim, S. Mitra, K.K. Sirkar, Facile fabrication of superior nanofiltration membranes from interfacially polymerized CNT-polymer composites, *Journal of Membrane Science,* 375 (2011) 81-87.

[133] E.-S. Kim, Y. Liu, M. Gamal El-Din, An in-situ integrated system of carbon nanotubes nanocomposite membrane for oil sands process-affected water treatment, *Journal of Membrane Science,* 429 (2013) 418-427.

[134] M. Amini, M. Jahanshahi, A. Rahimpour, Synthesis of novel thin film nanocomposite (TFN) forward osmosis membranes using functionalized multi-walled carbon nanotubes, *Journal of Membrane Science,* 435 (2013) 233-241.

[135] K.K.U. Venkata, G. Venkataramana, Appreciating the role of carbon nanotube composites in preventing biofouling and promoting biofilms on material surfaces in environmental engineering: A review, *Biotechnol. Adv,* 28 (2010) 802-816.

[136] M. Morikawa, Beneficial biofilm formation by industrial bacteria Bacillus subtilis and related species, *J. Biosci. Bioeng*, 101 (2006) 1–8.

[137] R.J. Palmer, D.C. White, Developmental biology of biofilms: implications for treatment and control, Trends. *Microbioogy,* 5 (1997) 435–440.

[138] L.R. Arias, L. Yang, Inactivation of bacterial pathogens by carbon nanotubes in suspensions, *Langmuir,* 25 (2009) 3003–3012.

[139] K.M. Cui, M.C. Tria, R.B. Pernites, C.A. Binag, R.C. Advincula, Carbon Nanotube-PVK Electropolymerized Conjugated Polymer Network Nanocomposite Films, *ACS Applied Materials & Interfaces,* (2011).

[140] J.M. Yeh, K.C. Chang, Polymer/layered silicate nanocomposite anticorrosive coatings, J*ournal of Industrial and Engineering Chemistry,* 14 (2008) 275-291.

[141] N.K. Guimarda, N. Gomezb, C.E. Schmidt, Conducting polymers in biomedical engineering, *Progress in Polymer Science,* 32 (2007) 876–921.

[142] C.M. Santos, M.C. Tria, R.A.M.V. Vergara, F.A. Ahmed, R.C. Advincula, D. Rodrigues, Antimicrobial graphene polymer (PVK-GO) nanocomposite films, *Chemical. Communication.*, DOI: 10.1039/c1cc11877c.

[143] T. Ahujaa, I. Ahmad, M.D. Kumara, Biomolecular immobilization on conducting polymers for biosensing applications, *Biomaterials,* 28 (2007) 791–805.

[144] E.b. Frackowiaka, F. Beguin, Interaction between electroconducting polymers and C60 *Journal of Physics and Chemistry of Solids,* 57 (1996) 983-989.

[145] L.W. Shaobin Liu, Lin Hao, Ning Fang, Matthew Wook Chang, Rong Xu, Yanhui Yang and Yuan Chen, Sharper and Faster "Nano Darts" Kill More Bacteria: A Study of Antibacterial Activity of Individually Dispersed Pristine Single-Walled Carbon Nanotube, *ACS Nano,* 3(12) (2009) 3891–3902.

[146] C. Yang, J. Mamouni, Y. Tang, L. Yang, Antimicrobial Activity of Single-Walled Carbon Nanotubes: Length Effect, *Langmuir Article,* 26 (2010) 16013-16019.

[147] E.N. Fox, R.S.J. Demaree, Quick bacterial fixation technique for scanning electron microscopy, *Microscopy Research and Technique,* 46 (1999) 338-339.

[148] J.F. Ambrose, R.F. Nelson, Anodic Oxidation Pathways of Carbazoles, *Journal of Electrochemical Society,* 115 (1968) 1159-1164.

[149] A. Baba, K. Onishi, W. Knoll, R.C. Advincula, Investigating Work Function Tunable Hole-Injection/Transport Layers of Electrodeposited Polycarbazole Network Thin Films, *Journal of . Phyical. Cheistry. B,* 108 (2004) 18949-18955.

[150] B. Mohanty, A.K. Verma, P. Claesson, H.B. Bohidar, Physical and anti-microbial charecteristics of carbon nanoparticles prepared from lamp soot., *Nanotechnology,* 18 (2007) 1-9.

[151] K.M. Cui, M.C. Tria, R.B. Pernites, C.A. Binag, R.C. Advincula, *ACS Applied Materials & Interfaces,* (2011).

[152] S. Kang, M. Pinault, L.D. Pfefferle, M. Elimelech, Single-walled carbon nanotubes exhibit strong antimicrobial activity, *Langmuir,* 23 (2007) 8670-8673.

[153] J.D. Schiffman, M. Elimelech, Antibacterial Activity of Electrospun Polymer Mats with Incorporated Narrow Diameter Single-Walled Carbon Nanotubes, *Acs Applied Materials & Interfaces,* 3 (2011) 462-468.

[154] R.M. Donlan, Preventing biofilms of clinically relevant organisms using bacteriophage, *Trends in Microbiology,* 17 (2009) 66-72.

[155] S. Aslan, C.Z. Loebick, S. Kang, M. Elimelech, L.D. Pfefferle, P.R. Van Tassel, Antimicrobial biomaterials based on carbon nanotubes dispersed in poly(lactic-co-glycolic acid), *Nanoscale*, 2 (2010) 1789.

[156] P. Taranekar, T. Fulghum, D. Patton, R. Ponnapati, G. Clyde, R. Advincula, Investigating Carbazole Jacketed Precursor Dendrimers: Sonochemical Synthesis, Characterization, and Electrochemical Crosslinking Properties, *ournal of American Chemical Society*., 129 (2007) 12537-12548.

[157] A.B. Bourlinos, D. Gournis, D. Petridis, T. Szabó, A. Szeri, I. Dékány, Graphite Oxide: Chemical Reduction to Graphite and Surface Modification with Primary Aliphatic Amines and Amino Acids, *Langmuir*, 19 (2003) 6050-6055.

[158] R. Pernites, A. Vergara, A. Yago, K. Cui, R. Advincula, Facile approach to graphene oxide and poly(N-vinylcarbazole) electro-patterned films, *Chemical Communications,* 47 (2011) 9810-9812.

[159] N. Hilal, V. Kochkodan, L. Al-Khatib, T. Levadna, Surface modified polymeric membranes to reduce (bio)fouling: a microbiological study using E. coli, *Desalination,* 167 (2004) 293-300.

[160] K.C. Khulbe, T. Matsuura, S. Singh, G. Lamarche, S.H. Noh, Study on fouling of ultrafiltration membrane by electron spin resonance, *Journal of Membrane Science,* 167 (2000) 263-273.

[161] C.X. Liu, D.R. Zhang, Y. He, X.S. Zhao, R. Bai, Modification of membrane surface for anti-biofouling performance: Effect of anti-adhesion and anti-bacteria approaches, *Journal of Membrane Science,* 346 (2010) 121-130.

[162] F. Peng, C. Hu, Z. Jiang, Novel ploy(vinyl alcohol)/carbon nanotube hybrid membranes for pervaporation separation of benzene/cyclohexane mixtures, *Journal of Membrane Science,* 297 (2007) 236-242.

[163] L.R. Arias, L. Yang, Inactivation of Bacterial Pathogens by Carbon Nanotubes in Suspensions, *Langmuir,* 25 (2009) 3003-3012.

[164] F. Ahmed, C.M. Santos, R.A.M.V. Vergara, M.C.R. Tria, R. Advincula, D.F. Rodrigues, Antimicrobial Applications of Electroactive PVK-SWNT Nanocomposites, *Environmental Science & Technology,* 46 (2012) 1804-1810.

[165] N.K. Guimard, N. Gomez, C.E. Schmidt, Conducting polymers in biomedical engineering, *Progress in Polymer Science,* 32 (2007) 876-921.

[166] T. Ahuja, I. Mir, D. Kumar, Rajesh, Biomolecular immobilization on conducting polymers for biosensing applications, *Biomaterials,* 28 (2007) 791-805.

[167] K.M. Cui, M.C. Tria, R. Pernites, C.A. Binag, R.C. Advincula, PVK/MWNT Electrodeposited Conjugated Polymer Network Nanocomposite Films, *ACS Applied Materials & Interfaces,* 3 (2011) 2300-2308.

[168] A.S. Brady-Estévez, M.H. Schnoor, C.D. Vecitis, N.B. Saleh, M. Elimelech, Multiwalled Carbon Nanotube Filter: Improving Viral Removal at Low Pressure, *Langmuir,* 26 (2010) 14975-14982.

[169] M.C.R. Tria, C.D.T. Grande, R.R. Ponnapati, R.C. Advincula, Electrochemical Deposition and Surface-Initiated RAFT Polymerization: Protein and Cell-Resistant PPEGMEMA Polymer Brushes, *Biomacromolecules,* 11 (2010) 3422-3431.

[170] T.M. Fulghum, P. Taranekar, R.C. Advincula, Grafting Hole-Transport Precursor Polymer Brushes on ITO Electrodes: Surface-Initiated Polymerization and Conjugated Polymer Network Formation of PVK, *Macromolecules,* 41 (2008) 5681-5687.

[171] H. Sloane, Infrared Differential Technique Employing Membrane Filters, *Analytical Chemistry,* 35 (1963) 1556-1558.

[172] D.Y. Lyon, P.J.J. Alvarez, Fullerene Water Suspension (nC60) Exerts Antibacterial Effects via ROS-Independent Protein Oxidation, *Environmental Science & Technology,* 42 (2008) 8127-8132.

[173] D.Y. Lyon, J.D. Fortner, C.M. Sayes, V.L. Colvin, J.B. Hughes, Bacterial cell association and antimicrobial activity of a C60 water suspension, *Environmental Toxicology and Chemistry,* 24 (2005) 2757-2762.

[174] D.F. Rodrigues, M. Elimelech, Toxic Effects of Single-Walled Carbon Nanotubes in the Development of E. coli Biofilm, *Environmental Science & Technology*, 44 (2010) 4583-4589.

[175] L.A. Pratt, R. Kolter, Genetic analysis of Escherichia coli biofilm formation: roles of flagella, motility, chemotaxis and type I pili, *Molecular Microbiology*, 30 (1998) 285-293.

[176] C. Yang, J. Mamouni, Y. Tang, L. Yang, Antimicrobial Activity of Single-Walled Carbon Nanotubes: Length Effect, *Langmuir,* 26 (2010) 16013-16019.

[177] D. García, P. Mañas, N. Gómez, J. Raso, R. Pagán, Biosynthetic requirements for the repair of sublethal membrane damage in Escherichia coli cells after pulsed electric fields, *Journal of Applied Microbiology*, 100 (2006) 428-435.

[178] M. Zator, M. Ferrando, F. López, C. Güell, Membrane fouling characterization by confocal microscopy during filtration of BSA/dextran mixtures, *Journal of Membrane Science,* 301 (2007) 57-66.

[179] N. Tufenkji, M. Elimelech, Correlation Equation for Predicting Single-Collector Efficiency in Physicochemical Filtration in Saturated Porous Media, *Environmental Science & Technology*, 38 (2003) 529-536.

[180] J. Cheng, M.J. Meziani, Y.-P. Sun, S.H. Cheng, Poly(ethylene glycol)-conjugated multi-walled carbon nanotubes as an efficient drug carrier for overcoming multidrug resistance, *Toxicology and Applied Pharmacology*, 250 (2011) 184-193.

[181] F. Tian, D. Cui, H. Schwarz, G.G. Estrada, H. Kobayashi, Cytotoxicity of single-wall carbon nanotubes on human fibroblasts, *Toxicology in Vitro*, 20 (2006) 1202-1212.

[182] T. Miyoshi, T. Aizawa, K. Kimura, Y. Watanabe, Identification of proteins involved in membrane fouling in membrane bioreactors (MBRs) treating municipal wastewater, *International Biodeterioration & Biodegradation*, 75 (2012) 15-22.

[183] W.S. Ang, M. Elimelech, Protein (BSA) fouling of reverse osmosis membranes: Implications for wastewater reclamation, *Journal of Membrane Science*, 296 (2007) 83-92.

[184] H. Liu, R. Liu, C. Tian, H. Jiang, X. Liu, R. Zhang, J. Qu, Removal of natural organic matter for controlling disinfection by-products formation by enhanced coagulation: A case study, *Separation and Purification Technology*, 84 (2012) 41-45.

[185] X. Zhang, C. Cheng, J. Zhao, L. Ma, S. Sun, C. Zhao, Polyethersulfone enwrapped graphene oxide porous particles for water treatment, *Chemical Engineering Journal*, 215–216 (2013) 72-81.

[186] A.K. Mishra, T. Arockiadoss, S. Ramaprabhu, Study of removal of azo dye by functionalized multi walled carbon nanotubes, *Chemical Engineering Journal*, 162 (2010) 1026-1034.

[187] C.-Y. Kuo, C.-H. Wu, J.-Y. Wu, Adsorption of direct dyes from aqueous solutions by carbon nanotubes: Determination of equilibrium, kinetics and thermodynamics parameters, *Journal of Colloid and Interface Science*, 327 (2008) 308-315.

[188] Y. Tian, B. Gao, V.L. Morales, L. Wu, Y. Wang, R. Muñoz-Carpena, C. Cao, Q. Huang, L. Yang, Methods of using carbon nanotubes as filter media to remove aqueous heavy metals, *Chemical Engineering Journal*, 210 (2012) 557-563.

[189] Y.-C. Lee, J.-W. Yang, Self-assembled flower-like TiO2 on exfoliated graphite oxide for heavy metal removal, *Journal of Industrial and Engineering Chemistry,* 18 (2012) 1178-1185.

[190] S.-T. Yang, Y. Chang, H. Wang, G. Liu, S. Chen, Y. Wang, Y. Liu, A. Cao, Folding/aggregation of graphene oxide and its application in Cu2+ removal, *Journal of Colloid and Interface Science,* 351 (2010) 122-127.

[191] A. Qureshi, I. Roci, Y. Gurbuz, J.H. Niazi, An aptamer based competition assay for protein detection using CNT activated gold-interdigitated capacitor arrays, *Biosensors and Bioelectronics,* 34 (2012) 165-170.

[192] Y. Kang, Y.-C. Liu, Q. Wang, J.-W. Shen, T. Wu, W.-J. Guan, On the spontaneous encapsulation of proteins in carbon nanotubes, *Biomaterials,* 30 (2009) 2807-2815.

[193] X. Cai, R. Ramalingam, H.S. Wong, J. Cheng, P. Ajuh, S.H. Cheng, Y.W. Lam, Characterization of carbon nanotube protein corona by using quantitative proteomics, *Nanomedicine: Nanotechnology, Biology and Medicine,* 9 (2013) 583-593.

[194] F. Bomboi, A. Bonincontro, C. La Mesa, F. Tardani, Interactions between single-walled carbon nanotubes and lysozyme, *Journal of Colloid and Interface Science,* 355 (2011) 342-347.

[195] H. Wei, W. Yang, Q. Xi, X. Chen, Preparation of Fe3O4@graphene oxide core–shell magnetic particles for use in protein adsorption, *Materials Letters,* 82 (2012) 224-226.

[196] F. Ma, Z. Zhang, H. Jia, X. Liu, Y. Hao, B. Xu, Adsorption of cysteine molecule on intrinsic and Pt-doped graphene: A first-principle study, *Journal of Molecular Structure: THEOCHEM,* 955 (2010) 134-139.

[197] W.S. Hummers, R.E. Offeman, Preparation of Graphitic Oxide, *Journal of the American Chemical Society,* 80 (1958) 1339-1339.

[198] T. Chakrabarty, M. Kumar, V.K. Shahi, pH Responsive Hybrid Zwitterionomer for Protein Separation: Smart Nanostructured Adsorbent, *Industrial & Engineering Chemistry Research*, 51 (2012) 3015-3022.

[199] Z. Adamczyk, Modeling adsorption of colloids and proteins, *Current Opinion in Colloid & Interface Science,* 17 (2012) 173-186.

[200] F. Meder, T. Daberkow, L. Treccani, M. Wilhelm, M. Schowalter, A. Rosenauer, L. Mädler, K. Rezwan, Protein adsorption on colloidal alumina particles functionalized with amino, carboxyl, sulfonate and phosphate groups, *Acta Biomaterialia,* 8 (2012) 1221-1229.

[201] M. Rabe, D. Verdes, S. Seeger, Understanding protein adsorption phenomena at solid surfaces, *Advances in Colloid and Interface Science,* 162 (2011) 87-106.

[202] X. Sun, C. Li, Z. Wu, X. Xu, L. Ren, H. Zhao, Adsorption of Protein from Model Wine Solution by Different Bentonites, *Chinese Journal of Chemical Engineering,* 15 (2007) 632-638.

[203] Q.H. Shi, Y. Tian, X.Y. Dong, S. Bai, Y. Sun, Chitosan-coated silica beads as immobilized metal affinity support for protein adsorption, *Biochemical Engineering Journal*, 16 (2003) 317-322.

[204] K.L. Jones, C.R. O'Melia, Protein and humic acid adsorption onto hydrophilic membrane surfaces: effects of pH and ionic strength, *Journal of Membrane Science,* 165 (2000) 31-46.

[205] S. Pasche, J. Vörös, H.J. Griesser, N.D. Spencer, M. Textor, Effects of Ionic Strength and Surface Charge on Protein Adsorption at PEGylated Surfaces, *The Journal of Physical Chemistry B*, 109 (2005) 17545-17552.

[206] X. Sun, Z. Liu, K. Welsher, J. Robinson, A. Goodwin, S. Zaric, H. Dai, Nano-graphene oxide for cellular imaging and drug delivery, *Nano Research.*, 1 (2008) 203-212.

[207] T. Yang, Z. Li, L. Wang, C. Guo, Y. Sun, Synthesis, Characterization, and Self-Assembly of Protein Lysozyme Monolayer-Stabilized Gold Nanoparticles, *Langmuir*, 23 (2007) 10533-10538.

[208] D.W. Boukhvalov, M.I. Katsnelson, Modeling of Graphite Oxide, *Journal of the American Chemical Society*, 130 (2008) 10697-10701.

[209] A. Brody, Nano and food packaging technologies converge., *Food Tecnology*, 60 (2006) 92-94.

[210] M. Endo, M.S. Strano, P.M. Ajayan, Potential Applications of Carbon Nanotubes, in: A. Jorio, G. Dresselhaus, M.S. Dresselhaus (Eds.) Carbon Nanotubes, *Topics Applied Physics, Springer-Verlag, Berlin, Hedelberg*, 2008.

[211] A.D. Eaton, L.S. Clesceri, E.W. Rice, A.E. Greenberg, Standard Methods for The Examination of Water and Wastewater, 2005.

[212] D. Goyal, X.J. Zhang, J.N. Rooney-Varga, Impacts of single-walled carbon nanotubes on microbial community structure in activated sludge, *Letters in Applied Microbiology*, 51 (2010) 428-435.

[213] I.E. Mejias-Carpio, C.M. Santos, X. Wei, D.F. Rodrigues, Toxicity of a polymer-graphene oxide composite against bacterial, planktonic cells, biofilms, and mammalian cells., *Nanoscale*, 4 (2012) 4746-4756.

[214] Q. Bao, D. Zhang, P. Qi, Synthesis and characterization of silver nanoparticle and graphene oxide nanosheet composites as a bactericidal agent for water disinfection, *Journal of Colloid and Interface Science*, 360 (2011) 463-470.

[215] A. García, L. Delgado, J.A. Torà, E. Casals, E. González, V. Puntes, X. Font, J. Carrera, A. Sánchez, Effect of cerium dioxide, titanium dioxide, silver, and gold nanoparticles on the activity of microbial communities intended in wastewater treatment, *Journal of Hazardous Materials*, 199–200 (2012) 64-72.

[216] Y. Yin, X. Zhang, J. Graham, L. Luongo, Examination of purified single-walled carbon nanotubes on activated sludge process using batch reactors, *Journal of Environmental Science and Health, Part A*, 44 (2009) 661-665.

[217] C.J. Kelly, N. Tumsaroj, C.A. Lajoie, Assessing wastewater metal toxicity with bacterial bioluminescence in a bench-scale wastewater treatment system, *Water Research*, 38 (2004) 423-431.

[218] B.P. McNicholl, J.W. McGrath, J.P. Quinn, Development and application of a resazurin-based biomass activity test for activated sludge plant management, *Water Research*, 41 (2007) 127-133.

[219] S. Ge, Y. Peng, S. Wang, J. Guo, B. Ma, L. Zhang, X. Cao, Enhanced nutrient removal in a modified step feed process treating municipal wastewater with different inflow distribution ratios and nutrient ratios, *Bioresource Technology*, 101 (2010) 9012-9019.

[220] C.D. Vecitis, M.H. Schnoor, M.S. Rahaman, J.D. Schiffman, M. Elimelech, Electrochemical Multiwalled Carbon Nanotube Filter for Viral and Bacterial Removal and Inactivation, *Environmental Science & Technology*, 45 (2011) 3672-3679.

[221] A. Shvedova, V. Castranova, E. Kisin, D. Schwegler-Berry, A. Murray, V. Gandelsman, A. Maynard, P. Baron, Exposure to Carbon Nanotube Material: Assessment of Nanotube Cytotoxicity using Human Keratinocyte Cells, *Journal of Toxicology and Environmental Health, Part A*, 66 (2003) 1909-1926.

[222] K. Riedel, K.P. Lange, H.J. Stein, M. Kühn, P. Ott, F. Scheller, A microbial sensor for BOD, *Water Research*, 24 (1990) 883-887.

[223] A.R.N. Reddy, Y.N. Reddy, D.R. Krishna, V. Himabindu, Multi wall carbon nanotubes induce oxidative stress and cytotoxicity in human embryonic kidney (HEK293) cells, *Toxicology*, 272 (2010) 11-16.

[224] G.P. Winward, L.M. Avery, T. Stephenson, B. Jefferson, Chlorine disinfection of grey water for reuse: Effect of organics and particles, *Water Research*, 42 (2008) 483-491.

[225] G.R. Chang, J.C. Liu, D.J. Lee, CO-conditioning and dewatering of chemical sludge and waste activated sludge, *Water Research*, 35 (2001) 786-794.